The Impact of Interstitial Air Pressure on Sand Acoustic Emissions in the Context of Mars Exploration

Paul Perez

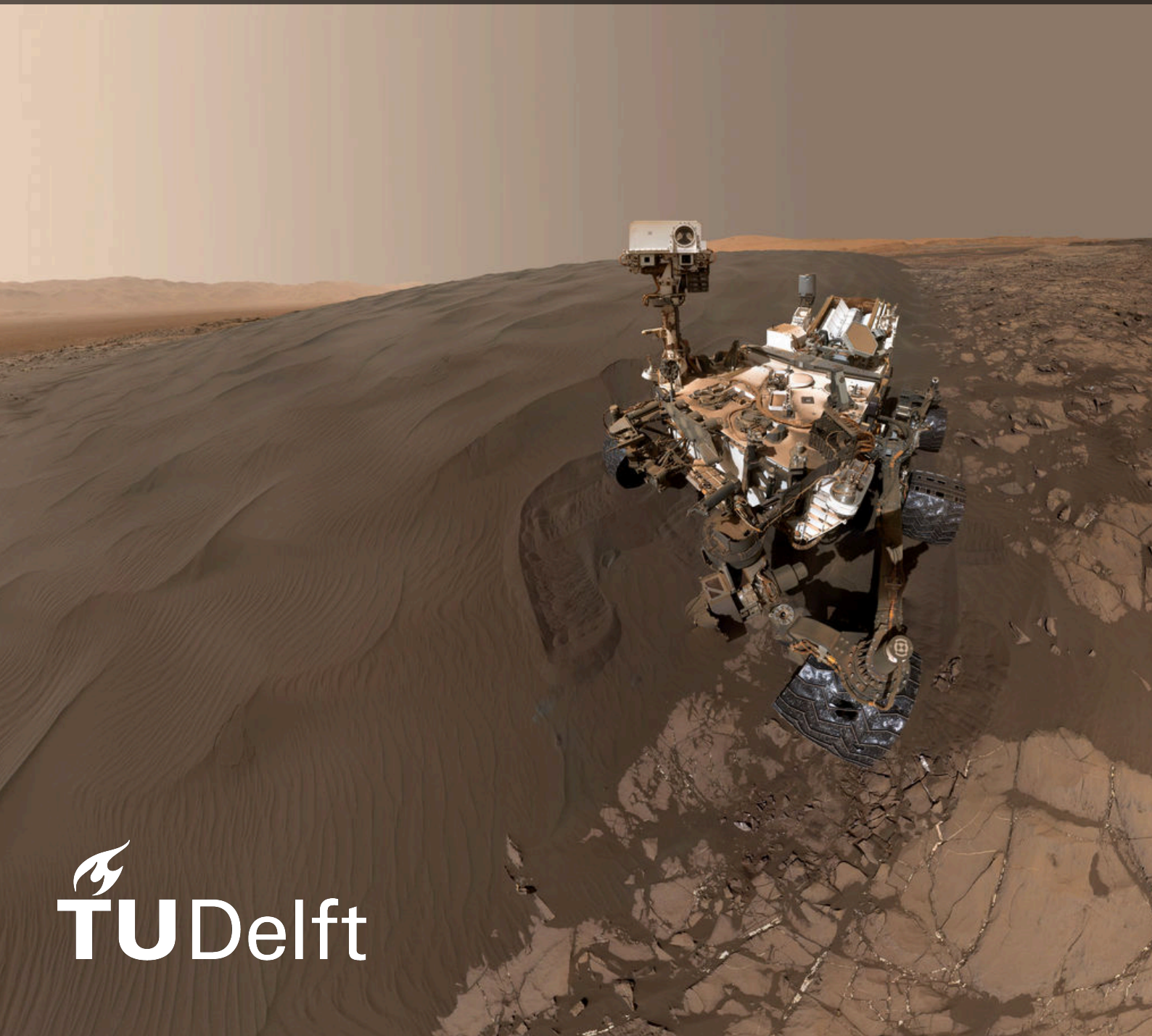

TU Delft

The Impact of Interstitial Air Pressure on Sand Acoustic Emissions in the Context of Mars Exploration

by

Paul Perez

to obtain the degree of Master of Science
at the Delft University of Technology,
to be defended publicly on Monday April 17, 2023 at 9:30 AM.

Student number: 5134773

Thesis committee:

Dr. ir. SJ. de Vet,	TU Delft, Responsible thesis supervisor
Dr. ir. D. Ragni,	TU Delft, Examiner
Dr. ir. F. Avallone,	TU Delft, Additional Examiner
Dr. ir. S. Cazaux,	TU Delft, Chair

TU Delft

Acknowledgements

I would first like to thank Sebastiaan for allowing me to work on such a unique topic, which also coincided with my interest in planetary sciences. Your constant enthusiasm and stream of ideas was not only helpful, but encouraging in its positive energy. Thank you also to Daniele, for your pragmatic approach to research, your straight to the point comments and your consistent availability, which all helped me become better at structuring a project efficiently. And finally, thank you Francesco, for your systematic feedback, which helped me in the completion of this project.

A special thank you to the technicians and engineers, Johan, Peter, Ferdinand and especially Stefan at the LSL, for helping me assemble the experimental setup used in this project, and giving me a place to perform my tests.

Fully creating and navigating this multi-disciplinary project presented me with numerous challenges and hurdles, both academically and mentally, from which I have learnt much about myself. I am also especially grateful for my parents who always supported me, despite the extended duration of this thesis.

To all my good friends and family, in Delft, Switzerland, Belgium, France and everywhere else, there is a little piece of all of you in these pages; let this be a memento of your support and our friendship, cheers!

Paul Perez
Delft, March 2023

Abstract

Desert sand acoustic emissions are produced when a “sonic sand” is sheared locally or by a natural dune slipface avalanche, resulting in a brassy sound between 50 and 400 Hz. This type of sediment exhibits particular granulometric, shape and surface characteristics, due to the grains’ erosion and transport history, and emits sounds when the sheared grain layer vibrates in a synchronized manner, much like the membrane of a speaker. Recording such sand acoustic emissions on Mars (and perhaps other planetary environments) using rover microphones could thus become a new form of observable for scientists to estimate the surface sediment’s characteristics and history from a distance, but also the granular flow dynamics taking place. To determine whether this approach could be viable in the future, it is essential to evaluate how the Martian environment may affect sand acoustic emissions differently than on Earth. After showing that the muted Martian soundscape would likely allow rovers to detect such signals from a few tens of meters, the present thesis studies the impact of the interstitial air pressure within the sand bed on the sound emission mechanism of such sonic desert sands.

In this project, silent and sonic desert sand shear flows are induced under a range of pressure levels, from terrestrial ambient pressure to Mars-like pressure, within two separate, manually operated vacuum chamber setups: a smaller chamber shaken to create the sounds, and another longer chamber that better replicates avalanche-like sand flows. The motion applied and sound produced are measured using an accelerometer and a microphone inside the chamber. Metrics in the time and frequency domains are defined to analyse the changes in sound energy, amplitude, and frequency components produced at different pressure levels. Firstly, the silent sand tests are used to establish how the air pressure level within the experimental setup affects the regular sound of sheared sand (i.e. grains impacting one another) and more generally the sound emission of “normal” sounds, whose emission mechanisms do not depend on grain packing and synchronized motion. Then, a simplified theoretical model of how the sound pressure level (*SPL*) of a sound evolves with decreasing acoustic impedance, is derived and validated using the silent sand measurements performed. Finally, the sonic sand measurements are compared to the *SPL* model and silent sand measurement results, which are used as a baseline for nominal sound production behavior, to evaluate how the interstitial air pressure affects the amplitude and signal energy of the sheared sonic sand emissions. Furthermore, differences in the sand acoustic emissions’ frequency spectra and time duration across pressure levels provide information about the possible physical changes occurring in the granular flow dynamics of the sheared sonic sand.

In both experiments, the dominant frequency very closely follows the trend of the motion metrics used, as described in the literature, and remains very consistent across pressure levels. This suggests that the maximum sheared sonic sand layer thickness is independent of the interstitial air pressure. Then, the sonic sand emissions see an increase in the sound amplitude and signal energy related metrics from ambient pressure to 413.25 mbar, unlike the gradual decrease predicted by the *SPL* model and the trend of silent sand measurements with decreasing pressure. Below 413.25 mbar, the results suggest a stabilized behavior, with the acoustic metrics of the emissions following the model. Furthermore, in the avalanche-like emissions, a new frequency component slightly higher than the dominant frequency emerges as the chamber pressure decreases. These observations are evidenced in the time-domain, where the sand acoustic emissions seem to initiate earlier in the granular flow at 413.25 mbar and below, resulting in greater acoustic pressure levels being produced, compared to those at terrestrial pressure. It is hypothesized that more sheared sonic sand grains synchronize at 413.25 mbar and below (compared to terrestrial air pressure), and thus increase the amplitude of the sound wave produced. For avalanche-like flows, the new frequency component that appears with decreasing pressure level seems to suggest that the minimum sheared layer thickness threshold required to produce an emission is lowered at lower pressure, which leads to a higher frequency produced initially until the full layer forms, ultimately decreasing the frequency. Further research is required to confirm these preliminary findings and theories.

Contents

List of Tables

List of Figures

1

Introduction

1.1. The Discovery of Sonic Sand

1.1.1. From Mystical Occurrence to Physical Phenomenon

For centuries and probably longer, natives and travellers have heard and described sounds coming from desert and coastal sand beds, in many regions on Earth (Andreotti, 2012). The neighbouring local communities ascribed the sounds to mystical occurrences. In Hawaii and Peru, the dunes were haunted with spirits and the dead (Tschiffely, 1933). In Bilma, Niger, it was rather the voice of the mountain, informing the villagers of an approaching caravan, while in California and Egypt, the sound was attributed to the bells and gong of old convents and monasteries (Ledoux, 1920). Opposing these mystical explanations, explorers and academics from the colonial era, such as Darwin and Curzon (Sholtz et al., 1997) generally related the downhill motion of a loose layer of sand to the sound, which they often compared to low string and wind instruments and even percussions (Curzon, 1923).

At the turn of the 20th century, many studies (Carus-Wilson, 1891; Poynting and Thompson, 1909; Richardson, 1919) were conducted, recognising the sonic sands' general properties and conditions propitious for sound emission. Later, in 1941, Ralph Bagnold wrote *The Physics of Blown Sand and Desert Dunes* (Bagnold, 1941), after being stationed in Egypt and exploring the Lybian desert for many years. This book provides the first piece of extensive research on aeolian sand transport and dune formation, using wind tunnel experiments, and is still widely considered one of the most complete references on the topic. It also proposes a theory for the sound emission mechanism of sonic desert sands, which has served as a key stepping stone for current theories. Although the scientific community has remained divided in the last 20 years regarding the sound production mechanism at play in sand acoustic emissions (Andreotti, 2012), the conditions and characteristics favourable for sonic sands are now rather well known. Indeed, many studies (Lindsay et al., 1976; Miwa et al., 1983; Sholtz et al., 1997) have extensively compared different sands and their sound emission capabilities.

1.1.2. Different Types of Sand Acoustic Emissions

Sand acoustic emissions can be produced in different environments, under various conditions, and thus also present distinct acoustic characteristics. The different types of sounds that emanate from these sonic sands are thus presented and compared in Table 1.1, using four parameters: the sand feature(s) where the emission can occur (beach, dune, slipface), the force or event that induces the emission, the frequency range reported in different locations and the timbre, which gives information about the differences in frequency components of the sounds. Indeed, while two sounds may have the same fundamental frequency, their timbre could differ greatly as the overtone frequencies vary, such as a guitar and a trumpet playing the same note.

Booming Emissions

The main sand acoustic emission type that fascinated travellers and natives is the booming emission, named as such due to its high amplitude and low frequency sounds. These emissions are known to occur in about 40 dune field sites around the world, such as Morocco, Oman, China and California (Han et al., 2017; Hunt and Vriend, 2010), when sand grains on the slipface of a dune avalanche downhill.

The emissions may reach up to a deafening 105 dB at the avalanche core, an amplitude comparable to that of a jet take-off around 300 meters away (Andreotti, 2012). When looking at most reports and recordings, the clear fundamental frequency ranges from 70 to 110 Hz (Andreotti, 2012). Harmonic overtones are also visible through spectral analysis (Hunt and Vriend, 2010), giving the sound a rich brassy timbre. One of the biggest points of contention within the literature, regarding the characteristics of the booming sounds emitted by avalanches has to do with the length of the sound. A team of researchers at the California Institute of Technology claims that the booming emission from avalanches is sustained and can remain audible for tens of seconds, if not minutes, after any sand movement has ceased on the slipface (Hunt and Vriend, 2010). Most authors however agree that the booming lasts until the excitation (and the slumping of sand) halts, and that no evidence of such sustained acoustic behaviour has been recorded nor published (Andreotti, 2012). Without concrete evidence, it is thus assumed that the sound does not extend after sand movement has ceased.

Burping Emissions
The second distinct type of sand acoustic emissions is the burping emission. These take place in the same dune fields as booming emissions, meaning that the sand at play is identical for both sounds (Vriend et al., 2007). This short localised sound is emitted when a portion of sand is sheared or impacted by an external source (Brantley et al., 2002; Douady et al., 2006), such as one's hand or foot. The sound generally ranges from 50 to 400 Hz (Brantley et al., 2002; Haff, 1979; Hidaka et al., 1988; Leach and Rubin, 1993), and can be described as rich and slightly noisy, as the fundamental frequency is recognisable, with a more broadband signal than the booming emission.

Squeaking Emissions
Lastly, the most common form of sand acoustic emission does not come from the desert; it is rather produced by sand from beaches all over the world, certain lake shores, like Lake Michigan, and even river banks (Bolton, 1890; Brown, 1964). The sand is often described as squeaking, as when sheared or impacted locally (similarly to the burping emission excitation), it emits a relatively high pitched sound, on the order of 1 kHz (Andreotti, 2012; Hunt and Vriend, 2010; Patitsas, 2012). The timbre of the squeaking sound can be described as somewhat noisy, with the spectral analysis showing a signal spanning a few hundreds of Hertz (Miwa et al., 1983).

Table 1.1: Comparison of the three different sand acoustic emission types and their main characteristics.

	Squeaking	Burping	Booming
Sand landform	Beach [1, 2, 3, 4, 5]	Dune field [6, 7]	Dune field [6, 7, 8, 9]
Driving excitation	Local disturbance [4, 10, 11]	Local disturbance [12, 13, 14]	Slipface avalanche [6, 7, 15]
Frequency range	1 kHz [5, 6, 14, 16]	50 Hz - 400 Hz [12, 17, 18, 19]	70 Hz - 110 Hz [10, 13, 16, 17]
Sound timbre	Noisy, broadband [4, 6]	Rich, broadband [12, 14]	Rich, narrowband with clear harmonic overtones [6, 9, 15, 20]

[1] Bolton (1890). [2] Brown (1964). [3] Humphries (1966). [4] Miwa et al. (1983). [5] Ridgway and Scotton (1973). [6] Hunt and Vriend (2010). [7] Vriend et al. (2015). [8] Van Rooyen and Verster (1983). [9] Vriend et al. (2007). [10] Criswell et al. (1975). [11] Sholtz et al. (1997). [12] Brantley et al. (2002). [13] Douady et al. (2006). [14] Patitsas (2012). [15] Dagois-Bohy et al. (2012). [16] Andreotti (2012). [17] Haff (1979). [18] Hidaka et al. (1988). [19] Leach and Rubin (1993). [20] Lindsay et al. (1976).

The differences between sand acoustic emissions and their origin can be explained by looking at the way the sound is created and identifying the demarcating characteristics of the types of sand at play.

1.2. The Physics Behind the Phenomenon

Sand acoustic emissions occur as a result of a combination of sand properties and environmental conditions, which lead to, under the right excitation, the sounds we hear. Although the actual sound emission mechanism of some of the emissions is still a heavily debated topic, the elements propitious

for the phenomenon are mostly agreed upon. Based on this classification, recording such sand acoustic emissions in other planetary environments could thus help estimate surface sediment characteristics in the context of planetary exploration.

1.2.1. Characteristics of Sonic Sands

Sonic Beach Sand

Sediment sorting is a measure of the statistical spread of grain sizes about the mean of the distribution, and thus depends on the standard deviation. Using the logarithmic φ scale, the following sorting classification of sediment, based on Folk and Ward (1957), is shown in Table 1.2.

Table 1.2: Sediment sorting classification using standard deviation expressed in the logarithmic φ unit, based on Folk and Ward (1957).

Characterisation	Standard deviation (in φ)
Very well sorted	< 0.35
Well sorted	0.35 - 0.50
Moderately well sorted	0.50 - 0.71
Moderately sorted	0.71 - 1.00
Poorly sorted	1.00 - 2.00
Very poorly sorted	2.00 - 4.00
Extremely poorly sorted	> 4.00

Based on this classification, studies (Humphries, 1966; Lindsay et al., 1976; Ridgway and Scotton, 1973) have found that squeaking sands are generally very well sorted, with a unimodal distribution, while silent beach sands are well sorted (Humphries, 1966; Lindsay et al., 1976). This trait seems to be correlated to the width of the coastal plain; wider coastal plains would provide longer periods of abrasion for the sand, leading to a more monodisperse distribution (Edwards, 2001). It remains to be seen whether squeaking beach sands occur mostly on wide coastal plains. Lindsay et al. (1976) and Sholtz et al. (1997) conclude that while size distribution and sorting does appear to be an important factor in the ability to emit sounds, certain silent sands exhibit similar size characteristics, meaning that other properties must be at play.

Another aspect related to the shape of the grains which seems to play a role in acoustic emissions is the sphericity, i.e. the degree to which the shape of grains resembles that of a sphere. When comparing silent and sonic beach sands, Ridgway and Scotton (1973) and Lindsay et al. (1976) found that the squeaking sands were slightly more spherical than their silent counterparts, which are already quite spherical. It is however difficult to quantify the exact level of sphericity, as different methods were used in those two studies to characterize the sediments. Furthermore, many other techniques exist, and generally, no unified sediment sphericity classification is agreed upon.

Using a scanning electron microscope (SEM), Sholtz et al. (1997) and Lindsay et al. (1976) identified two properties to qualify the surface of the grains: roundness and polish level. How well rounded a grain is indicates if its edges are rounded or angular, while the polish level has to do with the surface smoothness on the micrometer level. Those studies however do not make an attempt at classifying the sediments with respect to those parameters, but rather compare those qualities on a sonic sediment relative to a silent one. Based on the qualitative particle shape classification of Ulusoy (2019), further used in section 2.1.1, the grains in Figure 1.1 (and those studied in Sholtz et al. (1997)) show that squeaking beach sands are generally well-rounded to very well-rounded, more so than silent beach sands. Like the sorting of beach sand, the roundness of grains is likely correlated to the width of the coastal plain. On wider coastal plains, the sand abrades for longer periods of time, which increases the roundness of the grains (Edwards, 2001). It can also be seen on Figure 1.1 that although much more polished than silent beach sands, sonic beach sands still have small surface impact pits visible with the SEM (Lindsay et al., 1976).

Although some squeaking sands can make sounds under wet and even submerged conditions (Miwa et al., 1983), they are most acoustically effective and loud in dry conditions (Brown, 1964; Lindsay et al., 1976; Ridgway and Scotton, 1973). While the moisture content is not indicated, “dry” is usually used to describe loose and cohesionless sediment, which has been dried by the sun or an oven for a prolonged period of time. It was also shown that the more clean (free of fine dust and polluting particles)

a sand is, the louder and most effective the sound becomes (Miwa et al., 1983). This property could perhaps explain why squeaking seems to only occur at a certain distance from the shore, as described by Richardson (1919); the sand needs to be occasionally cleaned by the action of waves and tides, and dried by the sun, in order to produce emissions (Ridgway and Scotton, 1973; Sholtz et al., 1997). Thus, a balance exists between the natural cleaning of the sand and its moisture content, which explains why a beach will generally have squeaking sand only within a strip parallel to the shore.

Earlier research has indicated that lower shear strength of squeaking sand decreases its sonic ability (Hashimoto, 1951; Humphries, 1966). More recently, it has been shown that a higher shear resistance is obtained by washing the sand (Miwa et al., 1983). Perhaps this could come from the washing away of the polluting oil substances mentioned in the article. The oil could have formed a lubricating layer around the grains which could explain the lower shear resistance. When looking at the penetrative load by a rod, Miwa et al. (1983) indeed measured an increased static internal angle of friction, synonymous of increased static shear resistance, the more the sand was washed. This corresponds well with the shear box tests, which also show similar trends in angle of friction. Thus, part of the improvement in sonority could indeed come from higher shear resistance, as suggested by Hashimoto (1951) and Humphries (1966).

Although different characteristics are present, most silent beach sands seem to go through aeolian transport and erosion processes similar to their sonic counterparts, which begs the question: why are some beach sands very well-sorted and exhibit high shear resistance, compared to most other sands? For beach sand to combine the properties favourable for acoustic emission production, a few conditions must be met. Very well sorted, well rounded and somewhat polished grains are often obtained in high-energy beaches, where the wave action is high, and faster erosion of the sand grains takes place (Miwa et al., 1983). For the same grains to be cyclically eroded long enough for the favourable granulometric properties to appear, the beach's shoreline must remain about static, and no direct input of new sand particles, typically from rivers, should disrupt the refinement of the beach sand. Then, for sands to be clean, both the sea water and the sand itself must be free of polluting agents such as fine particles and oils, which can be produced by neighbouring industrial plants and general pollution (Miwa et al., 1983). Ridgway and Scotton (1973) additionally noted that sonic beaches visited on a regular basis by people can quickly lose their ability to produce sounds, as the abrasion of grains produces fine dust particles which disrupt the size distribution and mute the sand. These conditions seem to explain how squeaking sands gain their specific characteristics compared to silent beach sands.

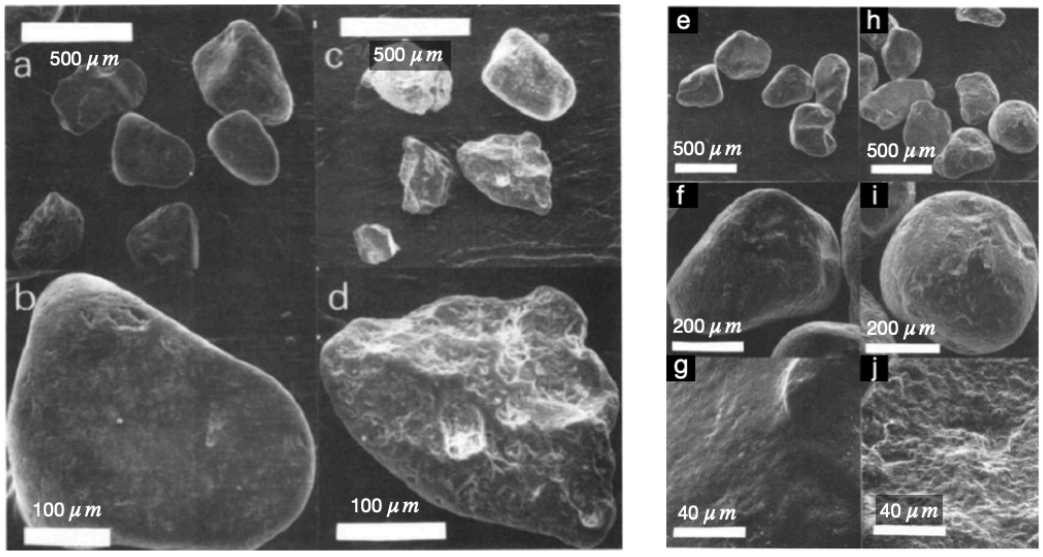

Figure 1.1: SEM of sonic and silent sand grains. On the left, squeaking beach grains (a and b) are compared to silent beach grains (c and d). The squeaking sand is notably more well-rounded and polished than the silent one. On the right, booming desert grains (e, f, g) are compared to silent desert grains (h, i, j). While sorting and sphericity seem similar, the booming sand is notably more polished than the silent one. (Lindsay et al., 1976).

Sonic Desert Sand

As mentioned earlier, booming and burping emissions are produced by the same desert sand within a dune field (Vriend et al., 2008). Although the size distribution of sand grains varies across any dune, due to the aeolian processes at play in sand transport, the sand remains generally well-sorted regardless of its geographical location in the world (Humphries, 1966; Lindsay et al., 1976; Nori et al., 1997; Van Rooyen and Verster, 1983). The average grain diameter for such sands ranges between about 180 and 320 µm (Hunt and Vriend, 2010). Adding dust, under 50 µm, to a sonic sand precludes emissions (Haff, 1986; Ridgway and Scotton, 1973). Van Rooyen and Verster (1983) noted that many desert sands exhibit similar well-sorted uniform distributions but remain silent, as illustrated in Figure 1.1 (h, i, j), and encourage looking at other properties.

Sonic desert sands generally have similar sphericity levels to that of silent ones, visible in Figure 1.1 (Lindsay et al., 1976). It is however speculated that the more spherical the grains, the more sonorous the sand is (Douady, 2016, February 18). Although not as essential as for squeaking sands, size distribution and shape still play a role in desert sands being sonic.

The surface texture of sonic desert sands differs from that of squeaking sands. The former are generally rounded, with some cases of more angular grains (Han et al., 2017; Lindsay et al., 1976), and are not necessarily very well-rounded like sonic beach sand. Then, sonic desert sands are very well-polished (Criswell et al., 1975; Lindsay et al., 1976; Sholtz et al., 1997), smooth on the 1 µm level, more so than the squeaking beach sands. This is clearly visible on the SEM images in Figure 1.1, which show the much more polished surface of the sonic grains compared to silent ones. This quality is only attainable if a certain degree of roundness has been achieved prior to polishing, as larger surface features such as angular edges are more likely to be eroded first before the much smaller surface pits. However, many desert sands go through such extended travelling and erosion, without gaining the ability to produce sound (Lindsay et al., 1976). A more recent study (Dagois-Bohy et al., 2010) points towards the presence of a layer of silts and oxides, called desert varnish, around the sand grains of the booming mega-barchan dune in Tarfaya, Morocco, making the grain surface seem more smooth and polished. Desert varnish has been discovered and studied for decades, with Engel and Sharp (1958) providing a thorough analysis of the chemical compositions of different varnishes. The main elements are generally Si, Al, Fe, Mg, Mn and water, but the formation mechanism remains uncertain (Perry et al., 2005). This coating is generally found on exposed rocks in dry, arid environments (Engel and Sharp, 1958), and not usually said to cover particles as small as sand grains. However, the chemical composition of the varnish corresponds to the elements identified by Douady (2016, February 18) in his research on the sonic desert sand coating. They suggest that unlike the sand of neighbouring smaller dunes which comes directly from the sea, the sand from this mega-barchan goes through a salt lake, where chemical reactions combining hot temperatures, water, salt and the various elements presented earlier lead to the formation of this desert varnish around the grains. Han et al. (2017) support this reasoning, by showing the presence of lakes and springs close to booming dunes in China, while encouraging more research to prove this theory. Reproducing this surface treatment in a laboratory setting has been shown to either greatly increase sonority or restore the latter in a sand which had previously been used extensively such that the layer was gone (Dagois-Bohy et al., 2010). It is possible that this rather uncommon occurrence and sojourn lead to the rarity of such sonic desert sands.

According to Sholtz et al. (1997) and Andreotti (2012), the increased shear resistance of desert sonic sand compared to silent sand, is the demarcating and critical parameter for booming to occur. Though Humphries (1966) showed that the shear resistance of one type of booming sand was significantly greater than another squeaking beach sand, it was not compared to that of normal desert sand. There is indeed a gap in the literature regarding the comparison in shear resistance of multiple sonic and silent desert sands, with resulting angle of friction values, to confirm this characteristic. Dagois-Bohy et al. (2010) also emphasize the key role of surface friction in desert sonic sand grains: similarly to the way rosin and magnesite (used to increase surface friction in string instruments and rock climbing respectively) mixed into regular silent glass beads can make them produce sounds comparable to sand acoustic emissions, the desert varnish covering the grains would increase their surface friction and allow for burping and booming emissions. This idea would also explain why repetitive shearing of sonic desert sand makes it loose its sound: the varnish erodes away, reducing the shear resistance, similar to a wheel tyre (Douady, 2016, February 18). A shear box test comparing the friction characteristics of a sonic desert sand after having lost its sound through repetitive shearing, and after restoring its desert varnish and sound, could further corroborate this argument. The reason increased grain surface friction

would lead to sand acoustic emissions is discussed in the following section.

Most studies (Andreotti, 2012; Douady et al., 2006; Haff, 1979; Hunt and Vriend, 2010) declare that this sand type must also be extremely dry to emit sounds, without a clear description of the moisture content. However, the idea is that humidity increases the cohesion forces in the sand bed which is undesirable, as it emits best when loose (Sholtz et al., 1997). This coincides with the fact that sonic desert sand is most acoustically active near the dune crest, which is where the sand dries the fastest (Sholtz et al., 1997). Only a surface layer of about 20 cm reaches the dryness level required due to sand's poor heat conducting properties. This very low humidity level thus only occurs for long periods of the year on very large dunes, as the surface layer almost always remains dry enough for emissions, compared to smaller dunes which can often only boom a few minutes over the entire year (Andreotti, 2012). This condition is another reason for the rarity of booming emissions.

Comparison & Discussion

Table 1.3 summarises the general granulometric characteristics of sonic beach and desert sands, and the favourable conditions for sound emission discussed in this section. The acoustic emission condition is often interpreted as a threshold, where sand characteristics combine to lower said threshold until a sound is emitted, with some being more critical than others (Andreotti, 2012). The sand washing experiment conducted by Miwa et al. (1983) reinforces this idea, as more favourable conditions, in this case the removal of dust and polluting particles, gradually reduce the threshold and sound is emitted with less effort. Similarly, most sonic desert dunes cannot emit booming sounds year round due to varying humidity content, although most characteristics remain the same. These examples show that sound emissions from sands can be produced when specific properties and conditions combine to lower an emission threshold.

Table 1.3: Summary of the general granulometric and surface characteristics of sonic sands, and the favourable conditions under which acoustic emissions are maximised.

	Sonic Beach Sand	Sonic Desert Sand
sorting	very well-sorted, unimodal size distribution [1, 2, 3]	well-sorted, polymodal distribution possible [2, 3, 4, 5, 6]
sphericity	high sphericity [3, 7]	high sphericity [2, 3]
roundness	generally very well-rounded [1, 3, 8]	rounded [3, 8, 9, 10, 11]
polish	more polished than silent grains, small surface pits still visible on the 1 µm level [3]	polished on the 1 µm level [3, 8, 9, 12, 13]
surface varnish	—	present [9, 13, 14], more research required to confirm relevance
moisture content	most acoustically active with low moisture content [3, 15, 16, 17], can still emit sound under water [3, 17]	very low level required [8, 16]
cleanliness	free of dust, and polluting agents thanks to wave action [7, 8, 17, 18]	free of dust [7, 19]
shear resistance	high shear resistance [2, 17, 20]	very high shear resistance [2, 8, 13, 21]
packing	—	loose [16]

[1] Edwards (2001). [2] Humphries (1966). [3] Lindsay et al. (1976). [4] Lämmel et al. (2018). [5] Nori et al. (1997). [6] Van Rooyen and Verster (1983). [7] Ridgway and Scotton (1973). [8] Sholtz et al. (1997). [9] Han et al. (2017). [10] Mazzullo et al. (1986). [11] Sharp (1966). [12] Criswell et al. (1975). [13] Dagois-Bohy et al. (2010). [14] Douady et al. (2006). [15] Brown (1964). [16] Haff (1979). [17] Miwa et al. (1983). [18] Richardson (1919). [19] Haff (1986). [20] Hashimoto (1951). [21] Douady (2016, February 18).

1.2.2. Sound Emission Mechanism

The Stick-Slip Instability

The stick-slip instability is widely used to describe the sound emission of sonic beach sands. Miwa et al. (1983) showed that silent beach sands have almost equal static angle of internal friction (the measure of how much a soil resists to a shear stress before failing and being entrained) and dynamic angle of internal friction (which describes the resistance to shear when in motion), meaning that when a load, like a pestle, is applied to them, the penetration is almost continuous. In the case of sonic beach sands, there is a noticeably larger difference between the two angles of internal friction, meaning that the load required for a static pestle to penetrate the sand increases, until it surpasses the threshold and the pestle slips through, after which the load decreases sharply due to the lower dynamic angle of friction, and so on. This step-like behaviour leads to the formation of shear bands, which would be at the origin of the sound according to the authors. Although the role of shear bands in the emission of sound has been contested by Andreotti (2004), their presence during the phenomenon (and absence with silent sand) has been observed and corroborated by the increase in the difference of the dynamic and static angles of friction of the sonic sand. This stick-slip instability, often compared to that in the singing wine glass trick, is thus generally used to explain the squeaking sounds of beach sands.

Dilation & Synchronisation

Poynting and Thompson (1909) provided an explanation for the mechanism of sound emission of sonic desert sand, based on the dilatation of sand in motion, explained by Reynolds (1885). In their model, sand grains are ideal spheres of the same size, which when sheared, move from one stable position to another by dilating the sand bed volume, as seen in Figure 1.2. The rate at which the grains move from one volume minimum to another is then equivalent to the frequency of the emitted sound. The sand avalanche surface would vibrate like the membrane of a speaker, which propagates in the air and produces sound (Andreotti, 2004; Douady et al., 2006). Andreotti (2004) adds that the well-defined sound obtained indicates that the grains must be partly synchronised, in phase; the simple rubbing of grains as first proposed by Carus-Wilson (1891) would only produce a noise, like ordinary sand. Since then, the dilation theory has been refined by Bagnold (1941), and later Andreotti (2004) and Douady et al. (2006), giving the simple shear rate equation $f = 0.4\sqrt{g/d}$, where *f* is the dominant frequency in Hz, *g* the gravitational acceleration on Earth in m.s^{-2}, and *d* the average grain diameter in m. More recently, Dagois-Bohy et al. (2012) studied the polydispersity of certain sonic sands' grain size distribution and the impact on the booming sound frequency. Grains of the same size regroup together quickly after an avalanche has started (Möbius et al., 2001; Savage and Lun, 1988), and form different layers of sand. Each layer has a constant shear rate $f = 0.4\sqrt{g/d_0}$ where d_0 is the peak in grain size diameter in m, for a specific layer, rather than the average of the total grain size distribution. These calculated shear rates then correspond to the peaks in frequency recorded. If the sand is very well-sorted like in Tarfaya, Morocco, with one peak in grain size, the booming is clear with a well-defined fundamental frequency. Multiple peaks in grain size distribution, such as the Al-Askhara dune in Oman, result in multiple clear peaks in frequency.

Multiple theories exist regarding the mechanism behind the synchronisation of the sand grains. Andreotti (2004) first proposed that the relative motion of grains excite coherent elastic waves in the

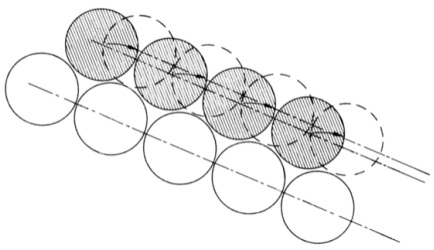

Figure 1.2: Dilatation model with idealised one-size spherical particles. The shaded ones represent the grains at rest, stable on the layer below. When sheared, during an avalanche for example, the grains move in a synchronised way, represented by the dashed circles. This behaviour causes the dilatation of the sand bed volume and leads to a vibrational mode. (Ridgway and Scotton, 1973).

avalanche layer, which in turn partly synchronise some grain collisions, which themselves reinforce the vibrations and so forth. The wave velocity of around 40 m/s has been confirmed by Vriend et al. (2015) to indeed be surface waves. However, the initial formation of such a coherent wave has been put into question (Douady et al., 2006). Douady's theory states that the increased grain to grain friction provided by desert varnish encourages synchronised grain motion rather than slipping (such as regular round glass beads for example). Although the proof of this theory could use more support, this synchronisation is visible in the fluid-like motion of the sand bed when put in motion, and the lack of slipping plates of grains, common in silent sand motion.

1.2.3. A Novel Method for Sediment Characterisation in Planetary Exploration?

As seen in Section 1.2.1, sonic sands have particular characteristics, which combine with certain conditions to produce their acoustic emissions. Because this combination of characteristics is unique and well agreed upon in the literature, this characterisation of sonic sediment could potentially be applied to planetary exploration. By recording sand acoustic emissions in other planetary environments, scientists could indeed estimate surface sediment characteristics presented in Table 1.3, such as sorting, morphology, etc. The refined shear rate equation of Dagois-Bohy et al. (2012) could also be used to approximate sediment size and distribution based on the frequency content recorded. Of course, sample collection will always be more accurate and desirable, to directly study sediment through imaging and testing, such as on Earth. Rather, this method could truly find a use in environments where such means are not (yet) available, such as on other planets. Using microphones onboard rovers and landers with other mission objectives could also prove much less costly than dedicated rovers for sediment analysis, especially in early planetary exploration phases.

This focus on sonic sediment can also lead to a better understanding of planetary surface conditions and sand motion dynamics, which would not be evident with classical sediment analysis. Desert varnish on booming sand grains occurs due to chemical reactions at high desert temperatures between water, salt and sand (Dagois-Bohy et al., 2010), meaning that from detecting booming emissions, one could deduce the presence of salt, water (or brines), and certain temperature levels on a planet's surface, all very valuable pieces of information in the context of planetary exploration. Furthermore, one could also infer from the sound, characteristics of the sand's motion dynamics, as the motion of sonic desert sand is often described as fluid-like, with grain synchronisation and little slipping. Thus, scientists could add this type of acoustic analysis to the list of observables in planetary exploration, even where rovers already study the sediments through sample collection, like on Mars.

1.3. Mars: A Suitable Host for Sand Acoustic Emissions?

It is currently unknown whether sand acoustic emissions occur on other planets, and whether sediment characterisation through acoustic analysis would be a realistic prospect. The purpose of this section is to evaluate the likelihood of these emissions occurring on Mars, which is primarily covered in granular material, and already has landers and rovers, equipped with microphones, studying its surface. This could then present the first opportunity to test this theory in the future.

1.3.1. An Active Sand Transport System

An active sand transport system is crucial for a planet to host sand acoustic emissions for different reasons. Firstly, the formation and shaping of sand, silent or sonic, comes from particle transport and erosion. Indeed, it all starts with weathering processes, where rain, heat fluxes and plants break down rocks and generate fine particles (Greeley and Iversen, 1985; Kokelaar, 1986), and volcanic eruptions, which produce pyroclastic rocks and particles ranging in size from dust to boulders (Fisher and Schmincke, 2012). Then, these small particles are entrained and transported by various media away from their source. Aeolian particle transport occurs when differential atmospheric pressure causes gas movements, or wind. The size of the transported particles depends on the planetary and atmospheric conditions present. On Earth, these aeolian processes illustrated in Figure 1.3, occur with particles smaller than 2 mm, namely sand and dust particles (Kok et al., 2012). Such transport also occurs in water, with rivers carrying weathered rock particles downstream. During their transport, particles are further eroded by the transporting medium (water or air) and by other grains when impacting one another (National Oceanic and Atmospheric Administration, 2021), which alters their shape and properties. From these processes, sand can travel and accumulate to produce various bedforms, from

coastal, lake and river beaches, to deserts and dune fields. Desert sand can come from many different places, from beaches to glacial till or river deposits (Ahlbrandt, 1979), which are then transported by wind induced processes depending on their size, as illustrated in Figure 1.3.

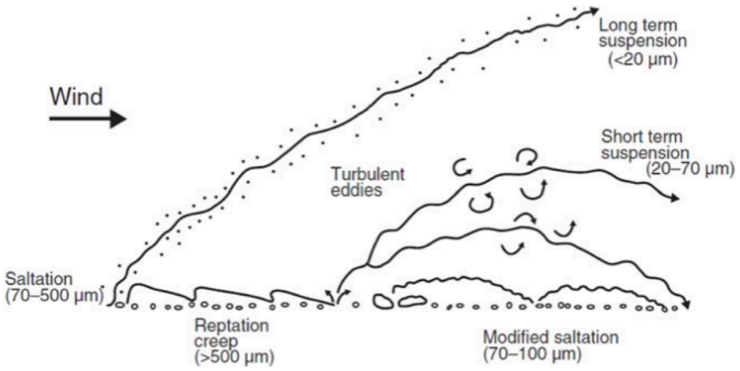

Figure 1.3: Aeolian sand and dust transport regimes. The size ranges indicated correspond to transport during moderate wind storms. (Nickling and Neuman, 2009; Pye, 1987).

The first particles to be blown by the wind are around 100 μm in diameter, when wind speeds exceed a particular fluid threshold velocity (Bagnold, 1941; Kok et al., 2012; Sharp, 1963). The sand bounces along the surface in the dominant wind direction, a process called saltation. The threshold velocity depends on the weight of the grains and the cohesive forces in the sand, both determined by the gravitational pull exerted on the sand grains (Musiolik et al., 2018). Finer sand and dust particles remain static in the first place due to their larger cohesive forces, while larger particles are too heavy for wind transport. Then, when falling back on the surface, saltating particles impact and displace other particles, giving the different modes of transport visible in Figure 1.3. This explains why grains in deserts tend to range between 70 and 500 μm. This also leads to an increasingly more monodisperse sand distribution with distance traveled (Lämmel et al., 2018). As booming dunes tend to be found downwind of their respective large dune fields (Sholtz et al., 1997), the sand grains are thus well-sorted, and free of dust. The roundness of desert grains also increases with the distance traveled from the source, due to the accumulative saltation erosion, and the preferential entrainment of more rounded grains by the wind (Mazzullo et al., 1986; Sharp, 1966), which explains the rounded nature of sonic desert sands. Similarly for sonic beach sand, wider coastal plains would provide longer periods of abrasion for the sand, leading to more rounded grains and a more monodisperse distribution (Edwards, 2001). Saltating sand particles can gain enough momentum to splash other similar sized grains, which themselves are accelerated and splash more particles, causing an initially exponential increase in saltating grains (Andreotti et al., 2010). This acts as an obstacle in the air flow, called saltation drag, which decreases the wind speed, and the consequent momentum of saltating particles until an equilibrium is reached (Kok et al., 2012). This decrease in local wind speed (which also arises from a change in surface landscape, or vegetation, rock formation, etc.) can lead to sand accumulation and dune formation (Cooke and Warren, 1973; Fryberger and Ahlbrandt, 1979).

It is now evident why a sand transport system is indispensable in creating sand, shaping and sorting it to be free of dust, and well-rounded, which are essential characteristics of sonic sand. However, one could argue that a planet which had an active aeolian system in the past but not anymore, could have already created this sonic sediment. Although this is true, an active aeolian system is needed to induce natural sand acoustic emissions, which only occur when sand grains avalanche down the slipface of dunes (while squeaking and burping emissions would require an external driving excitation). Indeed, dune avalanches and movement are a product of active aeolian transport. Though dunes can take different shapes due to multiple wind directions and patterns, this process is explained for cases where a dominant wind direction is present, such as the crescent-shaped barchan dunes, where most desert sand acoustic emissions occur. As illustrated in Figure 1.4, once an accumulation of sand gets large enough, sand grains on the stoss of the dune, or windward face, saltate past the crest onto the leeward face, or slipface, where the wind velocity is lower. Sand grains accumulate on the upper region of the slipface, which increases its slope relative to that of the windward face, giving most dunes their

characteristic asymmetrical structure. The sand accumulates in the described manner until it reaches its angle of repose, approximately 31-34° (De Vet, 2016; Hunt and Vriend, 2010), leading to the natural avalanching or slumping of a sand mass on the slipface. This combination of saltation and avalanching repeats such that dunes move with the dominant wind direction, namely transverse and barchan dunes.

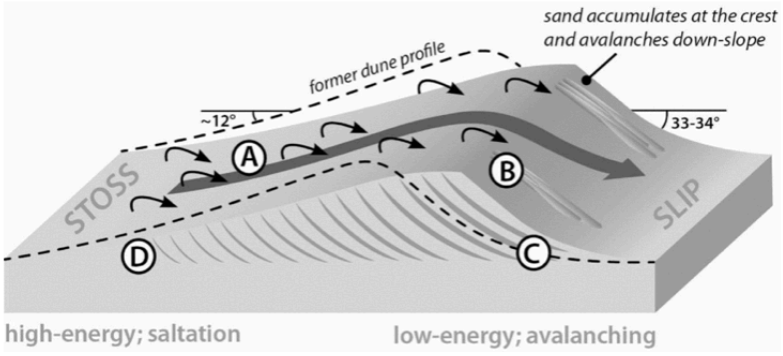

Figure 1.4: Sand transport cycle within a dune. The grains saltate across the stoss of the dune with the dominant wind direction (A), and reach the top region of the slipface, where they avalanche downslope once the angle of repose is exceeded (B). The grains are then buried cyclically, such that the dune migrates forward (C), until their saltation can start again on the stoss (D). (De Vet, 2016).

For Mars to qualify for sand acoustic emissions, it must first exhibit an active sand transport system. In 1659, the Dutch astronomer Christian Huygens was the first to identify a surface feature on another planet: the dark volcanic region of Mars, Syrtis Major. Since the early 1900s, scientists have been able to detect patterns and spots of different colours on Mars' surface seasonally shifting in position, a phenomenon interpreted in different ways. While many believed that vegetation cycles or lichens were at play, McLaughlin (1954) proposed that aeolian processes would entrain dust and volcanic particles with wind patterns corresponding to the observed colour features. This hypothesis was later confirmed when a global dust storm engulfed the planet in 1971. After it cleared off in 1972, the Mariner 9 Orbiter sent back the first satellite images of Martian surface features. It became clear to scientists that the patterns of varying position and albedo, such as streaks, indeed emanated from the erosion and deposition of wind-blown centimetre level particles (Greeley and Iversen, 1985). Furthermore, through this mission along with the Viking mission in the late 1970s, the existence of a sand sea larger than Rub Al Khali, the largest dune field on Earth, was discovered, populated with sand dunes. These discoveries already mean that some of the sonic sediments' characteristics may be present in Mars' surface material.

Although scientists discovered a large saltwater lake under Mars' south pole ice cap in 2018, and are still studying the possibility of transient liquid water traces on its surface (Martín-Torres et al., 2015), it is known that after billions of years of climate evolution and orbital variations, Mars is now very dry and devoid of abundant surface liquid water (Jakosky, 2021). As explained in section 1.2.1, sonic beach sand needs to be occasionally cleaned by the action of waves and tides, and dried by the sun, in order to produce emissions (Ridgway and Scotton, 1973; Sholtz et al., 1997), which explains the observation that squeaking seems to only occur within a strip parallel to the shore (Richardson, 1919). This would seem to indicate that though they may have existed once on Mars, squeaking sands are not present on the red planet anymore. The focus can thus shift mainly to sonic desert sands and related surface landforms.

Though it has now been stated that sand and dunes are present on Mars, as natural sand acoustic emissions require sand avalanches to occur, it is essential to discuss whether or not aeolian sand transport still takes place on Mars today. Since the early Martian missions in the 1970s, our understanding of sand and dust characteristics and behaviour on the red planet has greatly improved through more abundant and accurate data from landers and orbiters, along with the modelling of Martian aeolian bedforms and saltation processes. Some studies in the early 2000s (Malin and Edgett, 2001; Schatz et al., 2006; Zimbelman, 2000) did not find any evidence of dune migration and consequently argued that these visible landforms may have been shaped earlier in Mars' history, when its atmosphere was denser, as first hypothesised by Breed et al. (1979). This argument is consistent with both modelling

at different scales of the Martian atmosphere and rover data which agree that the weak winds present in Mars' low density environment don't generally exceed the fluid (or friction) threshold necessary for sand entrainment (Chojnacki et al., 2011; Holstein-Rathlou et al., 2010). However, unlike what was previously believed, the most recent studies looking at the evolution of surface features such as sand ripples and dunes over several months have confirmed the presence of active saltation in many areas on Mars (Bridges et al., 2012; Chojnacki et al., 2011; Fenton, 2006; Hansen et al., 2011; Horgan and Bell III, 2012; Silvestro et al., 2010), thanks to an increase in the resolution of satellite images, showing sand grain avalanches on dune slipfaces, and dune migration. These recent discoveries represent an important step in evaluating the potential of sand acoustic emissions on Mars, as sand avalanches are necessary for booming emissions. To confirm this, Musiolik et al. (2018) studied the behaviour of sand under Mars like gravity and found the resultant fluid threshold to be much lower than previously assumed, agreeing well with current global Mars dust cycle models. They suggest that anterior studies must not have accounted for the decrease in cohesive forces between grains due to the reduced gravitational pull, which ultimately renders sand entrainment more common than previously believed. Furthermore, although Martian winds are generally rather weak, local topography can lead to stronger winds in particular regions, such as the Nili and Meroe Patera, which house some of the fastest moving dunes on Mars (Davis et al., 2020). Once saltation is initiated, sand grains fall back down to the surface and impact other grains, which are consequently ejected into the air, perpetuating the saltation process. In Martian conditions, namely lower gravity and reduced atmospheric density, this impact threshold has been found to be substantially smaller than the fluid threshold (Kok, 2010a; Kok, 2010b), meaning that once initiated, saltation is likely to be sustained for long periods of time even with much weaker winds. All these elements show that Mars houses an active aeolian sand and dust transport system.

With the idea of recording sand acoustic emissions for sediment characterisation, it is also relevant to look at the frequency at which sand avalanches take place on another planet compared to Earth. Hence, dune migration rates, and thus avalanche recurrence intervals, from several places on both Earth and Mars can be compared to understand the orders of magnitude at play. Davis et al. (2020) summarise the motion of sand features (dunes and ripples) in some of the most active dune fields on Mars. In the Nili and Meroe Patera, dunes move up to 0.5-0.8 m/EY (meters per Earth Year) (Bridges et al., 2012). At Herschel Crater, a displacement of 0.1-0.6 m/EY has been recorded (Cardinale et al., 2016), while some of the fastest moving dunes reside in Hellespontus Crater, with close to 1 m/EY (Davis et al., 2020). Bridges et al. (2012) describes sand fluxes on Mars as Earth-like when looking at dunes in Victoria Valley, Antarctica, with migration rates of about 1.5 m/EY (Bourke et al., 2009). However, many places on Earth exhibit more active aeolian sand transport. Indeed, dunes in the Sahara desert in Morocco, in China's Quruq desert, and Namibia's Sperrgebiet, have been measured to migrate 15-90 m/EY (Aydda and Algouti, 2014), 9-32 m/EY (Yang et al., 2019) and 7-32 m/EY (Baird et al., 2019) respectively. The large variations come mainly from the diversity in dune size. This shows that although present on Mars, dune migration takes place at a much lesser rate (1 to 2 orders of magnitude) than on Earth, when comparing dunes of similar morphologies, due to the low density atmosphere (Bridges et al., 2012). Potential sand acoustic emissions from avalanches, consequently would occur on Martian dunes less frequently than on their terrestrial counterparts.

Furthermore, one must look at the grain flow dynamics present on Mars' dunes, as Douady et al. (2006) showed that a minimum grainflow thickness of 3 cm is required for sand acoustic emissions to be produced. Since 2015, the Curiosity rover has taken many pictures within the Bagnold dune field in Gale crater, providing the first high resolution images of an active Martian dune slipface. Cornwall et al. (2018) compared the avalanching processes on the Namib dune on Mars and a transverse dune in the very arid (Mars-like) Maspalomas dune field in Spain, an analog dune of similar size (2-4 meters in height). It was found that the grainflow morphologies on both dunes were similar, though those on the Martian dune were thinner (a maximum of 2 cm was calculated) and displaced less sediment. Although this thinness in the grainflow on Mars could appear to perhaps impede acoustic emissions from occurring, it is important to note that avalanche characteristics depend on seasonal changes and that the Curiosity images used in this study were taken during a time period with weak winds. It remains to be determined through future research whether or not the low density Martian atmosphere and thus thinner sediment grainflow on the slipface of dunes prevent booming emissions from occurring on Mars.

1.3.2. Characteristics of Martian Dunes and Sands

Knowing that Mars has an active sand transport system reveals that some regions of the planet most likely do have well sorted and rounded sediment, free of dust, which are all properties that lower the sound emission threshold. To confirm this, and to study in greater detail the likeness of Martian soils to sonic desert sand, data from different types of environments, namely the Curiosity rover (at Gale crater and the Bagnold dunes), the Mars Exploration Rovers (Spirit at Gusev crater and Opportunity at Meridiani Planum), and the Phoenix lander (at Mars' North pole), is analysed and presented in Table 1.4. Only data from Martian dune soils is described and compared to desert sonic sand in more length, due to the increased relevance for sand acoustic emissions.

Granulometry & Particle Morphology

Chojnacki and Fenton (2017) describe the sand at Gale crater as very well sorted and with a particle size generally smaller than 250 µm (Cousin et al., 2017) which fits well the characteristic of sonic desert sands. Dust particles, under 50 µm, which have been shown to negate the sound emission abilities of sonic sands (Haff, 1986; Ridgway and Scotton, 1973) and commonly found on the Martian surface, are almost completely absent in the Bagnold dunes sands (Ehlmann et al., 2017; O'Connell-Cooper et al., 2017). Similarly, soil particles at the El Dorado dune field exhibit very well sorted grains with a peak in grain size diameter at 270 µm (Cabrol et al., 2008), and a lack of dust particles. Ehlmann et al. (2017) have also noted that most grains sampled by the Curiosity rover at the Bagnold dunes are quasi-spherical, which is also the case for many sonic desert sands (and terrestrial desert sands in general). Figure 1.5 indeed shows the sand at the Namib dune in Gale crater being more spherical than a silent beach sand from Earth, and even than the booming sand of Sand Mountain, in Nevada. Sand grains from the Bagnold dunes are characterized as rounded to subrounded, with some samples of well-rounded particles, coming from the attrition of grains from recurrent saltation processes similarly to terrestrial desert sands (Ehlmann et al., 2017). It it important to note however that booming sand grains are not especially well-rounded, as is the case for sonic beach sand (Lindsay et al., 1976).

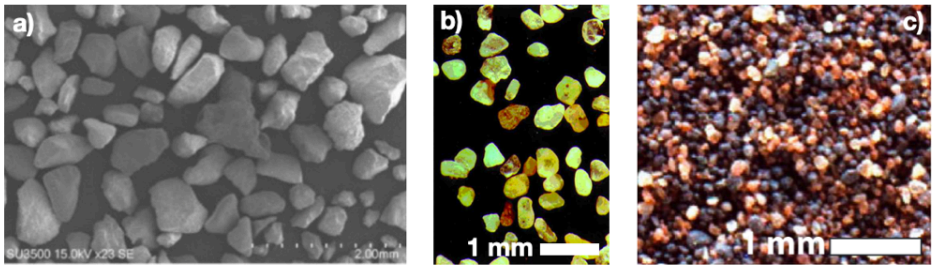

Figure 1.5: (a) Silent beach sand from Babolsar, Iran with low to moderate sphericity. (Zamanian et al., 2020). (b) Booming sand from Sand Mountain, Nevada, with medium to high sphericity. (Sholtz et al., 1997). (c) Sand from Namib dune, in Mars' Gale crater, with high sphericity. (Ehlmann et al., 2017).

Water Content & Soil Cohesion

Mars is generally described as a dry, frigid desert, which lost most of its surface water millions of years ago to space, due to climate evolution and orbital variations (Jakosky, 2021). One would thus instinctively think that the extreme dryness and loose packing required for booming, demonstrated by Haff (1979), would be found almost anywhere on the Martian surface. However, when the Viking landers studied Martian surface material for the first time, three classes of soils were identified, depending on their cohesion (Moore and Jakosky, 1989).

When analysing data from the Curiosity rover, researchers (Ehlmann et al., 2017; Leshin et al., 2013; Martín-Torres et al., 2015) found that very fine particles (< 45 µm) common on the Martian surface carry volatiles such as water, and chloride. However, when looking at the composition of sands of the Bagnold dunes, very low concentrations of water and Cl were measured compared to other Martian and Gale soils, which correspond to the lack of dust (Ehlmann et al., 2017). Consequently, the presence of fines and water content in soil affects the cohesive forces within the sand bed (Sholtz et al., 1997). Figure 1.6 compare the volatile rich soil at Rocknest which forms aggregates of sand and silts, to the silt and water depleted sand grains of the active Namib dune, which exhibit a cohesionless and loose packing.

This shows that Martian dune sand dominated by sand-sized particles, at low enough latitudes to avoid higher absorbed water and pore ice within the soil (seen in the soil at the Phoenix lander situated in Mars' North pole) (Moore and Jakosky, 1989; Shaw et al., 2009), can indeed have the necessary dryness and loose configuration, characteristic of booming desert sands.

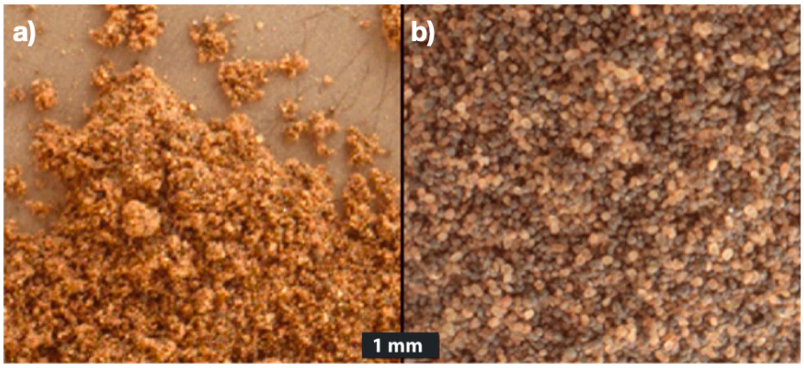

Figure 1.6: (a) Volatile rich soil at the Rocknest landform, in Gale crater, forming aggregates of sand and silts. (b) Silt and water depleted sand grains of the active Namib dune, in Gale crater, which exhibit a cohesionless and loose packing. (Ehlmann et al., 2017).

Desert Varnish

The micrometer level polish which differentiates (especially desert) sonic sands from silent ones on Earth is difficult to identify in Martian soils with the available data. Indeed, out of the three missions explored in this chapter that have studied Martian soils, the Phoenix lander is the only lander/rover to possess onboard instruments with resolution limits at the micron (Optical Microscope) and sub-micron levels (Atomic Force Microscope), necessary for this type of grain texture analysis. When looking at soil samples, the surface texture of particles varied from rough on some, to smooth and glossy on others, like the sand-sized particles seen in Figure 1.7 (a) (Goetz et al., 2010). It is worth noting that the red dust present on most of Mars' surface and at the Phoenix lander site, makes it difficult to study the surface quality of the grains in more depth, evident on the Optical Microscope images available.

As previously explained, Dagois-Bohy et al. (2010) and Han et al. (2017) have proposed that the surface quality of sonic desert grains is actually due to desert varnish, a layer of silts and oxides that forms on sand grains that temporarily reside in nearby salt lakes. After repetitive grain collisions from aeolian transport (and accelerated during sonic sand experiments where the sand is sheared repetitively), the layer wears off and the sand indeed becomes soundless (Dagois-Bohy et al., 2010). Though the existence of this varnish on Martian grains in unknown, available data from the Martian surface can be used to determine the presence or absence of the varnish's key ingredients, especially salt and water. Salt is known to exist on the surface of Mars in the form of perchlorates (Hecht et al., 2009; Martín-Torres et al., 2015). The latter decrease the freezing temperature of water and can absorb atmospheric water vapor, to then dissolve and form saline solutions called cryobrines (Fischer et al., 2019; Möhlmann and Thomsen, 2011; Zorzano et al., 2009). Though it is important to note that this process, depends on atmospheric temperatures and relative humidity, and thus on the latitude, seasonal changes and time of the day, these transient saline solution could perhaps provide the necessary conditions for the formation of desert varnish on Martian dune grains. Lastly, it remains to be seen whether the Earth-like daytime temperatures reached at mid to low Martian latitudes would be sufficient to induce the chemical reactions needed for the varnish to be formed, and the grains to be dried. However, at Meridiani Planum, a surface coating has been identified on some of the millimetre-sized granules and larger cobbles (Weitz et al., 2006) visible in Figure 1.7 (b), and has been hypothesised by Soderblom et al. (2004) to emanate from interactions between perchlorates and small amounts of moisture at the very surface of the soil. This does show that such chemical processes could be a reality on the Martian surface, and that desert varnish could thus perhaps form on Martian sand grains.

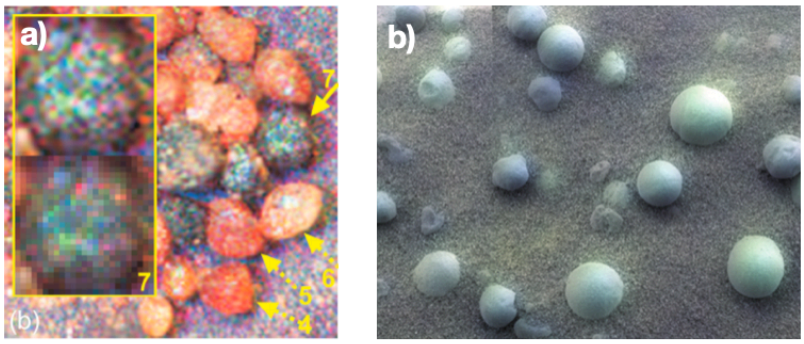

Figure 1.7: (a) Sand-sized particles at Phoenix lander site show high sphericity. The image is 500 µm wide. (Goetz et al., 2010). (b) Example of soil at Meridiani Planum, where dust and fine sands are mixed with larger, blue millimetre-sized granules, referred to as blueberries. Although no scale is provided, the larger spherical grains are around 3 mm in diameter. (Weitz et al., 2006).

Shear Resistance of Surface Material

The shear resistance of sonic desert sand has been found to be higher than that of silent sand of similar size and shape (Humphries, 1966; Sholtz et al., 1997). Similarly to the independence between gravitational acceleration and angle of repose (Atwood-Stone and McEwen, 2013; Chen et al., 2015; Karapiperis et al., 2020; Nakashima et al., 2011), results regarding the effect of reduced gravity on shear resistance are conflicting. Alshibli et al. (2003) and Karapiperis et al. (2020) find that in both numerical modelling and experimental results, the peak friction angle increases with decreasing gravity, suggesting that the latter allows grains at the shear band to dilate more, thus slightly increasing the shear resistance. On the other hand, Ng (2013) and later Zou et al. (2015) state that the impact of varying gravity on shear resistance is negligible, and thus that the dilating behaviour of granular matter does not depend on gravity. Marshall et al. (2018) support this conclusion, finding no difference in friction angles and angles of repose under Martian gravity and confining pressure, noting that the varying results and conclusions from different studies might come from the selection of different granular soils which can vastly differ in mechanical properties. The Phoenix lander and Mars Exploration Rovers have also estimated the shear resistance of Martian soils using wheel scuffing and trenching, resulting in an average angle of internal friction of 38°±5° (Shaw et al., 2009) and 30-37° (Sullivan et al., 2011) respectively. Considering the uncertainties associated to the estimation methods, and because factors like dust and moisture content can have an impact on the friction angle, it can only be concluded that the shear resistance of Martian soils is in the range of that for terrestrial sands, sonic or not.

Comparison to Terrestrial Sonic Sand

Table 1.4 summarises the general characteristics and properties of different Martian soils using data from the Curiosity, MER and Phoenix missions, and compares them to the favourable conditions and properties for terrestrial sonic sands, seen in Table 1.3. Firstly, it is evident that the highly spherical and rounded to subrounded shape of Martian sand-size particles, is similar to that of terrestrial sonic sands, and especially desert booming sand which can also be subrounded to angular (Lindsay et al., 1976). This is due to the long history of aeolian transport and erosion of sand and dust particles on Mars. Then, the particles range from being very poorly sorted in regions of composite soils, to very well sorted in bedforms like dunes, where the surface layer of dust present on most of Mars' surface along with larger granules and pebbles are absent. These dune soils are thus the closest to terrestrial sonic sands, in terms of granulometry and morphology. Furthermore, the similitude extends to their low moisture content and loose packing due to their well-sorted, dust depleted distribution. Indeed, most Martian soils are covered in dust, which often carries and deposits water on Mars (Ehlmann et al., 2017), increasing the grain-grain cohesion. This makes most Martian soils unlikely to emit any acoustic emissions, leaving only low latitude, well-sorted, dry sand from bedforms like dunes or ripples as potential Martian sonic sands. Data regarding the rest of the characteristics is more sparse, and thus inconclusive and speculative. Indeed, the polish of particles has only been studied at the Phoenix lander site, where some grains showed glossy surface textures. It is unknown however if this characteristic is present on other soils and especially on bedform sands.

Table 1.4: Summary of the general granulometric and surface characteristics of terrestrial sonic sands and different Martian soils.

	Sonic Beach Sand	Sonic Desert Sand	Bagnold Dune Soil (Curiosity rover)	Gusev Crater Soils (Spirit rover)	Meridiani Planum Soils (Opportunity rover)	Martian Arctic Soil (Phoenix lander)
sorting	very well-sorted, unimodal size distribution [1, 2, 3]	well-sorted, polymodal distribution possible [2, 3, 4, 5, 6]	very well-sorted [7, 8]	El Dorado dune field: very well-sorted, other non-dune soils: very poorly-sorted [9, 10]	overall poorly sorted, fine sand and blueberry granules well-sorted [11]	poorly sorted, with mix of dust, sand and gravel particles [12, 13]
sphericity	high sphericity [3, 14]	high sphericity [2, 3]	high sphericity [15]	high sphericity [10, 16]	high sphericity sand and blueberry granules, low sphericity pebbles [11, 17]	high sphericity [12]
roundness	generally very well-rounded [1, 3, 18]	rounded [3, 18, 19, 20, 21]	rounded to subrounded [15]	rounded to subrounded [10, 16]	rounded to subrounded dust, sand and granules, angular larger particles [17]	generally subrounded [12]
polish	more polished than silent grains, small surface pits still visible on the 1 µm level [3]	polished on the 1 µm level [3, 18, 19, 22, 23]	no available data	no available data [10]	no available data [10]	smooth, glossy surface on some grains [12]
surface varnish	–	present [19, 23, 24], more research required to confirm relevance	existence unknown, elements needed present [8, 15, 25], transient surface brines present [26, 27, 28]	–	surface coating on granules and cobbles [17], combination of perchlorates and moisture hypothesised [11]	perchlorates, brines and subsurface ice water present [29], but temperature likely too low [24]
moisture content	most acoustically active with low moisture content [3, 30, 31, 32], can still emit sound under water [3, 32]	very low level required [18, 31]	water depleted, dry [15, 25]	low in dust depleted soils, like ripples and dunes [33]	low in dust depleted soils, like ripples and dunes [33]	absorbed water and pore ice [34]
cleanliness	free of dust, and polluting agents thanks to wave action [14, 18, 32, 35]	free of dust [14, 36]	free of dust [15]	El Dorado dune field: free of dust, other non-dune soils: surface dust layer [9, 10]	some dust present, less than at Gusev crater [11]	dust present [12]
shear resistance	high shear resistance [2, 32, 37]	very high shear resistance [2, 18, 23, 38]	no available data	$\phi = 30° - 37°$ [33], similar to Earth sands, sonic or silent	$\phi = 30° - 37°$ [33], similar to Earth sands, sonic or silent	$\phi = 38° \pm 5°$ [34], similar to Earth sands, sonic or silent
packing	–	loose [31]	cohesionless, loose [15]	weakly cohesive in well-sorted bedform soils (dune, ripple), cohesive in dusty soils [17, 33]	weakly cohesive in well-sorted bedform soils (dune, ripple), cohesive in dusty soils [17, 33]	crusty to cloddy cohesion [34, 39]

[1] Edwards (2001). [2] Humphries (1966). [3] Lindsay et al. (1976). [4] Lämmel et al. (2018). [5] Nori et al. (1997). [6] Van Rooyen and Verster (1983). [7] Chojnacki and Fenton (2017). [8] Cousin et al. (2017). [9] Cabrol et al. (2008). [10] McGlynn et al. (2011). [11] Soderblom et al. (2004). [12] Goetz et al. (2010). [13] Leer et al. (2009). [14] Ridgway and Scotton (1973). [15] Ehlmann et al. (2017). [16] Greeley et al. (2006). [17] Weitz et al. (2006). [18] Sholtz et al. (1997). [19] Han et al. (2017). [20] Mazzullo et al. (1986). [21] Sharp (1966). [22] Criswell et al. (1975). [23] Dagois-Bohy et al. (2010). [24] Douady et al. (2006). [25] O'Connell-Cooper et al. (2017). [26] Martín-Torres et al. (2015). [27] Möhlmann and Thomsen (2011). [28] Zorzano et al. (2009). [29] Hecht et al. (2009). [30] Brown (1964). [31] Haff (1979). [32] Miwa et al. (1983). [33] Sullivan et al. (2011). [34] Shaw et al. (2009). [35] Richardson (1919). [36] Haff (1986). [37] Hashimoto (1951). [38] Douady (2016, February 18). [39] Moore and Jakosky (1989).

Then, the presence of desert varnish on Mars is also speculative, as the required chemical elements, salt and water do exist on the Martian surface, but sparsely, although the surface coating on larger granules and cobbles at Meridiani Planum has been hypothesised to come from such chemical reactions (Soderblom et al., 2004). Finally, the shear resistance of granular material on Mars can only be described as Earth-like, whether the sand is sonic or not.

It can be concluded from this table that most favourable conditions for sand acoustic emissions, such as the granulometric and morphological characteristics along with the cohesionless, water-depleted packing, are present in bedform soils, such as the sands of the Bagnold and El Dorado dune fields. The surface varnish, which increases the shear resistance and polish level of the grains, is the only element which may or may not occur on Martian sands. Studying the sub-micrometer surface texture of sand grains of Martian dunes (like the Bagnold dunes) would be required to answer this question.

1.3.3. Sound Emission and Propagation in Martian Atmosphere

In the previous section, certain Martian dune soils were shown to exhibit similar characteristics to sonic desert sands on Earth. If these sediments were to be sonic as well, how would their booming emissions sound like? Would rovers be able to detect them? Those questions are answered by looking at sound emission on Mars, and the attenuation of frequencies in the range of desert sand acoustic emissions.

Acoustic Impedance

A sound is created when a pressure wave propagates through a medium. The acoustic impedance measures the opposition of this medium to the propagation of the pressure waves. There are different types of acoustic impedances, depending on the application. In the case of a spherical wave propagating from a point source in free-field conditions, which is assumed for sounds produced on the surface of Mars, the wave can be approximated as a plane wave far from the source. The resultant characteristic impedance z_0 is expressed as follows (Hiremath et al., 2021):

$$z_0 = \rho_0 c_0$$

where ρ_0 and c_0 are the density and speed of sound of the medium respectively. Based on the surface atmospheric conditions of Mars (Petculescu and Lueptow, 2007; Williams, 2001), the characteristic impedance of Martian air is around two orders of magnitude smaller than that of Earth, which translates to the same sounds being approximately 20 dB weaker on Mars, without propagation losses (Maurice et al., 2022; Petculescu and Lueptow, 2007).

Assuming the emission mechanism of sonic sands is independent of the atmospheric pressure level, the loudest natural booming emissions on Mars would reach around 85 dB at the source, as those on Earth commonly approach 105 dB at the avalanche core (Andreotti, 2012). Irrespective of propagation attenuation of sound waves, the lower acoustic impedance on Mars would thus already greatly reduce the sound amplitude of sand acoustic emissions, and perhaps decrease their detection range for surface rovers. However, as the emission mechanism of sonic desert sands is based on grain synchronization within the sheared layer, it remains to be seen whether the phenomenon is actually independent of intergranular air pressure or not. This could have repercussions on the sound amplitude of booming emissions on Mars at the avalanche core.

Sound Attenuation

When pressure waves propagate through a medium, they are attenuated by various factors. As natural sand acoustic emissions are produced on the ground, hemispherical propagation is assumed. The hemisphere of propagated sound grows with the distance to the source r in m, while the power P of the emitted sound in W is a constant. This leads to geometrical attenuation (also called wavefront spreading), where, for a simplified case, the sound intensity I in W.m^{-2} is given by:

$$I = \frac{P}{2\pi r^2}$$

Because the human ear can sense a very wide range of pressures, a logarithmic scale in dB is commonly used to describe the pressure levels of different sounds with respect to a reference level, which corresponds to the human ear's hearing threshold. Thus, the relation between sound pressure level (*SPL*) and sound power level (*SWL*) can be expressed as follows (Attenborough, 2014):

$$SPL = SWL - 8 - 20\log(r)$$

The *SPL* of a sand acoustic emission thus reduces due to wavefront spreading by around 28 dB at a distance of 10 m, 42 dB at 50 m, and 48 dB at 100 m, both on Mars and Earth.

Other attenuating factors affect the propagation of sound waves, and are represented by the absorption coefficient α (where α [dB.m^{-1}] $= 8.686\alpha$ [m^{-1}]) (Simons and Snellen, 2021), such that:

$$SPL = SWL - 8 - 20\log(r) - \alpha r$$

Atmospheric absorption is the absorption of acoustic energy by a gas, and thus differs on Mars and Earth. Classical absorption describes the processes where gas molecules vibrate and collide with each other, leading to contact friction dissipating part of the energy into heat, which also leads to temperature fluctuations in the gas, and further heat dissipation (Morse and Ingard, 1986; Williams, 2001). The following expression gives the resultant classical absorption coefficient α_{v+T} in m^{-1} (Bass and Chambers, 2001):

$$\alpha_{v+T} = \frac{\omega^2}{2\rho_0 c^3}\left(\frac{4}{3}\mu + \frac{K(\gamma-1)}{\gamma c_v}\right)$$

with the angular frequency $\omega = 2\pi f$ in Hz, the local atmospheric density ρ_0 in kg.m^{-3}, the speed of sound c in m.s^{-1}, the shear viscosity coefficient μ in N.s.m^{-2}, the thermal conductivity K in W.m^{-1}.K^{-1}, the heat capacity ratio γ, and the heat capacity at constant volume c_v in J.K^{-1}. Using the surface atmospheric conditions of both Mars and Earth, the resultant classical absorption is greater on Mars than on Earth by almost two orders of magnitude (Petculescu and Lueptow, 2007).

The other component of atmospheric absorption is relaxation absorption, which describes the conversion of a part of the acoustic energy of the signal into vibrational and rotational molecular energy. Consequently, the relaxation time corresponds to the time the system takes to get back to equilibrium. The sound absorption related to this phenomenon would be maximised when the period of the passing pressure wave approaches the relaxation time of the gas it travels through (Williams, 2001). These processes have however been much more difficult to model, especially in gas mixtures such as planetary atmospheres, resulting in discrepancies between models (Maurice et al., 2022). In Figure 1.8, some models of the total atmospheric absorption are compared to the recent in situ acoustic attenuation measurements on Mars by the Perseverance rover, presented in Maurice et al. (2022), which shows that models by Bass and Chambers (2001) and Petculescu and Lueptow (2007) seem the most accurate. Classical absorption on both planets dominates for frequencies above 5-10 kHz, below which relaxation absorption plays a large role. In field measurements unfortunately do not yet reach frequencies below 1 kHz, which would further corroborate or disprove the models in the range where molecular relaxation dominates the acoustic absorption. However, these models can still be used to approximate the atmospheric absorption of sand acoustic emissions on Mars. As explained in section 1.2.2, the frequency f in Hz of a booming emission is dependent on the gravitational acceleration g on the planet in m.s^{-2}, and on the peak in grain size diameter d_0 in m, such that $f = 0.4\sqrt{g/d_0}$ (Dagois-Bohy et al., 2012). For the gravitational acceleration on Mars $g_M = 3.72$ m.s^{-2}, and a hypothetical sand with a

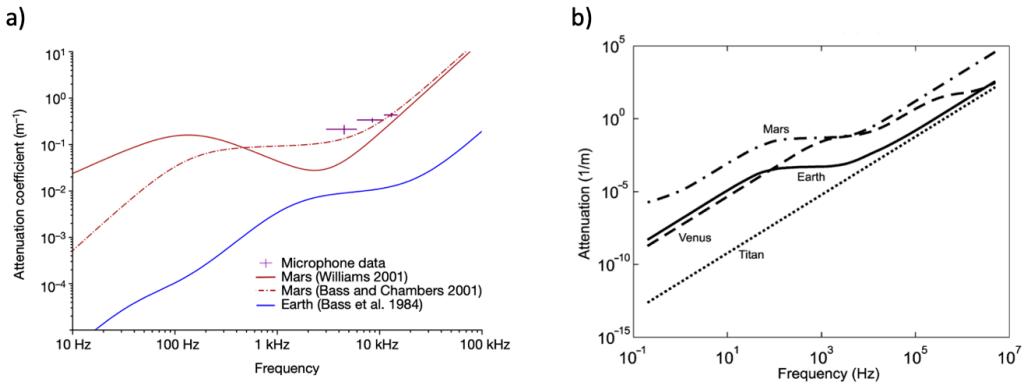

Figure 1.8: (a) Comparison between models of acoustic absorption at the surface of Mars, and Perseverance in situ measurements (Maurice et al., 2022). (b) Absorption coefficient as a function of frequency at the surface of Earth, Mars, Venus and Titan (Petculescu and Lueptow, 2007).

grain size diameter peak at around $d_0 = 200$ µm (which fits the granulometry of sonic desert sands and Martian dune sands), the corresponding booming frequency is estimated at 55 Hz. Based on the models of Bass and Chambers (2001) and Petculescu and Lueptow (2007), such a sound would be attenuated by around 0.18 dB.m^{-1}. The *SPL* of a natural sand acoustic emission on Mars would thus be reduced due to atmospheric absorption by around 1.8 dB at a distance of 10 m, 9 dB at 50 m, and 18 dB at 100 m.

When combining the estimated effects of geometrical attenuation and atmospheric absorption, the *SPL* of a Martian booming emission, assumed to be around 85 dB at the source, would be reduced to around 55 dB at 10 m, 35 dB at 50 m, and 20 dB at 100 m. Hence, sand acoustic emissions on Mars could potentially be detected by microphone equipped rovers up to almost 100 meters away from the avalanche flows responsible. It should be mentioned that other factors such as turbulence effects and meteorological events also affect sound propagation on Mars (Davidson, 1977; Henley and Hoidale, 1973; Maurice et al., 2022), and the resultant *SPL* levels of booming emissions. However, this section works only to give an estimate of these sound attenuation phenomena, and thus simplifies real conditions.

1.4. Research Questions & Thesis Outline

It was shown that most elements required for sand acoustic emissions seem present in the Martian dune sediment analysed and that the acoustic environment would likely allow rovers to measure such emissions using onboard microphones from a distance. What remains uncertain and will thus constitute the thesis' objective, is how interstitial air pressure within the sand bed affects the vibrating membrane-like emission mechanism of sonic desert sand, described in section 1.2.2. This idea is explored in the project, by inducing silent and sonic desert sand shear flows under a range of pressure levels down to Mars-like pressure. The following research questions can then be answered to reach the thesis goal:

1. How does the atmospheric pressure affect the sound emission of silent sand grains impacting one another? How does it compare with acoustic impedance models?

Before studying the sounds produced by sonic sand, one must first establish how the air pressure level within the experimental setup affects the sound emission of "normal" sounds (whose emission mechanisms do not depend on grain packing and synchronized motion). The results can then be validated using a simplified acoustic impedance model.

2. How do time domain characteristics, such as the acoustic pressure and signal duration, of sand acoustic emissions change with the air pressure level, independent of sound attenuation?

3. How does the frequency content of sand acoustic emissions change with the air pressure level, independent of sound attenuation?

The signal of sand acoustic emissions at different pressure levels can then be analysed in the time and frequency domains to evaluate how the burping sounds change with air pressure, compared to models, and hypothesize how the emission mechanism is affected.

Chapter 2 describes the methodology of testing, experimental setups produced, and metrics used, to answer the research questions formulated above. Then, Chapter 3 presents and discusses the results of the experiments, proposing some interpretations to the behaviors observed. Chapter 4 provides the experiment limitations met and recommended improvements for future work, before concluding and answering the research questions in Chapter 5.

2

Materials & Methods

2.1. Sonic Sand Acquisition

The first part of the project consisted in actually acquiring desert sonic sand, to then be able to test it. As listed by Hunt and Vriend (2010), this type of sand is only found in specific desert areas on Earth, and is thus not available in Europe. For this reason, the first approach was to attempt to create synthetic sonic sand, similarly to Dagois-Bohy et al. (2010). Although this part of the project was unsuccessful, the steps and process are described in section 2.1.1, to show how delicate the variables are in obtaining a working synthetic sonic sand. Then, section 2.1.2 takes a look at the natural sonic sand that was ultimately obtained, to replace the ineffective synthetic sonic sand originally produced. Both sediment types are compared to illustrate the driving characteristics of sonic sand.

2.1.1. Producing Synthetic Sonic Sand

The production of synthetic sonic sand was based on the research of Dagois-Bohy et al. (2010), and further help and descriptions from S. Douady (personal communication, March 18, 2022) and Douady (2016, February 18). The base sediment used as a starting point in this part of the project is sand from Bedaf, Netherlands, provided by SJ de Vet. It was used here as it was believed to be well sorted and quite spherical, which, as explained in section 1.2, are key components in the sonic sand phenomena. Thus, the steps were divided into three main categories, namely particle morphology, granulometry and chemical treatment, which together address all essential characteristics of desert sonic sand, presented in Table 1.3.

Particle Morphology

The morphology or shape of sand particles has generally been estimated by image analysis and qualitative comparison to 2D geometries (Altuhafi et al., 2013; Sochan et al., 2015). While new, much more complex analytical methods have recently arisen, such detailed analysis goes past the scope of this project. Furthermore, the available studies that have described sonic sand grains have done so using a qualitative approach. Thus, a similar characterisation method is used to describe the sand in this project. Indeed, as shown in Figure 2.1, the grains in microscope images (here of the beach sand used) are compared to a commonly used classification of particle shape by sphericity and roundness (Ulusoy, 2019). After a grain by grain evaluation of several samples, it could be inferred that around 15% of the grains had high sphericity, 50% medium sphericity and the rest, around 35% low sphericity. This sand was thus overall of medium sphericity. Based on this classification, it is rather difficult to differentiate between a well-rounded and rounded particle. However, it can be said that around 50% of the grains are rounded to well-rounded. The rest is separated into about 30% of sub-rounded particles, and 20% of sub-angular grains. Based on this approach, this batch of coastal sand is sub-rounded to rounded, and of medium sphericity. When comparing that to the shape characteristics of desert sonic sand, presented in Table 1.3, and depicted in Figure 1.1, it is apparent that this source of coastal sediment is slightly less rounded and spherical.

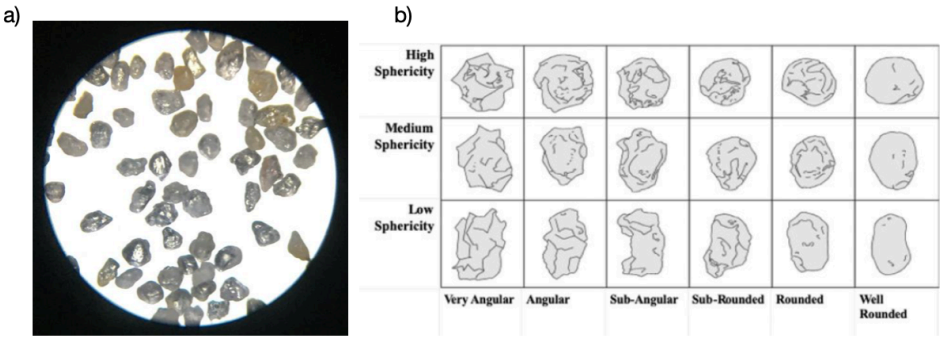

Figure 2.1: (a) Microscope image of coastal sand from Bedaf, Netherlands, used as base sediment for synthetic sonic sand experiment. (b) Particle shape classification by sphericity and roudness for microscope imaging assessment. (Ulusoy, 2019).

Granulometry

The granulometry of a batch of particles is a measure of its grain size distribution. In section 1.2.1, sonic sands are shown to exhibit at least a well-sorted distribution, which can even be polymodal for some sonic desert sands. To verify the granulometry of the test batch of coastal sand, a sieve analysis was performed. This procedure consists in passing a batch of sediment through a sieve shaker, which is comprised of multiple sieves of gradually decreasing mesh sizes that are mechanically vibrated at around 100 Hz in order for the particles to separate into their respective size range. As explained by W.S. Tyler, a leading manufacturer of sieve shakers, the amount of time the sieve shaker is in motion is determined by first performing a sieve analysis starting at 5 minutes and, using the same sediment batch, incrementally increasing the running time until the differences in final size distribution between analyses are under 1% (Tyler, 2023). Using this method, the duration used for the sieve analysis was 15 minutes. For the mesh size of the sieves, a range of 10 sieves with an opening diameter between 63 µm, the limit between dust and fine sand, to 0.9 mm, were selected, along with the bottom container that collects the finest particles. Firstly, the sieves and container are weighed while empty. Then, after placing the sand on the top sieve with the largest openings, the sieve shaker is sealed and turned on. After 15 minutes of vibrational motion, each sieve is removed and weighed whilst holding the sediment particles. The weight of the soil at each size bin is then obtained by subtracting the weight of the empty sieves from the combined weight. Finally, the weight ratio of the particles per size bin over the total batch weight is calculated. Three sand batches of 500 grams were analysed with this method to increase the accuracy of the study. The grain size distribution of this beach sand is plotted in Fig 2.2.

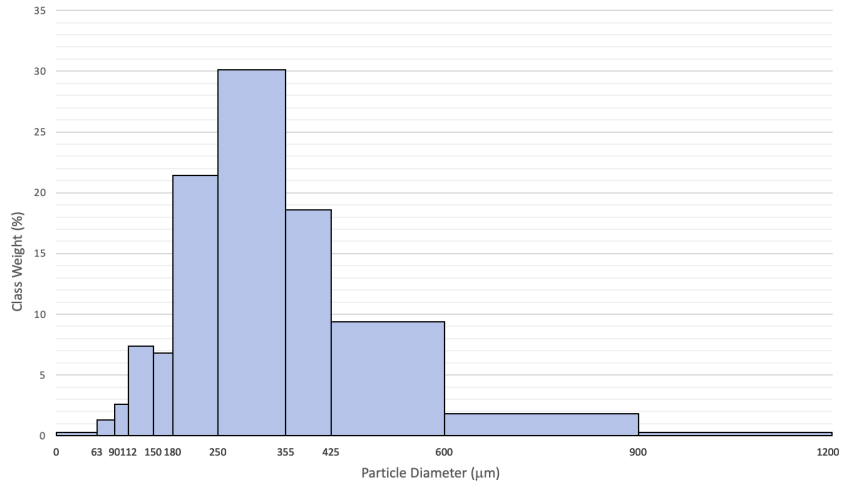

Figure 2.2: Particle size distribution of silent beach sand used for synthetic sonic sand production, from sieve analysis.

An Excel package called Gradistrat was used to analyse the grain size distribution of the sediment of interest. This program takes the values of the sediment mass per size bin obtained through sieving

or laser granulometry, input by the user, and calculates statistical metrics such as the mean, sorting, kurtosis and other relevant properties of the distribution at hand. It also uses methods of Folk and Ward (1957) to give physical descriptions of the granular material based on the statistics obtained, such as the sorting classification in Table 1.2. Using this program, the tested sand was described as moderately well sorted, with a mean size of 293 µm. While the mean grain diameter fits within the range of sonic desert sands, the distribution should be tighter to coincide with the well sorted sonic sediment. To achieve this, the extremities of the sand's distribution should then be reduced or removed. The limits were thus arbitrarily set such that all grains below 112 µm and above 425 µm were discarded from the samples. This resulted in a well sorted sand with a similar mean grain diameter as the original, and also without particles smaller than 63 µm, which preclude sand acoustic emissions.

Chemical Treatment

With the particle morphology and granulometry analysed and modified to be in the range of sonic desert sands, the last step resides in the formation of desert varnish on the grains. This aspect of sonic desert sand characteristics is by far the most uncertain and least reported on, with only the research team led by S. Douady asserting that the surface varnish provides added friction for the grains to roll over one another without slipping, which enhances synchronisation. With their successful attempt at creating a sonic sediment based on glass beads (Dagois-Bohy et al., 2010; Douady, 2016, February 18), by focusing on the three main pillars followed in this section, namely particle morphology, granulometry and desert varnish, and the fact that no research has emerged since to disprove this theory, the idea of desert varnish being necessary for desert sonic sand production is followed.

However, an important obstacle in trying to form desert varnish on the sand grains in the laboratory was the unavailability of data and information on the matter. While Dagois-Bohy et al. (2010) do touch on this, the steps to recreate the varnish are not precisely described, and the targeted sediment was worn sonic sand (which had lost its singing abilities through extensive shearing) and not a naturally silent granular material. Furthermore, the other, albeit unofficial source on the matter, is a conference talk by S. Douady from the same research team (Douady, 2016, February 18), with a slight difference in the process description. As explained in section 1.2.1, the goal is to reproduce the chemical reactions that occur in desert salt lakes where sonic grains would attain their desert varnish. The theory states that when water is evaporating from the salt lakes, the chloride and sodium from salt become more aggressive, and dissolve silica, magnesium and other minerals from nearby decomposing rocks. As the evaporation continues, the silicates and oxydes are deposited onto the sojourning sand grains in a thin clay-like paste until the newly coated grains are completely dry. With the desert varnish formed, the dry sand grains are then transported away by the wind and form the rare booming desert dunes.

Based on the literature and these researchers' information (Dagois-Bohy personal communication, December 2, 2021), a laboratory protocol was developed. The first step consisted in mixing the sieved sand samples with a saturated salt solution. Regular desert sand obtained from L. Geeven, with grains of slightly more various compositions (unlike the quartz dominant coastal sediment used as the base, visible in Figure 2.1), was then reduced to dust and added to the mixture to provide some minerals required for the varnish. Additional aluminium shavings were incorporated into the mix, as they were

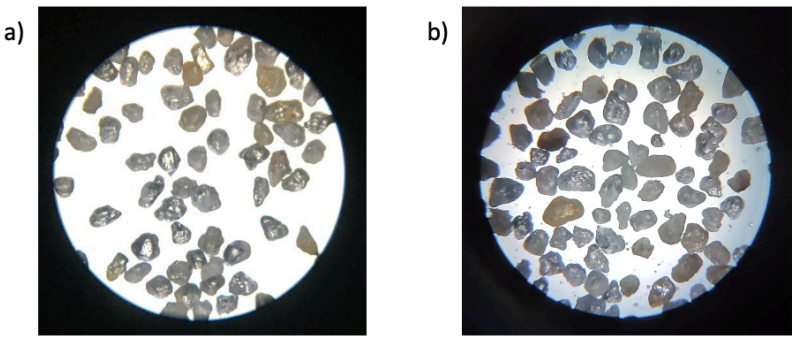

Figure 2.3: (a) Microscope image of original coastal sand used for synthetic sonic sand experiment. (b) Chemically treated coastal sand for desert varnish deposition.

also shown to provide minerals found in the desert varnish. The second step consisted in leaving the mix in a laboratory oven at 80°C for 72 hours to recreate desert-like conditions for the chemical reactions to take place, and for the sand mixture to be completely dried. This step was repeated 4 times. The last step consisted in first washing the concoction to remove the salt, dust particles, and metallic shavings, to then once again dry the resultant sediment in the oven at 80°C for 72 hours. This step was also repeated 4 times. The final sediment was passed through the sieve shaker once to ensure no unwanted dust particles were left behind. The obtained sediment is compared to its original form through microscope imaging in Figure 2.3. From this figure, it is unclear whether desert varnish was successfully deposited onto the grains' surface; some grains do look slightly more opaque and smoothed than the original more glassy quartz grains, as shown by Douady (2016, February 18), but most grains still look very similar to their original form.

Sound Test

A simple method often used in the literature to rapidly test if a sand sample is sonic or not, is to place a layer of at least 5-10 cm of sediment in a jar or bottle, and shaking the recipient side to side or up and down (Andreotti, 2012; Haff, 1979). Other than the regular trickling sound of sand grains, a resulting burping sound will be emitted if the sediment is indeed desert, or in this case synthetic sonic sand, and vibrations are felt through the fingers holding the recipient.

When sound testing the sediment obtained through chemical treatment, no emission resulted from the motion of the jar, which indicates that the sand grain characteristics present did not allow for grain synchronisation in the sheared layer and subsequent acoustic emissions. In hindsight, slightly more rounded and spherical grains could have helped to decrease the sound emission threshold. However, the main issue resides in the lack of a clear desert varnish deposition on the grains. The theory is that the mixture produced was lacking the variety of minerals required for the coating. Indeed, sediment from a source much closer to a rock weathering location, such as a river bank, should have been used instead of the regular desert sand, because the latter most likely did not contain the minerals of interest in high enough quantities, compared to the former. The reason is that most minerals erode into very fine particles much faster than the very resistant quartz particles, which is why river bank sediment closer to where rocks pieces are weathered would still present these minerals while most much older desert sands do not as much. This highlights the sensitivity of sonic desert sand characteristics and exposes an opportunity for future research to fill-in the blanks in the current body of literature on this topic.

2.1.2. Finding Natural Sonic Sand

After the unsuccessful attempt at producing synthetic sonic sand in the laboratory, multiple researchers in the field of sand acoustic emissions were contacted to inquire about the availability of natural sonic sand used in their past experiments. S. Douady who has explored this phenomenon in great depth and previously helped with the synthetic sonic sand production process, agreed to provide some natural sediment he had left in his laboratory in Paris. The sand comes from the Al-Askhara double barchan dune in Oman, which is known to be one of the most sonic desert sand dunes, and was also used by Dagois-Bohy et al. (2012) for their laboratory avalanche experiments. The sand grain characteristics are thus presented and compared to the ineffective synthetic sonic sand to show what is believed to be the critical parameters missing.

Particle Morphology

Similarly to the silent coastal sand in section 2.1.1, the morphology of the sonic sand from Oman was determined using microscope imaging, to get a general understanding of the shape and geometry of such sonic grains and what differentiates them from silent ones. The sphericity and roundness of the sonic grains in Figure 2.4 can also be classified using Figure 2.1 (b). After a grain by grain evaluation of several samples, it could be inferred that around 30% of the grains had high sphericity, 50% medium sphericity and the rest, around 20% low sphericity. This sand overall exhibited medium to high sphericity. When looking at the roundness of the particles, close to 50% of the grains are well-rounded, with a smooth opaque surface texture. The rest is separated into about 20% of rounded particles, 20% of sub-rounded grains, and the remainder 10% sub-angular. Based on this approach, this batch of sonic desert sand is rounded to well-rounded, and of medium to high sphericity. When comparing that to the shape characteristics of the silent coastal sand in Figure 2.1 (a), it can be concluded that the sonic

sediment is more spherical and rounded than the silent sand used. It is indeed common for any desert sand to be more spherical than regular beach sand (Lindsay et al., 1976), as longer aeolian transport has given the grains a more spherical shape. The increased roundness however, is certainly a trait from the desert varnish clearly visible in the microscope image, giving a lot of the grains the smooth, white to orange texture. The coating covers any irregularities on the grain surface making those grains very well-rounded, while the rest of the grains, similar to those from the silent beach sand used, are glassy quartz grains, whose desert varnish has probably already been eroded due to previous testing by Dagois-Bohy et al. (2012).

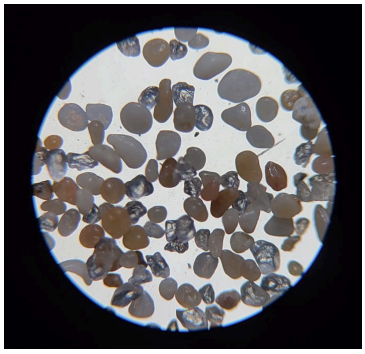

Figure 2.4: Microscope image of desert sonic sand from the Al-Askhara double barchan dune, Oman.

Granulometry

A sieve analysis was not necessary for the grain size distribution of the sonic desert sand from Oman, as it was obtained based on Dagois-Bohy et al. (2012), and plotted in Figure 2.5. The greater number of size bins between 0 and 400 µm used for the analysis of the Oman sand compared to that of the silent beach sand in section 2.1.1 (constrained by the equipment available), results in a more precise grain size distribution graph, with different peaks.

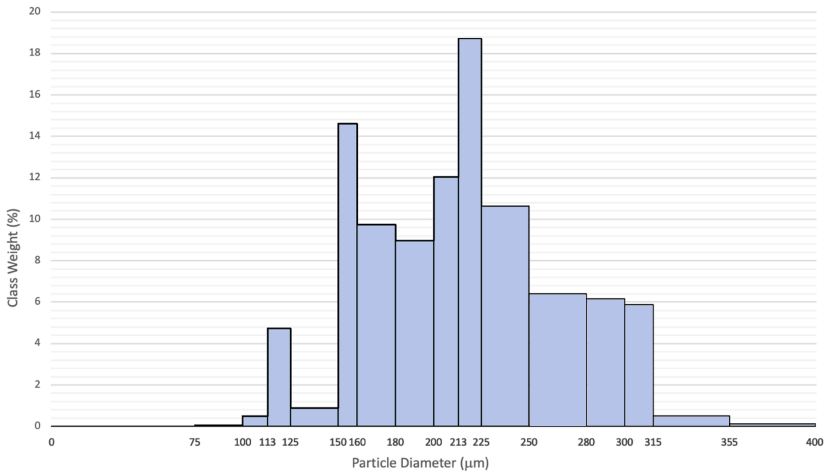

Figure 2.5: Particle size distribution of sonic desert sand from Oman, used for experiments, based on Dagois-Bohy et al. (2012).

Similarly to the silent beach sand, the Excel package Gradistrat was used to analyse the grain size distribution of the Oman sonic sand. The latter was described as well sorted, with a trimodal distribution, which fits the sonic desert sand characteristics described in section 1.2.1. Importantly, the sonic sediment is also devoid of particles below 75 µm, or dust.

Sound Test

Once again, the same sound test as in section 2.1.1 was performed to test the sonic sand from Oman. After placing the sediment in a jar, the shaking motion induced clear low frequency burping emissions,

with additional vibrations felt in the hand holding the recipient. As described by Douady et al. (2006), an emission threshold is here apparent based on the acceleration of the jar motion. Indeed, under a certain shear induced in the sand bed, no emission is produced. This is due to the minimum sheared layer thickness required for a sand acoustic emission to be produced (Andreotti, 2012; Douady et al., 2006). Regardless of the direction in which the jar is shaken, the sand grains synchronize and create a sound before coming to a rest.

Flowability
As previously mentioned in section 1.2.2, the theory of the grains synchronising to form a vibrating surface layer that creates a sound similarly to a speaker membrane, still needs further corroboration to be widely accepted. However, this trait can be observed when paying close attention to the sheared surface layer's motion when shaking a jar with sonic desert sand. A clear shear layer can be identified, within which a synchronization of grains rolling one over the other can be seen, without any slipping. This gives an overall fluid-like motion to the entire sand bed, similarly described by Bagnold (1941) and Humphries (1966), almost devoid of any slipping and irregular plate motion found in ordinary sand. This observation strongly goes in the direction of the desert varnish theory by Dagois-Bohy et al. (2010), and the idea that the varnish provides added friction between the grains to not slip, like a tyre to a wheel. The lack of this motion in the attempted synthetic sonic sand when placed in motion also coincides with the clear absence of desert varnish deposition visible in the microscope images.

2.2. Experimental Vacuum Chamber Setups & Methodology

2.2.1. Sound Production Methods & Equipment

In the past, there have been many types of experiments to study the topic of sonic sands (Andreotti, 2012; Dagois-Bohy et al., 2012; Douady et al., 2006; Hunt and Vriend, 2010). From those in a laboratory setting, two in particular presented interesting advantages considering the constraints of vacuum chamber experiments, and the fact that only a limited amount of sonic sand was available. This section explains how they are adapted to answer the research questions and fit the project.

Shaking Jar Experiment
The first kind of experiment used in this project is based on the shaking jar or beaker test as Haff (1979) called it, whereby sonic sand is placed in a jar and shaken to induce sand acoustic emissions. The resultant sound frequency has been shown to decrease with increasing the sand layer present in the jar (Kilkenny et al., 1997; Leach et al., 1999). No data exists regarding the dependence of the frequency on the jar radius, but from simple testing, it is evident that decreasing the jar radius increases the frequency, until a limit radius of around 60 mm, where the sheared sonic sand layer doesn't have enough space to create the sound when shaken side to side. In another laboratory experiment, Douady et al. (2006) also showed that the greater the velocity at which sonic sand is displaced, the higher the frequency emitted, which can also be applied to the shaking jar experiment. As the goal is to measure the impact of low pressure environments on the sound emission mechanism, which the emitted frequency components can give information about, it is important to remove as many external variables as possible that could affect the frequency spectrum. Thus, all the measurements are taken with the same sand layer thickness, inside the same recipient. The experiment was performed by manually shaking the container. To measure how this human factor affects the results, the jar motion is monitored during testing using a sensor discussed in section 2.2.2.

Now that the original experiment is defined and the variables understood, it must be modified to introduce the component of the low pressure environment. This is done by replacing the jar by a small vacuum chamber that can be shaken side to side after having reduced the chamber pressure using a vacuum pump. Figure 2.6 (a) shows the 1 l vacuum chamber, with a radius of 90 mm and a height of 180 mm. It is made of stainless steel to resist the vacuum conditions during use, and comes with a 1.5 cm thick polycarbonate lid that sits on a silicone gasket. It is also equipped with an analog vacuum gauge, and an intake air filter which is key for this experiment in order not to get sand grains aspirated into the vacuum pump, which would damage it.

This smaller scale experiment is useful because after repetitive testing and shearing, the desert varnish on the surface of sonic desert sand grains erodes and the sand loses its acoustic properties. It is thus advantageous to use small amounts of sonic sand to preserve this limited resource. This

experiment is performed using the desert sonic sand, and regular silent beach sand. The latter is used to determine the general frequency spectrum of regular sand sounds when sheared, and to understand how the lower air pressure affects the creation of those sounds. These results can then be compared to those with the sonic sand to isolate the affect of low interstitial air pressure purely on the sound emission mechanism of sonic sands.

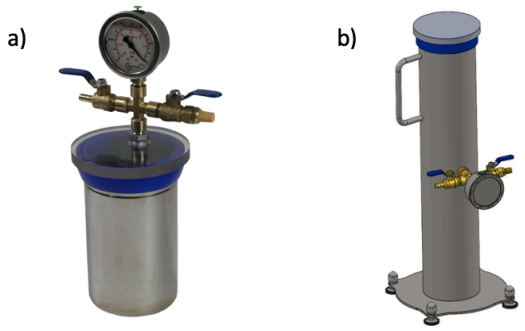

Figure 2.6: (a) 1 l vacuum chamber for shaking jar experiment. (b) Long 14.8 l vacuum chamber for laboratory avalanche experiment.

Laboratory Avalanche Experiment

The second type of laboratory experiment used is based on the laboratory avalanche setup by Dagois-Bohy et al. (2012) and Dagois-Bohy et al. (2010), which consists in using a 2 m long by 40 cm wide channel inclined at the angle of repose (31-34°) and releasing desert sonic sand down the slope to record and study the booming sound produced. With this setup, they were able to recreate the booming sound heard in the field for 3 seconds. Due to the limited sediment available for this project, it is not possible to achieve such extensive booming sounds which can only occur with a minimum avalanche thickness of around 2-3 cm (Andreotti, 2012; Dagois-Bohy et al., 2012). Instead, the sand produces short burping emissions at the end of the slope as the sand thickness inevitably increases. The avalanche channel is oriented at the same angle for each test to ensure that the sand motion and resultant sound frequency remain consistent.

Similarly to the shaking jar experiment, the laboratory avalanche is adapted such that the air pressure in and around the sand bed is decreased. This is done by replacing the channel by a long vacuum chamber that can be tilted to the angle of repose after having reduced the chamber pressure using a vacuum pump. Figure 2.6 (b) shows the 14.8 l vacuum chamber that was purchased for this purpose, with a radius of 97 mm and a height of 500 mm. The remaining equipment (lid, gauge, etc.) is identical to that with the 1 l vacuum chamber.

The main difference with the original experiment lies in the way the sand avalanche is produced. The setup in the Dagois-Bohy et al. (2012) experiment has a gate at the beginning of the channel that holds the sand back, until it opens which releases the sediment, creating the avalanche. Such a setup within a vacuum chamber is much more complex to achieve, as the gate would have to be remotely operated. Thus, to mimic such a gate effect that releases the sand all at once, the sand is first placed inside the vacuum chamber, which is then closed and tilted such that most of the sand is on the side of the chute that represents the top of the dune slipface. The chamber is then left in a horizontal, lying down position, with most of the sediment on one side. The testing can then begin once the vacuum chamber is tilted at the angle of repose and most of the sand still concentrated on one side can flow down in an avalanche-like motion. Finally, this experiment is also performed using both the desert sonic sand, and the regular silent beach sand, to identify the sole impact of low interstitial air pressure on the synchronisation of sonic sand grains and thus on the sound emission mechanism of the sonic sediment. This experiment also brings the added benefit that it better reproduces natural sediment grain flow on the slipface of dunes compared to the shaking jar type experiment.

2.2.2. Sensors

Accelerometer

As the frequency spectrum of sand acoustic emissions depends on the shearing velocity (Andreotti, 2012), small variations in the manually induced chamber motion may lead to differences in the produced sounds. While the initial proposition was for a machine or actuator to create the motion, which would then be perfectly reproducible and invariant, this solution proved too difficult and costly. Instead, a simpler option was selected in the form of an accelerometer attached to the chamber. When the chamber is shaken manually, the accelerometer is used to monitor the consistency of the motion across measurements. A selection is made post-testing, where outlier tests in the motion data are discarded. The acoustic signals with the closest acceleration data can then be compared, hence minimizing the uncertainty from the experiment's inherent variability. The accelerometer is also used in the laboratory avalanche experiment, to ensure that the motion of the vacuum chamber from its initial horizontal position to its final 35° angled position remains mostly unchanged throughout the measurements. The data selection criteria used in both experiments are further described in section 2.3.3.

The accelerometer used is the ADXL326 which is a 3-axis analog sensor, which can thus measure the chamber's motion in all directions. The specified sensitivity is then used to convert the voltage readings into usable acceleration data. The accelerometer is attached to the top of the vacuum chamber's polycarbonate lid, in a fixed position during all testing.

Microphone

A microphone is used to measure the acoustic signals produced by the sonic and silent sediments in the experiments. The sensor is placed inside the vacuum chamber rather than outside. Not only does the vacuum chamber block out most of the outside noise, but this also avoids having to consider the signal interference of the vacuum chamber walls and lid if the microphone were outside. As a result, the microphone must have a hole in its membrane for the pressure on both sides to equalise when the air pressure is lowered, to prevent it from being damaged. A simplified trade-off is performed in Table 2.1 to select between a wired and wireless microphone setup. Though the wired microphone involves a setup modification in the form of a hermetic seal connector and fitted hole in the chamber lid, its advantages regarding the unlimited battery life, minimal volume inside the chamber and lack of transmission interference, make it the right choice for this project.

Table 2.1: Trade-off between wired and wireless microphone.

	Setup Modification	Power Source	Space	Interference / Attenuation
Wired ✓	Manufacturing of jar lid hole + Hermetic connector	Unlimited	Only microphone	None
Wireless	None	Few hours	Microphone + Transmitter + Battery	Attenuation from transmitter to receiver distance + Interference from jar material

The microphone model selected was the Sonion 8010T. Its cylindrical shape gives it a flat frequency response between 150 Hz and 10 kHz, meaning that the signal of a sand acoustic emission produced during testing is uniformly translated across frequencies. At 2.56 mm in diameter and 3 mm in length, it takes minimal space within the vacuum chamber and does not interfere with the rest of the setup elements. It also has a compensation hole on the membrane to equalise the pressure on both sides when the air pressure is lowered during experiments. Finally, this microphone offers high sensitivity (-33.5 dB re 1 V/Pa in the 150 Hz - 10 kHz range) compared to similar models. As explained in section 1.3.3, the acoustic impedance at low pressure levels decreases which inherently brings the amplitude of an acoustic signal down (even for very short distances without much sound propagation attenuation). The high sensitivity microphone is thus useful to still be able to measure the acoustic signal at low pressure levels. The specified sensitivity is then used to convert the voltage readings into usable acoustic pressure data, to analyse the signals.

Setup Modifications

The microphone type selected presents some characteristics which require modifications being brought to the vacuum chamber setup. Firstly, as mentioned in the microphone trade-offs, a hermetic seal connector is necessary to ensure the electrical connections at the pressure interface, while preventing any leakage of air. The selected pin-pin connector is illustrated in Figure 2.7. It offers six pins on each side, which is sufficient for the microphone's output, power and ground connections, along with one additional pin each, for redundancy. As pictured in Figure 2.7 (c), female dupont crimp connectors are used to connect the wires to the hermetic seal connector's pins, instead of the commonly used solder joints, due to their reliability and sturdiness under motion and vibration.

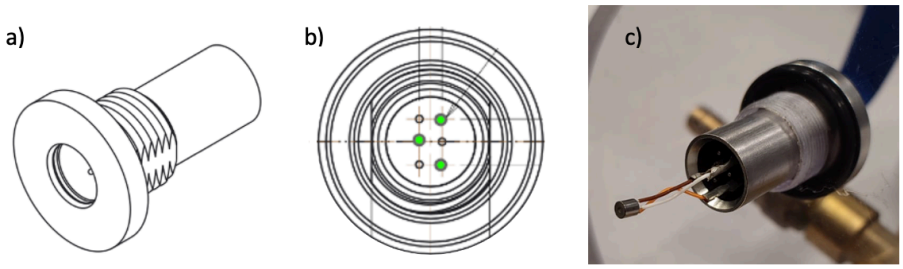

Figure 2.7: (a) Orthographic type view of hermetic seal connector. (b) Bottom view of hermetic seal connector, with six pins for electrical connections. The three pins colored in green depict the used pins for the microphone's output, power and ground connections. (c) Hermetic seal connector fitted into chamber lid, with microphone connected.

Because the sand grains were in direct contact with the chamber walls when put in motion and creating the sound, a large part of the signal measured by the microphone came from the sound propagating directly through the walls of the vacuum chamber. As the goal is to study the impact of low pressure air on the sound emission mechanism of sonic sand, any noise coming from sound propagating through any other medium but the air inside the chamber is undesirable. Identifying and removing the signal component belonging to the sound propagating faster through the solid walls in post-processing could not be achieved due to the very short sand to microphone distance. For the shaking jar experiment, the sand is thus placed in a smaller container hung inside the vacuum chamber using six radially distributed strings attached to the walls, and taped for stability, as shown in Figure 2.8 (a) and (b). The resultant signal measured is much closer to levels expected from the decreasing acoustic impedance. The jar radius threshold mentioned in section 2.2.1 was however passed, and the sonic sand didn't produce any sound when shaken side to side. The motion was thus converted to an up and down shake, which gave enough space for the sand grains to synchronise and produce the desired sound.

As depicted in Figure 2.8 (c) and (d), for the laboratory avalanche experiment, two sets of four radially distributed foam blocks are fitted between the inner container and vacuum chamber to provide a stable position for the sand chute, whilst greatly dampening the sound propagated through the walls of the vacuum chamber. The sand is weighted such that 500 g of sediment is used for all tests. Furthermore, an important variable that greatly impacts the sound produced by avalanching sediment, sonic or not, is its initial position in the inner container before tilting the vacuum chamber to the angle of repose. Thus, transparent material is employed at the visible end of the inner container (where the sand avalanches from), such that before every test, the vacuum chamber is tilted until the sand visibly reaches a pre-defined level on that end of the chute. Once this is achieved, the vacuum chamber is orientated at the angle of repose, the sand avalanches, and the sound is recorded. Figure 2.8 (e) shows the front view of the inner container fitted into the laboratory avalanche vacuum chamber, with the transparent material exposing the sediment. The marked rectangle in black represents the level the sand is adjusted to before every measurement.

2.2.3. Data Acquisition Device & Software

The data acquisition (DAQ) device used to record the data measured by the sensors in the setup is the NI 9234 module fitted into an NI CompactDAQ chassis. This module offers four input channels, each able to acquire data at rates reaching 51.2 kS/s simultaneously. For this project, the microphone output takes up one of the input channels, while the accelerometer the remaining three, one per spatial

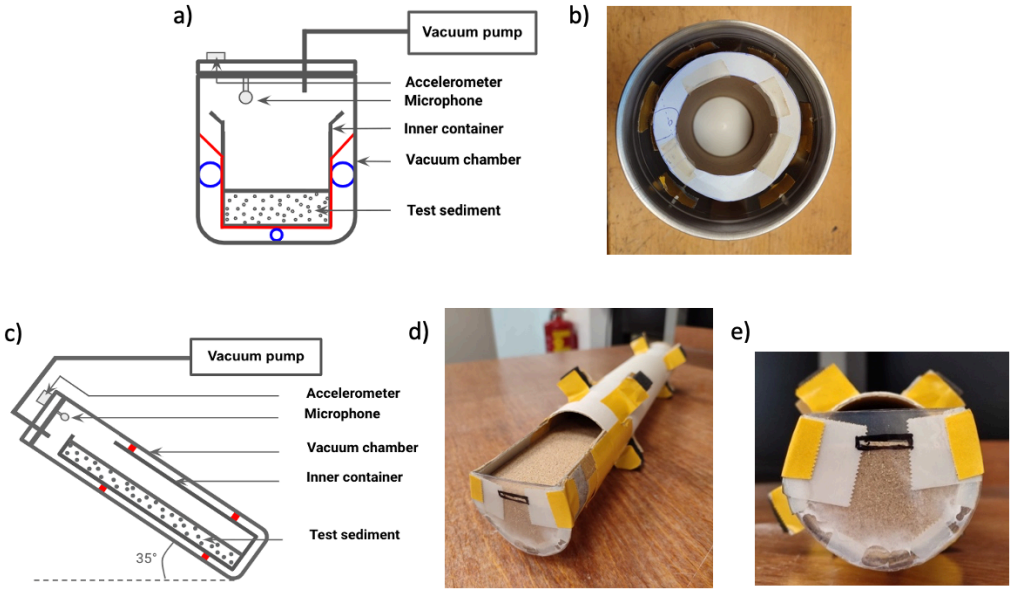

Figure 2.8: (a) Sketch of modified shaking jar experiment setup to avoid sound propagation through vacuum chamber walls. The red lines represent the radially distributed strings that hold the inner container in the air. The blue circles represent tape pieces that add stability to the inner container. (b) Top view of modified shaking jar experiment setup. (c) Sketch of modified laboratory avalanche experiment setup to avoid sound propagation through vacuum chamber walls. The red squares represent foam blocks that fixate the inner container and dampen the sound transmission through the vacuum chamber walls. (d) Orthographic type view of filled laboratory avalanche inner container. (e) Front view of filled laboratory avalanche inner container.

dimension. According to the Nyquist theorem, the sampling rate required to accurately reproduce a signal must be at least twice as large as the highest frequency of interest (Nyquist, 1928). For the accelerometer data, the frequency of the motion is very low, of the order of 5 Hz, and any DAQ device can thus accurately record and reproduce the signal. However, the entire audible frequency range should be accurately represented to study the sound produced by sand when put in motion. Thus, the sampling rate must be larger than the Nyquist frequency - here, twice the upper hearing limit of 20 kHz - equating to 40 kS/s, which is achievable with the NI 9234. Finally, this module also applies anti-aliasing filters which stop any frequencies above the Nyquist frequency from being misrepresented and converted to frequencies in the range of interest.

The DAQ device is connected to a computer, where a LabVIEW program stores the acquired data into binary format files. LabVIEW is a graphical programming software commonly used in applications related to control systems and data acquisition, among others. A graphical interface built for live visualisation of the acquired data is used to monitor the microphone and accelerometer's performance.

2.2.4. Testing Protocol

Common Steps

First, the sonic and silent sediment are to be tested at eight different chamber pressure levels ranging from Mars-like pressure to ambient pressure. The analog vacuum gauge in the setup (see Figure 2.2.1 (a)) has ticks in bar with negative numbers between 0 and -1, which must be subtracted from the ambient pressure of 1013.25 mbar to get the corresponding chamber pressure. The eight pressure levels for the measurements are thus fit on this scale, and tested in the following ascending order: 13.25 mbar, 63.25 mbar, 113.25 mbar, 213.25 mbar, 413.25 mbar, 613.25 mbar, 813.25 mbar, 1013.25 mbar. This series of pressure levels gives an opportunity to look at how sand acoustic emissions and their emission mechanism evolve with decreasing the intergranular air pressure, not just at Mars level. This opens the door to a potentially broader understanding of the topic, and recommendations for future work. The duration of each measurement is set at four seconds, which gives enough time to initiate the LabVIEW program, and manually induce the vacuum chamber motion.

Then, the greater the number of measurements per pressure level, the more the possible outliers in the data can be identified and not skew the results. However, repeatedly shearing sonic sand leads

to a loss in singing properties (Dagois-Bohy et al., 2012; Douady, 2016, February 18). A balance must thus be found. For the silent sand, the characteristics of the sound created when put in motion (in either experiments) largely depend on the way the grains impact one another, which is always slightly different from one shearing event to another due to the inherent chaotic nature of sand grain motion. However, when variables like the sand quantity and motion are controlled, the sound produced remains very consistent. Thus, a total of 10 measurements are taken per pressure level. For the sonic sand, whose burping sound depends on the coherent synchronization of sheared grains and is thus a lot more difficult to characterise and control than regular grain to grain sounds, 20 measurements are taken at every pressure level.

It was mentioned in section 1.2.1 that after repetitive shearing of sonic desert sand, a loss in sound is observed, hypothesized to come from the erosion of the desert varnish layer covering the grains. It is therefore also important to measure this variable by testing the sonic sand at ambient pressure after each pressure level. Thus, after the measurements at 13.25 mbar, the air is introduced back into the chamber, and five new measurements are taken. This is repeated for each pressure level, to capture how much, if at all, sand deterioration plays a role in the evolution of the sonic sand emissions along the experiments.

Measurement Definition

The shaking jar experiment consists in a singular continuous up-down motion of the chamber, illustrated in Figure 2.9. A measurement is taken when this motion is induced once, starting and ending at rest. The acceleration values to create the sound are large enough such that the sand moves as far upwards as possible, as in Figure 2.9 (b), but not too large which would eject the sand out of the inner container. The burping sound is emitted during the downwards motion where the sand grains roll down the created slope, as seen in Figure 2.9 (c).

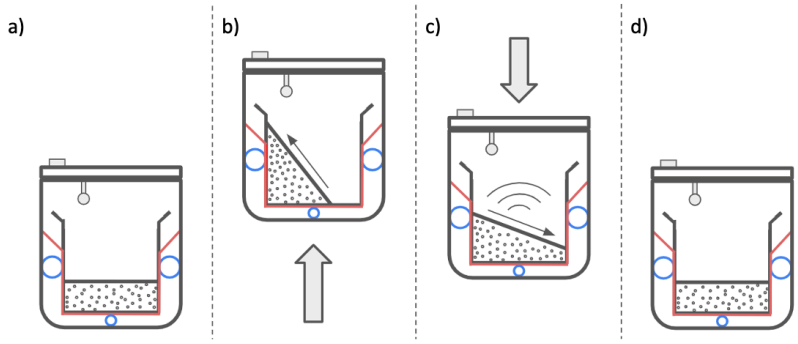

Figure 2.9: Up-down vacuum chamber motion in shaking jar experiment. (a) Starting position at rest. (b) Upwards motion such that sand layer angle increases past angle of repose. (c) Downwards motion where sand grains roll onto one another and burping emission is produced for sonic sand. (d) Final position at rest.

For the laboratory avalanche experiment, the first step is to tilt the vacuum chamber in order to accumulate the tested sand on the side of the container which will represent the brink of a dune, where the sand avalanches from. A line on the transparent end of the inner container (where the sand avalanches from) marks the level the sand must reach before each measurement, as depicted in Figure 2.8 (e). Then, the vacuum chamber is placed in a horizontal starting position, at 0°, illustrated in Figure 2.10 (a). A single measurement consists in rapidly tilting the vacuum chamber to a 35° angle from horizontal, slightly past the sand's angle of repose, to get all the sand grains flowing down the chute and maximize the sound produced, such as in Figure 2.10 (b). In order to constrain the starting and final vacuum chamber positions (and consequently the 35° angle discussed), foam blocks are fixated onto the workbench used during the experiment: two foam blocks delimit the starting position, and the third is attached to the back of the workbench such that the vacuum chamber cannot rotate further than the 35° position desired (see Figure 2.10).

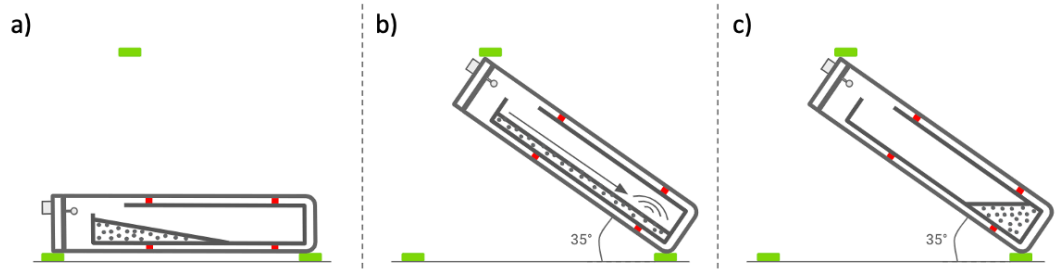

Figure 2.10: Vacuum chamber motion in laboratory avalanche experiment. (a) Starting horizontal position with sand grains already accumulated on "dune brink" side. (b) Vacuum chamber rapidly oriented at 35° angle such that sand grains avalanche down the chute, and burping emission is produced for sonic sand. (c) Final position after sand avalanche has stopped. The green rectangles represent blocks of foam fixated onto the workbench used during experiments, to constrain the vacuum chamber's initial horizontal and final 35° positions.

2.3. Data Processing of Measurements

2.3.1. Pre-Processing Raw Data

The data from the experiments is acquired by the DAQ device and stored using LabVIEW into .tdms format files. Using the npTDMS Python package, the data is retrieved and formatted into simple matrices. From there, the accelerometer and microphone data is processed and converted into usable data with specific units. Some further filtering is applied to the microphone data to remove some setup-related noise.

Unit Conversion and Zero Centering

The raw accelerometer data is composed of a series of voltage values per axis. The first step consists in removing the DC offset present in each series, such that the accelerometer at rest is represented by 0 V values in all three directions. Then, the accelerometer's sensitivity is used to convert the voltage values into acceleration data. For the ADXL326, the average sensitivity is specified at 57 mV/g, at a 3 V input. As the sensitivity is ratiometric and the chip operates at 3.3 V, it must multiplied by the ratio of 3.3 / 3, giving a sensitivity of 62.7 mV/g. Using this parameter, the acceleration data is obtained in the unit g, standing for Earth's gravitational acceleration. The absolute value of the motion data is taken, as the direction of acceleration is not of interest as will be seen further in section 2.3.2.

Similary to the accelerometer data, the DC offset present in the microphone data is subtracted from the signal to avoid any complications during further signal processing and analysis. Then, the microphone sensitivity is used to convert the voltage readings into acoustic pressure values in Pa. For the Sonion 8010T, the sensitivity between 150 Hz and 10 kHz (in which sand acoustic emissions and much of silent sand sound are contained) is constant, specified at -33.5 dB re. 1V/Pa. This unit can be converted into mV/Pa, which can then allow for the simple transfer to acoustic pressure. The sensitivity used is then 21.13 mV/Pa.

Identifying Motion Induced Noise

After the pre-processing steps, some tests were carried out to make sure the setups were performing correctly. Sonic sand was placed inside the shaking jar vacuum chamber setup, and the whole was shaken. When converting the microphone data back into .wav audio files, sub 50 Hz noise which did not come from the sand, was identified in the signal. It then became apparent that this noise came from two sources. First, the microphone put in motion leads to some sub 20 Hz noise in the signal. Then, the fit between the vacuum chamber's air manifold and lid was not perfectly tight (though the vacuum level was not compromised), which led to slight movement and noise under motion. As sand acoustic emissions in the setups used reach a minimum frequency of approximately 160 Hz however, these sources of noise importantly did not contaminate the frequencies of interest. A high-pass Butterworth filter with a 100 Hz cut-off frequency is used to show in Figure 2.11 the difference between the total signal obtained in (a) and that only coming from the sand sound in (b).

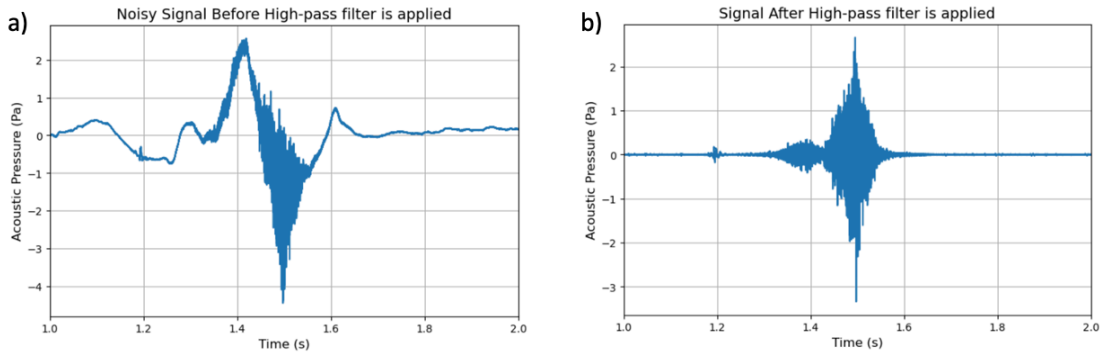

Figure 2.11: Comparison between (a) raw noisy signal on the left, and (b) signal after high-pass filter is applied, on the right.

2.3.2. Metrics Definition

Motion Metrics

The vacuum chamber motion in the shaking jar experiment mainly takes place in the z axis and can be decomposed into an upward and a downward section. In Figure 2.12, these upward and downward phases are represented by peaks, sudden changes of more than 0.5 g, in acceleration. All other smaller fluctuations in acceleration visible in the plots only represent negligible motion variations of the vacuum chamber at rest. In Figure 2.12 (a), the first peak represents the chamber accelerated upwards, the second peak is the deceleration (or negative acceleration in the z axis), then a pause is marked before the third peak, which corresponds to the downwards acceleration, and the final peak is the deceleration, bringing the chamber to a stop. Figure 2.12 (b) shows the acceleration data when the pause in between upward and downward phases is reduced, until it is removed completely in Figure 2.12 (c), giving a continuous motion. The second and third peaks, namely the upward deceleration and downward acceleration (both negative accelerations in the positive z direction), are thus combined into one. For clarity, the first peak is henceforth referred to as the upward acceleration, the second as the downward acceleration, and the third as the stopping acceleration. The absolute value of the acceleration data is used, such as in Figure 2.12 (d), as the sign is not relevant for the analysis. The exact shape of the

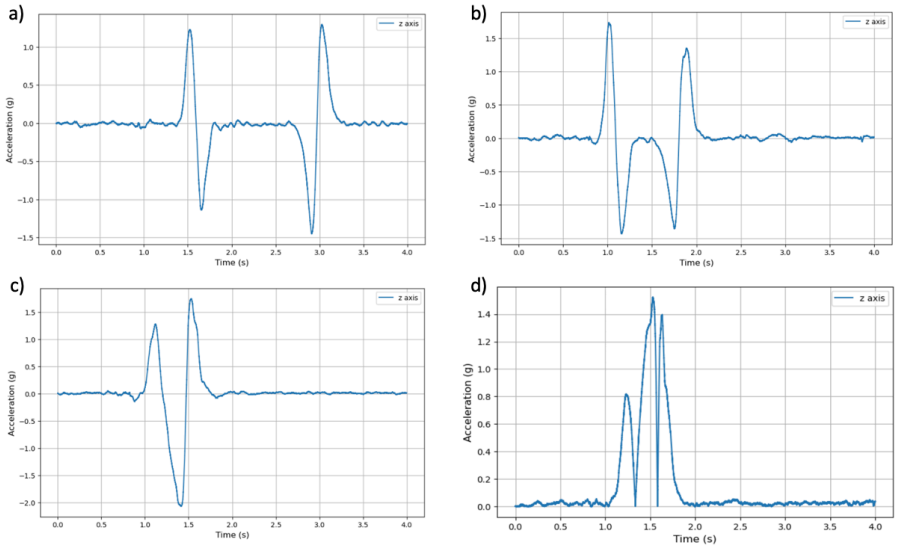

Figure 2.12: Shaking jar motion data explained: (a) Slow up-down chamber motion with clear pause in between. (b) Sped-up up-down chamber motion with short pause in between. (c) Up-down chamber motion without pause, performed during testing. (d) Absolute value of up-down chamber motion without pause, used for metrics.

peaks is not of interest, and the acceleration in the x and y directions is only monitored to ensure it remains minimal in the overall shaking motion. Finally, the magnitude of the three acceleration phases is also calculated to give an overall measure of the vacuum chamber motion.

For the laboratory avalanche experiment, the vacuum chamber is displaced from its original horizontal position to the measurement starting position, at around 35° from horizontal. The goal is for this motion to be fast enough such that most of the sand avalanches down the chute at the same time to ensure a thick enough sheared layer can synchronize and produce an acoustic emission, but not too fast where the sand grains could be ejected out of the inner container, and possibly onto the microphone. The time the vacuum chamber takes to travel between its resting horizontal position to the desired 35° inclination from horizontal is determined, and compared between measurements. It is not necessary to use the acceleration components of the vacuum chamber because unlike the shaking jar setup, they are in this case not as closely related to the sand motion and subsequent emission mechanism.

Acoustic Signal Characterisation

The first step consists in delimiting the signal to be analysed further. The burping emissions produced by the sonic sand in either experiments are identified in the signals by a clear dominant frequency, and are thus manually delimited where the latter begins and ends, as seen in Figure 2.13. Henceforth, the metrics are determined for this part of the signal only. Then, for the comparison to the regular sound of sand grains impacting one another, the signal of the silent sand measurements is also delimited, from where the sound begins to where it ends.

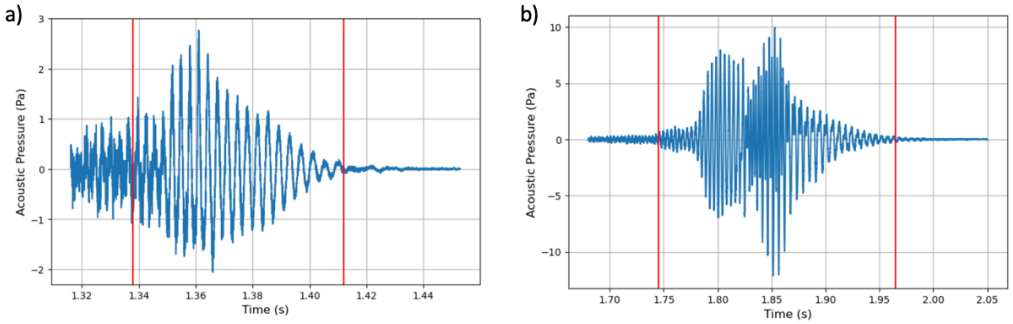

Figure 2.13: Manual delimitation of burping emission acoustic signal for (a) shaking jar measurement, and (b) laboratory avalanche measurement. The red lines represent where the sound starts and ends.

The characterisation of the burping emissions and sand grain impact emissions is based in both the time and frequency domain. In the time domain, the metric calculated is related to the *SPL*. The *SPL* is generally expressed in decibels, and represents the logarithmic ratio between the acoustic pressure of a sound P, and the smallest pressure disturbance the human ear can detect, called reference pressure $P_0 = 20$ µPa, such that:

$$SPL = 20 \log_{10}\left(\frac{P}{P_0}\right)$$

As expressed by Burkard (1984), the acoustic pressure value used to calculate the *SPL* is a root-mean-square (rms) value. This method inherently takes more signal information into account than using only a peak value which does not represent well the rest of the signal, and is thus preferred for *SPL* calculations of longer acoustic signals. This is most likely used in the case of extended booming emissions of desert sonic dune avalanches, lasting multiple seconds. However, burping emissions are by nature much more transient sounds, around 200 ms for the laboratory avalanche emissions and shorter than 100 ms for the shaking jar emissions. Indeed, to better represent the pressure disturbance of even shorter sounds for example, it is common to look at the peak-to-peak pressure (Burkard, 1984; Haughton et al., 2003; Laukli and Burkard, 2015), the range from the lowest negative pressure value in the signal to the highest positive value. Furthermore, the *rms* value depends on the signal delimitation, which in this case is done by hand and might slightly differ from one set of measurements at a certain pressure level, to another. What's more, measures of the entire signal's "strength" are covered by other

metrics. Thus, the maximum peak-to-peak acoustic pressure is used to calculate an *SPL*-like metric of each signal, which is named SPL_{pp}.

The impact of lower chamber pressure on the *SPL* of a same sound, can be modelled (see section 2.4). The sound emission mechanism of silent sand sound is only dependent on the grain to grain impact, and is not affected by changes in pressure. The experimental SPL_{pp} results of this sound at different pressure levels can thus be used to validate the models. The SPL_{pp} results of the sonic sand measurements can then be compared to this reference, to assess if the acoustic pressure of the burping sound produced differs from model predictions, which would give some insight on the potential impact on the emission mechanism at lower and Mars-like pressure levels.

The SPL_{pp} metric is first calculated for the raw signal - this refers to the signal after the motion induced noise filtering, but before any other kind of filtering related to the analysis - of the silent and sonic sand acoustic emissions to capture the acoustic pressure of both sound sources, namely the burping emission and the grain to grain impact sound sources. However, it would also be of interest to obtain the SPL_{pp} of the burping sound without the grain sound. Burping emissions generally range from 50 to 400 Hz (Brantley et al., 2002; Haff, 1979; Hidaka et al., 1988; Leach and Rubin, 1993), while regular rustling sound of sand grains is a broadband sound ranging the entire audible spectrum, but mainly sitting in the 5-15 kHz range, as seen in Figure 2.14 (a). Also considering that in the spectrum of a sonic sand emission (example shown in Figure 2.14 (b)), the burping sound dominates the signal over the grain to grain impact sound, it is considered that below 1 kHz (to also take into account possible higher harmonics of burping emissions), the sound mainly comes from the burping emission. Hence, a low-pass Butterworth filter with a cut-off frequency at 1 kHz, is applied to the signal to retain mostly the burping sound emission. The SPL_{pp} of the filtered signal is then obtained. This process is also performed for the silent sand measurements in order to later compare the evolution with pressure of the SPL_{pp} below 1 kHz between the two sound emission mechanisms, and see if differences with the raw signal SPL_{pp} appear.

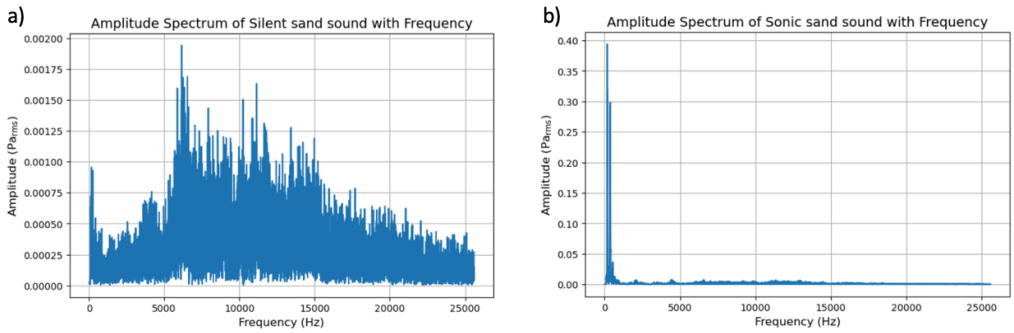

Figure 2.14: Examples of FFT-based amplitude spectrum used to visualise the acoustic signals in the frequency domain for this project. (a) Frequency response of the silent sand sound emission in the laboratory avalanche experiment. (b) Frequency response of the sonic sand sound emission in the laboratory avalanche experiment.

The rest of the metrics used to characterise the acoustic signal are defined in the frequency domain. This begins by performing a Fourier analysis, which decomposes the signal in the time domain into its periodic components, which can then be mapped in the frequency domain. The Fourier transform of a continuous time function $g(t)$ can be expressed as follows (Fourier, 1822; Papoulis, 1962):

$$\hat{g}(f) = \int_{-\infty}^{+\infty} g(t) e^{-i2\pi f t} dt$$

The resulting Fourier transform $\hat{g}(f)$ is a complex number for every frequency f, and evaluates which frequencies are part of the function, and which are not. This becomes evident when looking at the magnitude of the complex numbers; for a finite time, very small values close to 0 indicate frequencies not contained in the function, while positive values evidence frequency components that are. How large the value is is a measure of the amplitude of the frequency in the signal. This value can be plotted for an infinite number of frequencies, giving a representation of all periodic components of the signal, and their amplitude, in the frequency domain (Bracewell, 1986).

The Discrete Fourier Transform (DFT) is used for real signals, which are inherently made up of a finite number of points (Smith, 2003). This results in a similarly discrete frequency spectrum, where frequency components rather fall in bins. The size and number of bins is decided by the rate at which the time-domain signal is sampled, and the signal duration. The Fast Fourier Transform (FFT) is an algorithm that performs the DFT in a more efficient way by reducing the number of product computations in the Fourier transform integrals (Cooley and Tukey, 1965). This algorithm is widely used across domains related to signal processing for its efficiency, and is thus also used in this project.

The metrics for this project defined in the frequency domain focus on the amplitude spectrum of the frequencies rather than the phase, which gives information about how shifted the constituent waves are relative to each other. The first step after performing the FFT of the discrete acoustic signal of the measurement at hand, is to take the magnitude of each complex number in the series. The Fourier Transform is defined such that it results in a double-sided frequency spectrum, with mirrored positive and negative values. Thus, the amplitude of a frequency component in the frequency domain is half its peak amplitude in the time domain, being distributed between the positive and negative values. However, as it is generally more desirable to only visualize the positive side of the frequency spectrum, the negative side is discarded and the positive side (other than the 0 frequency bin) multiplied by two (Cerna and Harvey, 2000). Furthermore, the FFT values scale with the signal duration, such that the longer a frequency component lasts, the greater its amplitude in the frequency spectrum. To normalise the amplitude, it is divided by the number of points in the signal N. Finally, a better way than the peak amplitude for assessing the effective energy of a wave, is the *rms* of the quantity measured, here Pa. The peak amplitude is hence divided by $\sqrt{2}$ to obtain the amplitude *rms* of each frequency components (Cerna and Harvey, 2000). As shown in Figure 2.14, this project uses the one-sided amplitude spectrum in Pa_{rms} of the discrete time signal $g_s(t)$ such that:

$$\text{Amplitude Spectrum Pa}_{rms} = |FFT\,(g_s(t))\,| \times \frac{\sqrt{2}}{N}$$

This amplitude spectrum is used to compare the frequency components of burping emissions at different pressure levels. This gives an insight into the sand layer thickness of synchronising grains (Andreotti, 2012; Douady et al., 2006), and the emission threshold at different pressure levels.

Another method for determining how much of the sonic sand sound comes from the burping emission itself, rather than the grain-grain friction sounds, to then better analyse the relation between air pressure and the emission mechanism at play, is to look at signal energy. Indeed, Parseval's theorem for the DFT states that there is conservation of energy across the time and frequency domain (Smith, 2003), with the following expression:

$$\sum_{j=0}^{N-1} |x_j|^2 = \frac{1}{N} \sum_{k=0}^{N-1} |X_k|^2$$

where x_j and X_k is a discrete FFT pair, with *N* number of data samples. The energy of the entire acoustic signal can thus be computed in either domains. This theorem however becomes useful when wanting to determine the signal energy in a certain frequency range, which is only possible in the frequency domain. As explained earlier, because much of the grain to grain friction sound resides at higher frequencies than the burping emission, the signal energy in the sand acoustic emission frequency range is dominated by the burping sound itself. Thus, the energy in the frequency range of the burping emission can be calculated, and be compared to the behavior of the SPL_{pp} metric used in the time domain. The frequency range depends on the setup parameters, such as the sediment quantity and shearing velocity, and as a result differs between the shaking jar and the laboratory avalanche experiment. For the shaking jar experiment, the burping frequency range is composed of the burping emission's dominant frequency peak which lies in the 200-400 Hz region, and a second harmonic region in the 500-700 Hz range. For the laboratory avalanche, it became evident upon inspecting the frequency spectrum of different measurements that multiple frequency peaks were present between 100 and 550 Hz, which was thus defined as the burping range for energy calculations. These energy calculations are also executed for the silent sand measurements, to then compare between sediment type the evolution of the signal energy in different frequency ranges.

Finally, the last aspect to be analysed in the frequency domain of the sonic sand measurements is the evolution of the frequency peaks with chamber pressure. Changes in dominant frequency can

give information about the thickness of the main synchronised grains layer (Andreotti, 2012). The amplitude of the burping emission frequency peaks compared to the rest of the frequency spectrum (regular sand sound) at similar frequencies is also indicative of if the pressure level affects the sound emission mechanism of sand acoustic emissions in a similar way to how it affects regular rustling sand sound. Furthermore, if some higher frequency peaks are present in measurements at certain pressure levels and not others, an interpretation could be for example that the sound emission threshold is lowered and thinner synchronised layers can form at lower interstitial pressure.

To summarise, the acoustic signal is first manually delimited, before calculating the SPL_{pp} for the raw and filtered signal of both sonic and silent sand. The characterisation then shifts to the frequency domain, where a Fourier analysis is performed. Using Parseval's theorem, the energy of the signal over the entire spectrum and within the burping emission frequency range, is obtained for both sediment types. Finally the frequency of the main constituent peaks in the sonic sand measurements are recorded and analysed.

2.3.3. Data Selection Criteria

As mentioned in section 2.2.2, a selection of the measurements is made post-testing to remove outliers in the microphone and motion data, caused by the manually produced vacuum chamber motion, or the slight changes in initial sand position which may affect the sound.

Firstly, the median of the SPL_{pp} of the filtered signal of all measurements taken at one pressure level is calculated. For silent sand measurements, the sound produced is normally very consistent. A ±1 dB window around the median is set, such that measurements outside of it are discarded. For sonic sand measurements, where the burping emissions are more variable and sensitive to small changes in inputs, a ±2 dB window about the median is the threshold set.

Secondly, for the shaking jar experiment measurements, the median of the magnitude of the three acceleration phases is calculated. In the case of the sonic sand, the 10 measurements with the closest acceleration magnitude to the median value are selected. For silent sand, the five (out of the original 10) measurements closest to the corresponding median represent the final selection. The same selection criterion is applied to the motion metric of the laboratory avalanche experiment (i.e. the time between initial and final position).

For the sand deterioration measurements, as the goal is to measure large changes (if present) in the burping emissions, caused by a loss in the sand's singing ability rather than the human factor or sand grain position, the selection criterion related to the dB window about the median is not applied. The motion metric criterion on the other hand is used to select out of the initial five measurements, three that will be analysed further.

2.4. Sound Emission & Propagation Models

The measurements of silent sand in both experimental setups are used as a reference for how sound emission and propagation are normally affected by air pressure, to then compare with sonic sand measurements. The impact of the sound emission and propagation at different pressure levels on the *SPL* can also be modelled to ensure the silent sand reference results follow expected trends. In this section, the differences in acoustic impedance and propagation absorption between the surface of Earth and Mars, described in section 1.3.3, are first verified to validate the models used. The latter can then be applied to the experimental setup conditions, and later compared to silent sand measurement results.

2.4.1. Acoustic Impedance

The acoustic impedance for a spherical wave propagating from a point source in free-field conditions was previously described in section 1.3.3. Although to be fully accurate, the experimental setups developed should not be considered free-field-like environments, the resultant acoustic impedance would become a complex number, with the corresponding *SPL* being a function of many different variables (Hiremath et al., 2021). As the goal is only to approximate the impact of the acoustic impedance on the sound produced to ensure the general plausibility of the silent sand results being taken as a reference for the sonic sand measurements, the plane wave characteristic impedance is assumed. Thus, the impact of Mars' acoustic impedance on the *SPL* of sounds, described by Petculescu and Lueptow (2007) and Maurice et al. (2022), is first verified to validate the calculation method used. A model is

then computed to measure the theoretical relation between *SPL* and pressure level in the experimental setup conditions, which will later be compared to SPL_{pp} values of silent sand measurements.

As previously described by Petculescu and Lueptow (2007) and Maurice et al. (2022), sounds on Mars are approximately 20 dB weaker than on Earth, without propagation losses. To verify this, the air density on Earth ρ_{0_E} and Mars ρ_{0_M} is first obtained by using the ideal gas law:

$$\rho_{0_E} = \frac{P_{0_E}}{R_E T_{0_E}} = 1.225\ kg.m^{-3}$$

$$\rho_{0_M} = \frac{P_{0_M}}{R_M T_{0_M}} = 0.014\ kg.m^{-3}$$

with the sea level pressure on Earth $P_{0_E} = 101325$ Pa, specific gas constant of Earth air $R_E = 287.1$ J.kg^{-1}.K^{-1}, average Earth temperature $T_{0_E} = 288$ K, average pressure on Mars $P_{0_M} = 600$ Pa, specific gas constant of Mars air $R_M = 191.7$ J.kg^{-1}.K^{-1}, and average Mars temperature $T_{0_M} = 220$ K (Petculescu and Lueptow, 2007; Williams, 2001). Similarly, the speed of sound on Earth c_{0_E} and Mars c_{0_M} is calculated:

$$c_{0_E} = \sqrt{\gamma_E R_E T_{0_E}} = 340.3\ m.s^{-1}$$

$$c_{0_M} = \sqrt{\gamma_M R_M T_{0_M}} = 237.5\ m.s^{-1}$$

with the specific heat ratio of air on Earth $\gamma_E = 1.4$ and Mars $\gamma_M = 1.338$ (Williams, 2001). This gives the corresponding characteristic impedance:

$$z_{0_E} = 416.9\ kg.m^{-2}.s^{-1}$$

$$z_{0_M} = 3.3\ kg.m^{-2}.s^{-1}$$

Assuming free-field conditions, the *SPL* is equal to the sound intensity level (*SIL*) (Soares, 2015) such that:

$$SIL = 10\log_{10}\left(\frac{I}{I_0}\right)$$

where I is the acoustic intensity and I_0 the reference intensity. The reference intensity relates to the reference pressure P_0 and characteristic impedance z_0 such that for Earth and Mars:

$$I_{0_E} = \frac{P_0^2}{z_{0_E}} = 5.595 \times 10^{-13}\ W.m^{-2}$$

$$I_{0_M} = \frac{P_0^2}{z_{0_M}} = 1.203 \times 10^{-10}\ W.m^{-2}$$

For example, if one takes a signal on Earth with an $SPL_E = SIL_E = 100$ dB, the corresponding signal intensity is:

$$I = I_{0_E} \times 10^{SPL_E/10} = 5.595 \times 10^{-3}\ W.m^{-2}$$

Because the reference intensity is much higher on Mars, the *SPL* of this same 100 dB sound then becomes:

$$SPL_M = 10\log_{10}\left(\frac{I}{I_{0_M}}\right) = 77\ dB$$

A 23 dB decrease in *SPL* is obtained for this example, which is close to the estimation given in the literature. The difference seems to come from slightly different values of atmospheric conditions used.

This method can then be used for the experimental setup: the SPL_{pp} of a signal measured at ambient pressure in the experiments represents the “original” *SPL*, such that the theoretical *SPL* with the same sound intensity is calculated for multiple different pressure levels all the way down to around 10 mbar. However, the characteristic impedance in the experimental setup at around 10 mbar slightly differs from that on the Martian surface. Indeed, assuming a close to constant temperature, the speed of sound is independent of the atmospheric pressure, and for a pressure level $P_{exp} = 10$ mbar, the density becomes:

$$\rho_{exp} = \frac{P_{exp}}{R_E T_{0_E}} = 0.012\ kg.m^{-3}$$

This gives an equivalent characteristic impedance z_{exp}:

$$z_{exp} = \rho_{exp} c_{0_E} = 4.1\ kg.m^{-2}.s^{-1}$$

The acoustic impedance in the experimental setup at around 10 mbar is very close to that on the Martian surface, and results in a 20 dB decrease in *SPL*. Figure 2.15 shows a curve that follows the model described above, with an "original" *SPL* value at ambient pressure of 100 dB, and a final *SPL* at 10 mbar of 79.9 dB.

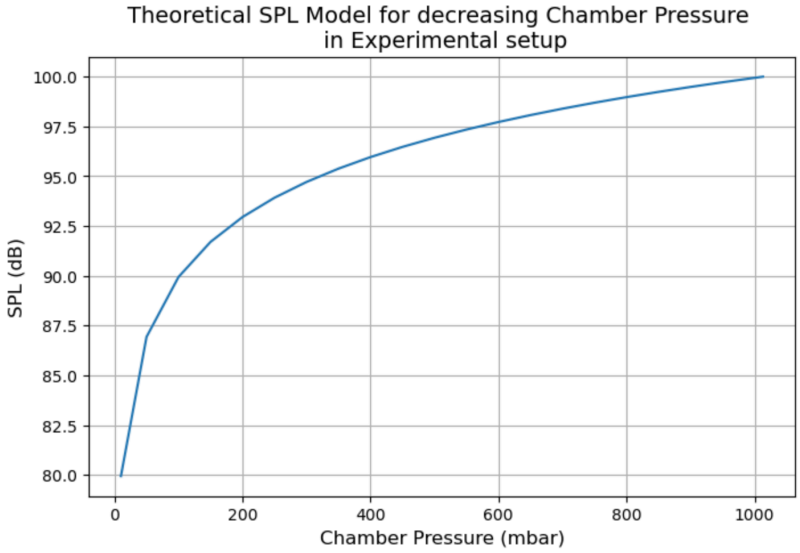

Figure 2.15: Theoretical *SPL* model for decreasing chamber pressure in the experimental setup.

2.4.2. Propagation Absorption

Atmospheric absorption is the attenuation of sound wave intensity when travelling through a medium, and combines classical and relaxation absorption processes, described in section 1.3.3. Modelling this phenomenon for the experimental setups is necessary to evaluate how the different pressure levels affect the propagation of the sand sounds. The model used is that developed by Liu et al. (2017), which successfully determines the relaxation absorption in gas mixtures. In comparison, previous, more simplified models used for planetary acoustics in Bass et al. (1984) and Williams (2001) do not correspond well with in-situ microphone data from the Perseverance rover (Maurice et al., 2022) in the frequency range where relaxation absorption dominates.

The total propagation absorption as a function of frequency is first calculated for average surface conditions on Earth and Mars, to compare and validate the model with that of Bass and Chambers (2001) and Petculescu and Lueptow (2007), which are both closer to Perseverance acoustic measurements in Maurice et al. (2022). The surface atmospheric conditions of Earth used are a temperature of 288 K, a pressure of 101325 Pa, and a composition of 78.5% N_2 and 21.5% O_2 (Bass and Chambers, 2001). Those for Mars are a temperature of 220 K, a pressure of 600 Pa, and a composition of 96% CO_2 and 4% N_2 (Maurice et al., 2022; Petculescu and Lueptow, 2007). The atmospheric composition of both environments was simplified to their two main elements, as the role of the other gases in the relaxation absorption is minimal, and the computation time greatly reduced. All parameter values and intermediate equations necessary for the calculations of the acoustic relaxation absorption were found in Tanczos (1956), Dickens and Ripamonti (1961), Dain and Lueptow (2001), Ejakov et al. (2003), Petculescu and Lueptow (2005), Zhang et al. (2014), and Liu et al. (2017). The calculation steps are described in Liu et al. (2017). The resultant model applied to terrestrial and Martin surface conditions is plotted in Figure 2.16, alongside that of Petculescu and Lueptow (2007).

Figure 2.16 shows that the model of Liu et al. (2017) applied to the surface atmospheric conditions of Earth and Mars agrees well with that of Petculescu and Lueptow (2007), and most importantly with

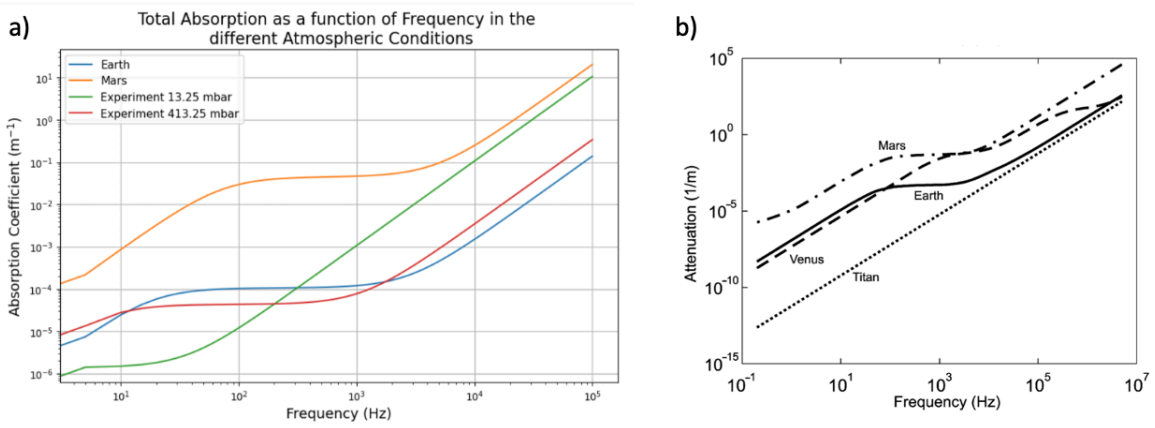

Figure 2.16: (a) Absorption coefficient as a function of frequency, for atmospheric conditions on Earth, Mars, and the experimental setup at 413.25 mbar and 13.25 mbar, based on Liu et al. (2017). (b) Absorption coefficient as a function of frequency at the surface of Earth, Mars, Venus and Titan (Petculescu and Lueptow, 2007).

microphone data from Perseverance plotted in Maurice et al. (2022) (and shown in section 1.3.3). The model is then used to calculate the propagation absorption in the experimental setup conditions, where only the pressure level differs from the surface conditions of Earth. The results are plotted for a pressure of 413.25 and 13.25 mbar. While the absorption coefficient α is commonly expressed in m^{-1}, it can be converted to $dB.m^{-1}$, where α [$dB.m^{-1}$] $= 8.686\alpha$ [m^{-1}] (Simons and Snellen, 2021). Thus, considering the sand to microphone distance of around 10 cm and 50 cm in the shaking jar and laboratory avalanche setups respectively, it can be deduced that the propagation absorption only becomes relevant over 10 kHz, especially at lower pressure levels. This might hence affect the SPL_{pp} of the sound of sand grains impacting one another (in the 5-15 kHz range), such that with a decrease in chamber pressure, the SPL_{pp} would decrease more than what the acoustic impedance model predicts alone. Then, in the frequency range of burping emissions in the experimental setups, between 150 and 700 Hz, the absorption coefficient remains between around 4.5×10^{-4} $dB.m^{-1}$ and 6×10^{-3} $dB.m^{-1}$, and the consequent acoustic absorption is thus negligible at the distances mentioned prior. The SPL_{pp} of the burping sound alone is thus expected to follow the acoustic impedance based model.

3
Results

The results obtained in the two experiments are presented and discussed in the following sections, where the metrics defined in Chapter 2 are plotted and compared for the silent and sonic sand, in the entire frequency range and the burping sound range. To begin, the SPL_{pp} in the time domain is presented, along with the motion data. Then, the sand deterioration measurements taken at ambient pressure after each set of tests at a certain pressure level, reveal whether the sound production of the sonic sand has remained consistent throughout testing and hence affected or not the results of the experiments. The results then shift to the frequency domain. The signal energy in the burping frequency region is compared between sonic and silent sediments. Finally, the dominant frequency and amplitude spectrum under 1 kHz give more information about the timbre characteristics of the sound produced by sand acoustic emissions at lower pressure levels. The results are then synthesized and compared across the two experiments, to reflect on the findings and their implications.

3.1. Shaking Jar Results

3.1.1. SPL_{pp} Analysis

Sensitivity Analysis of Motion Acceleration w.r.t SPL_{pp}

It was explained in section 2.2 that the human factor in the shaking jar experiment inherently introduces some variability in the resulting burping emission. The motion is hence measured using the accelerometer on the setup, to ensure that the measurements that are used for the results differ the least in their motion data. The accelerometer data can also be plotted against the resultant SPL_{pp} to establish if a relation between the acoustic and motion metrics defined can be deduced. In Figure 3.1, the three motion acceleration components and their magnitude are plotted against the SPL_{pp} of the burping emission produced during the shaking jar experiment. The data points used are of the measurements at ambient pressure, in both the main experiment and the sand deterioration tests. The outliers where no clear burping emission is produced are removed from the data set, and 45 total data points remain.

Studying the relation between two variables can be done using different methods. At first, the Pearson correlation coefficient, which gives a measure of the strength of the linear relationship between two variables, was determined for the relation between each acceleration metric and the SPL_{pp}. The strongest correlation was found with the acceleration magnitude metric, which was expected; the magnitude metric was indeed intended to better represent the overall vacuum chamber motion, compared to the individual acceleration phases. However, more data points in the middle to higher SPL_{pp} range (106-112 dB) would be needed for such a correlation to become more meaningful and accurate. This would also give a better indication of the relationship's linearity, which remains an assumption. To avoid these uncertainties, the relation between the acceleration and the SPL_{pp} is analysed differently: it can be seen in Figure 3.1 that for the acceleration magnitude, most data points are regrouped inside a range of SPL_{pp} values between around 102 and 107 dB, with no visible correlation, while the data points with higher SPL_{pp} values, above about 108 dB tend to correspond to measurements with higher acceleration values. The approach used thus divides the data into two populations, the first with low acceleration and SPL_{pp} values, and the second with high values of both variables, which avoids the limitations met with the correlation analysis while still providing a measure of the association between

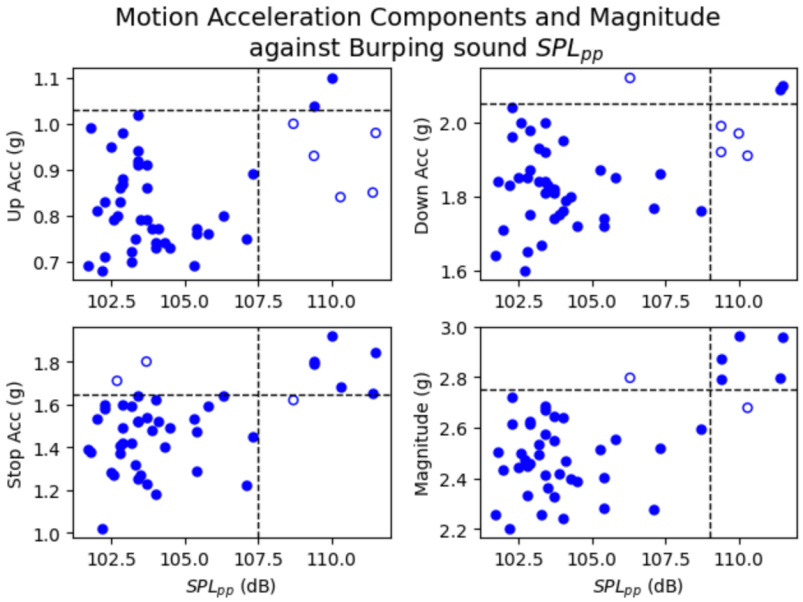

Figure 3.1: Motion acceleration components and magnitude against the SPL_{pp} of the burping emission in the shaking jar experiment. The dashed black lines delimit the two populations based on the Cate-Nelson model. The filled circles correspond to data points that fit the model, while the hollow circles, data points that do not.

the variables. The model used is the Cate-Nelson model, described in Cate and Nelson (1971), where the critical x-axis value which divides the two populations is calculated following an iterative process. The y-axis separation is subsequently determined graphically to minimize the number of points outside of the two populations. The separations are marked in the Figure 3.1 plots by the dashed black lines. The points outside of the delimited populations are marked by hollow circles, and their quantity gives a measure of how well the model describes the relation between the variables.

Using this method, it is apparent that a stronger association exists between the acceleration magnitude and the SPL_{pp}, especially compared to the upwards and downwards acceleration components, as all but two data points (or 96 %) fit within the two delimited populations. Though no clear correlation can be established between the induced motion and sound produced, these plots do show that for measurements where the acceleration magnitude remains between 2.2 and 2.75 g, the burping sound SPL_{pp} can have any value between 102 and 109 dB. Sounds with an SPL_{pp} of around 110 dB however will most often be due to a greater acceleration magnitude being applied to the vacuum chamber. The lack of clear relation between motion and sound metrics could perhaps come from the motion of the vacuum chamber not corresponding well enough to that of the sand, of which the exact initial grain position and motion dynamics are difficult variables to measure and control.

SPL_{pp} of Silent Sand Emission

The SPL_{pp} of the silent sand recordings is used to ensure that this sound is purely produced by the impact of grains with one another, by comparing the results to the theoretical model of the *SPL* at different pressure levels obtained in section 2.4.1. Figure 3.2 shows this comparison for the raw signal and the sub 1 kHz filtered signal, by plotting the trend of the measured SPL_{pp} in the shaking jar experiment along with the theoretical *SPL* model where the *SPL* at ambient pressure coincides with the experimental value. The motion metrics are also plotted to determine the impact on the SPL_{pp}.

Figure 3.2 (a) shows that the SPL_{pp} results of the filtered signal fit well with the *SPL* model, while the raw signal exhibits a greater decrease in the metric at lower pressure levels. This is most likely due to the increase in propagation absorption of frequencies above about 10 kHz in this setup, compared to those under 1 kHz which are essentially unaffected regardless of the air pressure (see section 2.4.2). This would explain the slight difference between the raw signal SPL_{pp} results and the corresponding *SPL* model, which greatly reduces in the filtered signal values. In Figure 3.2 (b), the acceleration magnitude exhibits a steady value from 13.25 mbar to 613.25 mbar, with a small decrease up to ambient pressure measurements. This behavior could explain the plateau experienced in SPL_{pp} values from

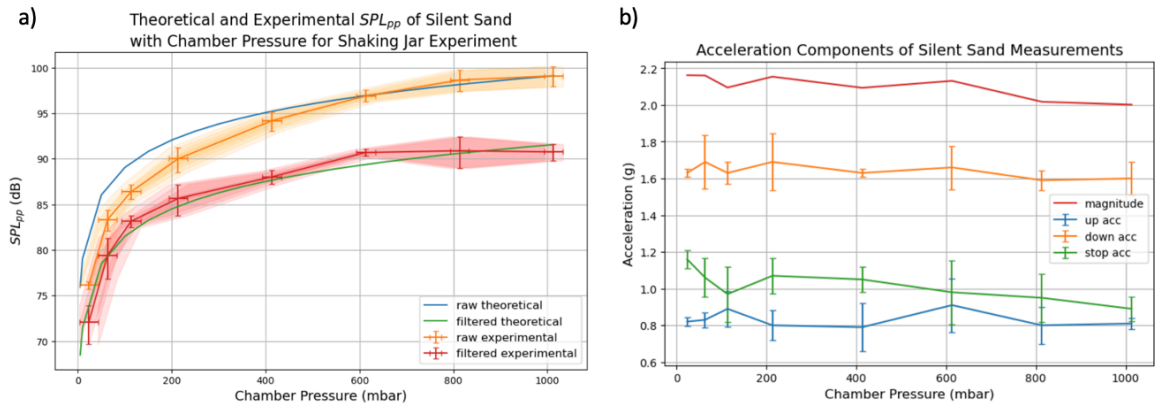

Figure 3.2: (a) Theoretical and experimental SPL_{pp} with chamber pressure, of the silent sand emission in the shaking jar experiment. (b) Corresponding motion acceleration components and magnitude of the silent sand measurements.

613.25 mbar to ambient pressure. Overall, the silent sand measurements agree very well with the *SPL* model, showing that the sound emission of grains impacting one another is affected by atmospheric pressure nominally. The *SPL* model can thus further be compared to the SPL_{pp} of burping emissions to analyse how the air pressure affects the sound emission of sonic sand.

SPL_{pp} of Sonic Sand Emission

The SPL_{pp} of the sonic sand measurements at various pressure levels can give an insight into the impact of the interstitial air pressure on the emission mechanism of the sonic sand. It is hence plotted in Figure 3.3 against the *SPL* model for the raw and filtered signal, along with the corresponding motion acceleration data.

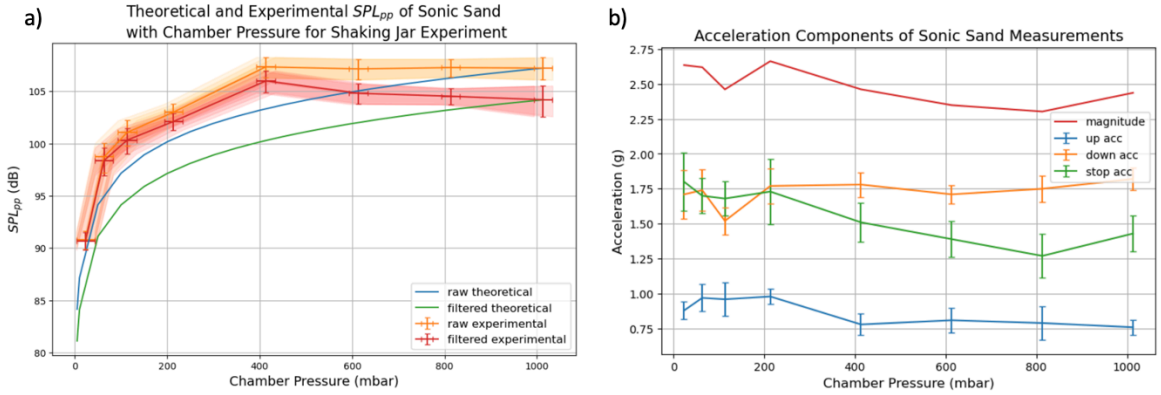

Figure 3.3: (a) Theoretical and experimental SPL_{pp} with chamber pressure, of the sonic sand emission in the shaking jar experiment. (b) Corresponding motion acceleration components and magnitude of the sonic sand measurements.

Similarly to the silent sand measurements, the higher frequencies of the raw signal are absorbed increasingly more with a decrease in air pressure, which is evidenced in Figure 3.3 (a), where the raw and filtered signal become very close at pressure levels below 200 mbar. For the filtered signal, which as explained in section 2.3.2 mainly represents the burping emission, it is apparent that the SPL_{pp} values are greater than the *SPL* model predicts; the SPL_{pp} increases from ambient pressure to 413.25 mbar, below which it fits well the model. The acceleration magnitude metric plotted in Figure 3.3 (b) shows a relatively similar value from 13.25 mbar to 413.25 mbar, after which the magnitude decreases slightly. However, all measurements remain between 2.25 and 2.7 g, within which the resultant SPL_{pp} does not correlate to the chamber motion (as shown in Figure 3.1). This increase in SPL_{pp} with decreasing pressure, which is unlike regular sounds (such as the silent sand sounds), is thus most likely not due to the small differences in chamber motion. This constitutes the first indication that the sound emission mechanism of sonic sands may depend on the surrounding air pressure.

3.1.2. Sand Deterioration

The erosion of the desert varnish on the surface of sonic sand grains causes the burping emission to fade. This occurs when extensive testing and shearing of sonic sand is performed (see section 1.2.1). It is thus important to measure this evolution to understand how it affects the results obtained in the main experiments. This is achieved by taking five measurements of burping emissions at ambient pressure, after each series of measurements at the different pressure levels, and keeping three. Figure 3.4 shows how the SPL_{pp} of the sound during these deterioration tests, along with the corresponding acceleration magnitude of the motion evolve over the number of measurements.

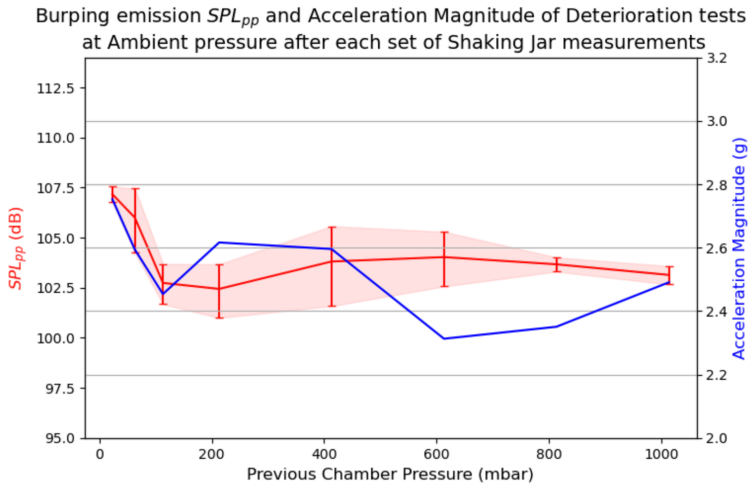

Figure 3.4: Burping emission SPL_{pp} and acceleration magnitude of deterioration tests in the shaking jar experiment. These tests are performed at ambient pressure after each set of measurements at the different pressure levels, labeled in the x-axis.

All deterioration measurements show an acceleration magnitude between 2.3 and 2.75 g, and an SPL_{pp} value between 102 and 107.5 dB, with no apparent correlation, which agrees well with the data and model in Figure 3.1. Furthermore, the burping emission always remained evident in the sound produced in these tests, which is not the case when desert varnish erodes away. Thus, the slightly larger SPL_{pp} values (2-3 dB) after the series at 13.25 and 63.25 mbar (which are the first measurements performed), seen in Figure 3.4, are likely due to the small sample size, and not any physical changes in the sound production. This would also indicate that the decrease in burping emission SPL_{pp} with increasing chamber pressure observed in Figure 3.3 would not be coming from a deterioration of the sonic sand.

3.1.3. Signal Energy

The SPL_{pp} metric in the time domain might be subject to biases in that the peak to peak measurement of the acoustic pressure might be affected by noise, and that it inherently only represents a small portion of the signal. Hence, to get a more complete view of the signal obtained, it can be beneficial to calculate the signal energy, which takes the entire delimited signal into consideration. Figure 3.5 thus compares the trend of this metric for the burping emission of the sonic sand, and for the sound of the silent sand in the burping frequency range, at the different pressure levels.

The signal energy of the silent sand sound in the burping frequency range (where propagation absorption plays a negligible role in the sound recorded) follows a roughly linear trend, with the signal energy more or less proportional to the chamber pressure. On the other hand, the signal energy of the sonic sand's burping emission follows a relatively linear trend from 13.25 to 413.25 mbar, past which it decreases. Similarly to the SPL_{pp} behavior in Figure 3.3 (a), the signal energy of the burping emission increases with decreasing pressure until 413.25 mbar, under which it follows a trend close to the silent sand measurements. The results with the SPL_{pp} and signal energy metric are thus in good agreement, both showing that the emission mechanism of sonic sand would seem to produce "louder" sounds than expected at pressure levels below terrestrial pressure.

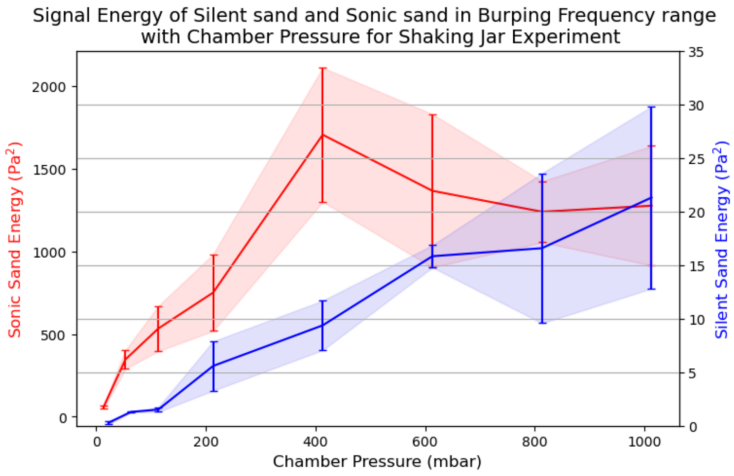

Figure 3.5: Signal energy of silent and sonic sands in burping frequency range with chamber pressure in shaking jar experiment.

3.1.4. Frequency Components

Analysing the frequency components of the burping emission signal at the different pressure levels can provide valuable information about the potential detection of sand acoustic emissions in other planetary environments, and about the grain dynamics of sheared sonic sand at lower pressure.

Firstly, the dominant frequency of the sound emitted by sonic desert sand is driven by the shearing force applied to the sand bed and the thickness of the sheared layer. This applies for both local emissions, such as in the laboratory experiments performed in this project (Douady et al., 2006), but also in naturally occurring dune slipface avalanches (Andreotti, 2004; Dagois-Bohy et al., 2012; Douady et al., 2006). To understand if the interstitial air pressure affects the rate at which the synchronized grain layer shears and vibrates, and its thickness, the dominant frequency of the burping emission and the acceleration magnitude of the chamber are plotted in Figure 3.6.

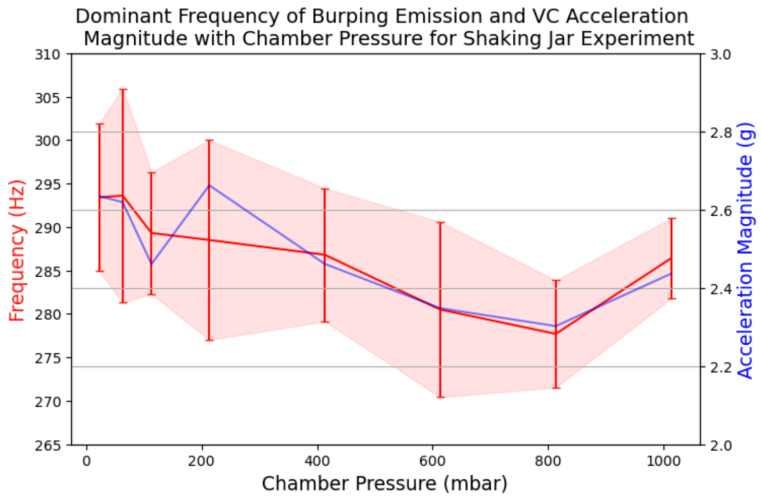

Figure 3.6: Dominant frequency of the burping emission and vacuum chamber acceleration magnitude at the different pressure levels in the shaking jar experiment.

Overall, the dominant frequency revolves around 285 Hz, and clearly follows the trend of the acceleration magnitude, as discussed in the literature. This could either mean that the chamber pressure does not significantly affect (if at all) either the shear rate nor the thickness of the sheared sonic sand layer, or that their individual changes cancel out in the resultant dominant frequency.

The entire frequency spectrum can give additional insights regarding the frequency components, harmonics, their amplitude relative to each other and to the regular sand noise, and whether these characteristics change with the air pressure level. Figure 3.7 (a) shows the amplitude spectrum of a

burping emission at ambient pressure, 413.25 mbar and 13.25 mbar. Figure 3.7 (b) shows the amplitude spectrum of the same three emissions, scaled by multiplying the frequency response by a constant such that the amplitude of the dominant frequency peaks matches, in order to better compare the relative amplitude of other components present in the signal. Signals with very close dominant frequency values are selected as this metric is already featured and studied in Figure 3.6.

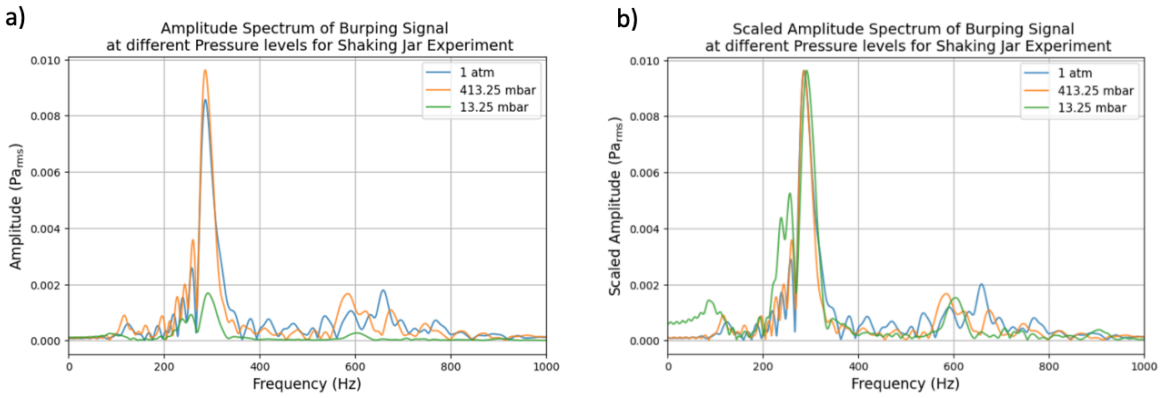

Figure 3.7: (a) Amplitude spectrum of burping emissions at ambient pressure, 413.25 mbar and 13.25 mbar, in the shaking jar experiment. (b) Scaled amplitude spectrum of burping emissions at ambient pressure, 413.25 mbar and 13.25 mbar, in the shaking jar experiment. The scaling is done by multiplying the frequency response by a constant such that the peak amplitude of all spectra match.

Figure 3.7 (a) mainly shows that the amplitude of the dominant frequency peak of the burping emission increases from terrestrial air pressure to 413.25 mbar, which is in accordance with the SPL_{pp} and signal energy behavior observed earlier. To better analyse the other frequency components, and the spectrum at 13.25 mbar, the scaled amplitude spectra are preferred.

Figure 3.7 (b) shows that the dominant frequency peak around 290 Hz generally remains similar in width and shape at different pressure levels. Some variability does appear in other measurements, but it is not correlated to the chamber pressure. The spectra of signals at 413.25 and 13.25 mbar are very similar: the second harmonic peak at around 600 Hz is very clear, and the amplitude of the non-burping emission components relative to the dominant frequency peak is comparably small. At ambient pressure however, the relative amplitude of the non-burping frequency components around the first and second harmonics noticeably increase, and the second harmonic peak becomes less visible. This agrees well with the time domain metrics, in that the amplitude of the sand grains sound decreases from ambient pressure to 413.25 mbar, while that of the burping sound increases. Below 413.25 mbar, the amplitude decreases similarly to the silent sand sounds. The results all suggest that sand acoustic emissions become louder as the interstitial air pressure decreases to around 400 mbar, below which the sound emission follows expected trends. The reason why lower air pressure seems to enhance the vibrating membrane-like emission mechanism of sonic sand remains unclear.

3.2. Laboratory Avalanche Results

3.2.1. SPL_{pp} Analysis

SPL_{pp} of Silent Sand Emission

Like in the shaking jar experiment, the SPL_{pp} of the silent sand recordings is used to validate the theoretical model of the *SPL* at different pressure levels obtained in section 2.4.1, and make sure it represents well the way “regular” sound is affected by a decrease in acoustic impedance. Figure 3.8 shows this comparison for the raw signal and the sub 1 kHz filtered signal, by plotting the trend of the measured SPL_{pp} in the laboratory avalanche experiment along with the theoretical *SPL* model where the *SPL* at ambient pressure coincides with the experimental value. The motion metric for this experiment, i.e. the duration of the vacuum chamber’s motion from horizontal position to its final 35° position, is also plotted to ensure its consistency over the measurements, and determine the potential impact on the SPL_{pp}.

Figure 3.8 shows that the SPL_{pp} results of the filtered signal fit well with the *SPL* model, while the

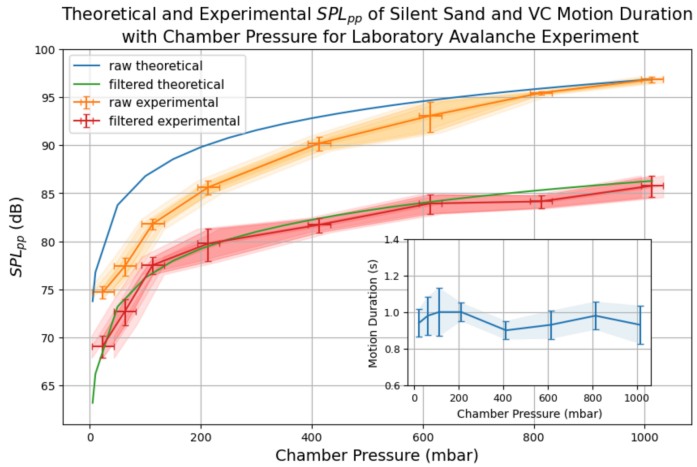

Figure 3.8: Theoretical and experimental SPL_{pp} with chamber pressure, of the silent sand emission in the laboratory avalanche experiment. The inset plot is the corresponding motion metric of the silent sand measurements, i.e. the duration of the vacuum chamber's motion from horizontal position to its final 35° position.

raw signal exhibits a greater decrease in the metric at lower pressure levels. Similarly to the shaking jar setup, it most likely comes from higher frequencies being absorbed more as the air pressure decreases. In comparison, the propagation absorption for those under 1 kHz remains negligible regardless of the air pressure (see section 2.4.2). This would explain the difference between the raw signal SPL_{pp} results and the corresponding *SPL* model, which isn't present in the filtered signal values. The inset graph shows that the vacuum chamber's motion duration average consistently remains between 0.9 and 1 s throughout the measurements. This stability translates to the filtered signal fitting the *SPL* model very well. As with the shaking jar setup, the *SPL* model represents well how the sound production of normal sounds is affected by air pressure, and it can thus further be used to evaluate the behavior of the SPL_{pp} of sonic sand sounds.

SPL_{pp} of Sonic Sand Emission

The SPL_{pp} of the sonic sand emissions in the laboratory avalanche experiment is plotted in Figure 3.9 against the *SPL* model for the raw and filtered signal, along with the corresponding motion metric in the inset plot.

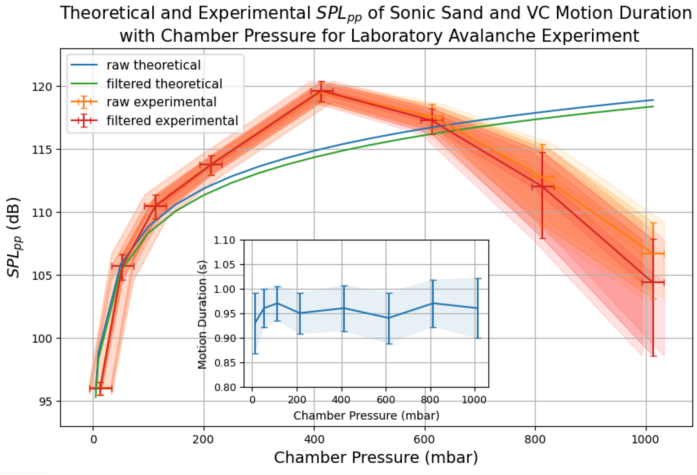

Figure 3.9: Theoretical and experimental SPL_{pp} with chamber pressure, of the sonic sand emission in the laboratory avalanche experiment. The inset plot is the corresponding motion metric of the sonic sand measurements, i.e. the duration of the vacuum chamber's motion from horizontal position to its final 35° position.

The graph shows that from 13.25 to 413.25 mbar, the raw and filtered signals are very close to one another, indicative of the burping emission dominating the overall signal. For an SPL_{pp} close to the

theoretical model at the lower pressure levels, the metric increases with pressure to surpass the model values by almost 5 dB at 413.25 mbar. The standard deviation remains relatively constant throughout this range of measurements, which suggests a nominal variability of the burping emissions. From 413.25 mbar to ambient pressure however, the SPL_{pp} significantly decreases (unlike the shaking jar experiment where only a slight decrease of 2-3 dB takes place), by around 15 dB gradually. Furthermore, the standard deviation also greatly increases, unlike in the shaking jar experiment, which implies that the amplitude of the burping emissions is becoming more sporadic. The difference between raw and filtered signal also becomes larger than the previous experiment and sets of measurements, which shows that the burping emission is not dominating the total signal over the sand grain sound as much anymore. As the motion metric in the inset exhibits a consistent value across pressure levels, it is evident that the behavior observed between 413.25 mbar and ambient pressure does not come from a significant change in the applied chamber motion. The characteristics described above seem to indicate that the sonic sand is not producing consistent burping emissions as reliably, most likely as a result of overuse from the experiments, rather than a physical consequence of the air pressure on the sonic sand emission mechanism. This interpretation is further discussed in the following section.

3.2.2. Sand Deterioration

The deterioration of sonic sand is more likely to occur and become apparent in the laboratory avalanche experiment because all the sediment is used at once, compared to the shaking jar experiment where much smaller samples are used and replaced if needed. It thus becomes even more essential to control this phenomenon. This is achieved by taking five measurements of burping emissions at ambient pressure, after each series of measurements at the different pressure levels, and keeping three. The SPL_{pp} and signal energy of the induced burping emissions are plotted in Figure 3.10. The inset graph plots the corresponding motion metric of the measurements to determine its variability and impact on the acoustic metrics.

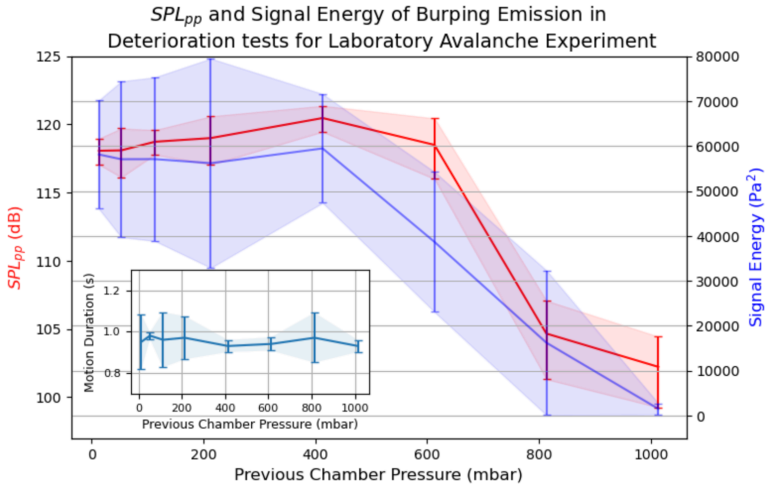

Figure 3.10: SPL_{pp} and signal energy of the burping emissions in the deterioration tests of the laboratory avalanche experiment. These tests are performed at ambient pressure after each set of measurements at the different pressure levels, labeled in the x-axis. The inset plot is the corresponding motion metric of the deterioration measurements, i.e. the duration of the vacuum chamber's motion from horizontal position to its final 35° position.

The SPL_{pp} and signal energy of the burping emissions follow very close trends over the series of sand deterioration measurements. The tests performed at ambient pressure after the series at 13.25 mbar (which are the first measurements performed) all the way up to 413.25 mbar exhibit a stable, close to constant SPL_{pp} and signal energy, which translates to no physical sign of changes in sound production. However, the measurements taken after the series at 613.25 mbar begin to show a clear decrease in signal energy. This behavior further continues for both acoustic metrics after the series at 813.25 mbar and ambient pressure, exhibiting strongly attenuated values compared to previous measurements. The motion metric plotted in the inset graph shows no significant variation over the deterioration measurements taken, and thus does not play a role in the reported behavior of the SPL_{pp}

and signal energy.

Slight changes in the acoustic metrics of different burping emissions are common and simply come from small differences in the motion metrics and from the stochastic variability in exact sand grain dynamics or initial position. However, in the laboratory avalanche experiment and deterioration tests, a significant gradual attenuation in both SPL_{pp} and signal energy after the tests at 413.25 mbar, are clear signs that the sonic quality of the sand has declined. This behavior may come from the deterioration of the surface desert varnish due to extensive shearing, as described by Dagois-Bohy et al. (2012) and Dagois-Bohy et al. (2010). When verifying the audio recordings of the microphone, the deterioration measurements (and hence the main laboratory avalanche experiment measurements) past the series at 413.25 mbar clearly exhibit a burping sound lower in volume and less frequent. Furthermore, this could perhaps also explain why the dominant frequency of the sound increases though the shearing rate remains consistent. Indeed, as Douady et al. (2006) and Andreotti (2012) explain, this occurs when the sheared layer thickness decreases. The hypothesis would be that as the sand is sheared repeatedly, the desert varnish which is believed to encourage grain synchronization (Dagois-Bohy et al., 2012; Douady, 2016, February 18) erodes, and the depth of the synchronised sheared layer would decrease. Though this would explain the observed increase in emitted frequency, and decrease in burping signal energy and SPL_{pp}, it remains to be confirmed.

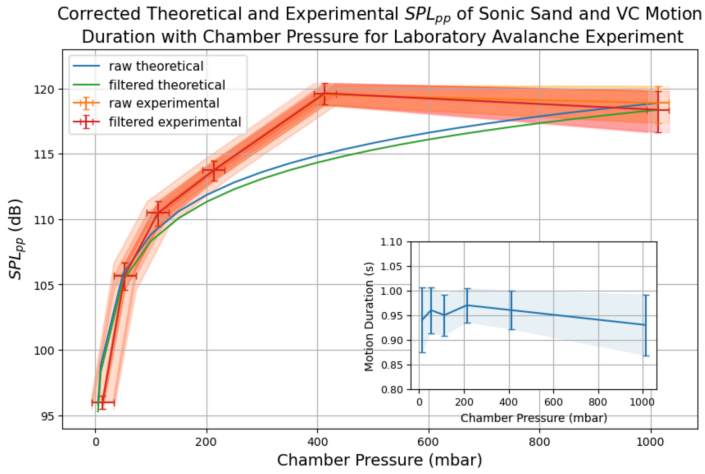

Figure 3.11: Theoretical and experimental SPL_{pp} with chamber pressure, of the sonic sand emission in the laboratory avalanche experiment, corrected to remove decrease in burping emission. The inset plot is the corresponding motion metric of the sonic sand measurements, i.e. the duration of the vacuum chamber's motion from horizontal position to its final 35° position.

Whether or not sand deterioration is the cause of this decrease in sonic sand sound production, the main measurements in the laboratory avalanche experiment and their corresponding data points in Figure 3.9, at 613.25 mbar, 813.25 mbar and ambient pressure, are indeed affected by this decrease in sound production by the sand. To remedy this and remove this variable from the results, the data points of these measurements are discarded. This creates a gap in the results for values at 613.25 and 813.25 mbar. At ambient pressure however, the data points are replaced by the deterioration measurements (which are performed at ambient pressure) for which the acoustic metrics remained constant in Figure 3.10, taken before the signs of sound production decrease appeared. These corrections are shown in Figure 3.11.

In this updated plot, it now becomes apparent that the behavior of the SPL_{pp} of burping emissions from ambient pressure to 413.25 mbar is actually very similar to that in the shaking jar experiment, with a slight but clear increase in the metric as the chamber pressure level decreases. Similarly to the shaking jar setup, the emission mechanism thus seems to produce louder burping sounds with lower interstitial air pressure. From 213.25 down to 13.25 mbar however, the SPL_{pp} decreases back down, and is close to the SPL model, with the value at 13.25 mbar even becoming slightly lower than the model. This trend does not agree well with the shaking jar experiment, and will be further analysed in section 3.3.

3.2.3. Signal Energy

As for the SPL_{pp} metric, the signal energy of the measurements at 613.25 mbar, 813.25 mbar and ambient pressure was affected by the decrease in sound production of the sand. Similarly, those data points were discarded, leaving a gap at 613.25 and 813.25 mbar. Once again, the first sets of deterioration measurements at ambient pressure were used to replace the main experiment measurements at ambient pressure. Figure 3.12 compares the resultant corrected signal energy for the burping emission of the sonic sand, and that for the sound of the silent sand in the burping frequency range, at the different pressure levels.

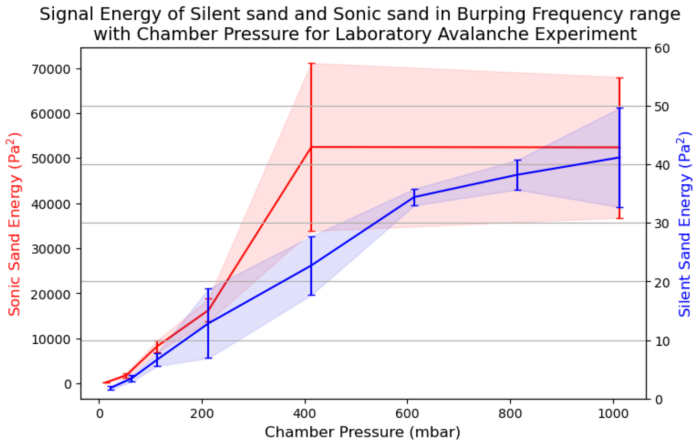

Figure 3.12: Signal energy of silent and sonic sands in burping frequency range with chamber pressure in laboratory avalanche experiment.

The signal energy of the silent sand sound in the burping frequency range follows a roughly linear trend, and is approximately proportional to the chamber pressure, similarly to the shaking jar experiment. The signal energy of the sonic sand's burping emission also matches well with the SPL_{pp} plot. First, a slight increase occurs from ambient pressure to 413.25 mbar, unlike the consistent decrease present in the silent sand measurements and the models. This agrees well with the shaking jar experiment results. The main difference lies in the significant decrease in both SPL_{pp} and signal energy from 413.25 to 213.25 mbar in the laboratory avalanche experiment. The signal energy of the sonic sand sound, like the SPL_{pp}, then follows a trend similar to that of the silent sand sound. While the data at 413.25 mbar does suggest an enhanced emission mechanism compared to ambient terrestrial pressure, the following values as the pressure decreases further do not coincide well with observations in the shaking jar experiment.

3.2.4. Frequency Components

As previously explained, in a setup where the sonic sand quantity is constant, the dominant frequency of the burping sound emitted is dictated by the shearing force applied, measured with the motion metric selected, and the thickness of the sheared layer. Thus, measuring the evolution of the dominant frequency at different pressure levels gives insight into the possible role of interstitial air pressure in the dynamics of the sonic sand flow, i.e. the rate at which the synchronized grain layer shears and vibrates, and its thickness. This metric along with the motion metric are plotted together in Figure 3.13 (a).

The dominant frequency average consistently remains around 170-175 Hz, and the average vacuum chamber motion duration between 0.93 and 0.98 s. Very small variations in the produced burping sound are unavoidable and depend on many factors that are difficult to characterize. However, similarly to the shaking jar experiment, the overall trend does follow that of the motion metric, which remains very stable over the whole set of measurements. This seems to suggest that the maximum thickness of the sheared layer is independent of the interstitial air pressure.

The entire spectrum of the burping signal produced can give further information about the sound frequency components at different pressure levels, and the possible implications in the sonic sand flow.

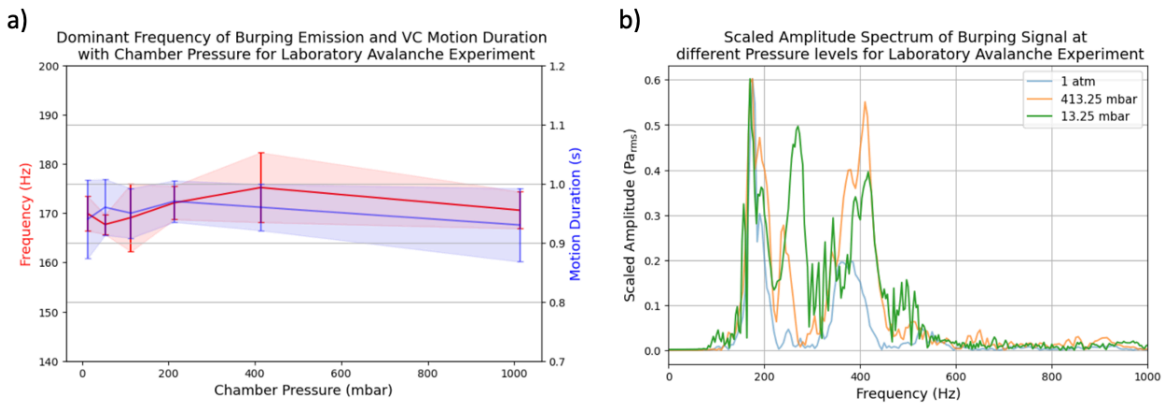

Figure 3.13: (a) Dominant frequency of the burping emission and vacuum chamber motion duration at the different pressure levels in the laboratory avalanche experiment. (b) Scaled amplitude spectrum of burping emissions at ambient pressure, 413.25 mbar and 13.25 mbar, in the laboratory avalanche experiment. The scaling is done such that the peak amplitude of all spectra match.

Figure 3.13 (b) shows the amplitude spectrum of a burping emission in the laboratory avalanche setup at ambient pressure, 413.25 mbar and 13.25 mbar, scaled by multiplying the frequency response by a constant such that the amplitude of the dominant frequency peaks matches, in order to better compare the relative amplitude of other components present in the signal. Signals with very close dominant frequency values are selected as this metric is already featured and studied in Figure 3.13 (a).

Figure 3.13 (b) shows that the dominant frequency peak around 175 Hz, spanning from around 160 to 210 Hz, generally remains similar in width and shape at different pressure levels. The variability in this area that does appear between certain measurements did not show any correlation with the chamber pressure. Then, a second peak in the spectrum, on average at around 240 Hz (slightly higher for the measurement at 13.25 mbar in Figure 3.13 (b)), can be identified. Relative to the dominant frequency peak, this component becomes increasingly more prevalent in the burping emission as the pressure level decreases. Finally, a wide peak between 350 and 430 Hz, likely the second harmonic, appears in the spectra. Its relative amplitude at different pressure levels seems to vary across measurements rather than exhibit a relation with the chamber pressure. These changes in the relative amplitude of certain frequency components as the air pressure lowers, could suggest changes in the sonic sand sound production. The implications of such changes are discussed in the following section.

3.3. Synthesis

3.3.1. SPL_{pp} and Signal Energy Behavior

The results show that in both the shaking jar and laboratory avalanche experiments, multiple SPL_{pp} data points of the sonic sand sound lied significantly above the *SPL* model, while the latter corresponded well with the silent sand data. Similarly, the signal energy in the burping frequency range for the sonic sand did not decrease approximately linearly with the decrease in chamber pressure, as that of the silent sand sound did. These observations could lead one to believe that interstitial air pressure lower than ambient terrestrial pressure in the sonic sand bed could somewhat enhance the sound emission mechanism as the resultant acoustic metrics exceed their natural progression with decreasing air pressure. However, some differences do appear in the results between the two experiments, which must be analysed and discussed.

Agreement across Experiments

The results show good agreement between the two experiments, from ambient pressure to 413.25 mbar, where the SPL_{pp} and signal energy of the sonic sand emissions are greater than at ambient pressure, which is not the case for “regular” sound emissions, such as the silent sand sound. To ensure this behavior does not emanate from noise, the time domain signal and frequency spectrum of two burping emissions in the shaking jar experiment at ambient pressure and 413.25 mbar are compared in Figure 3.14. The signals in the time domain show that the maximum peak to peak acoustic pressure

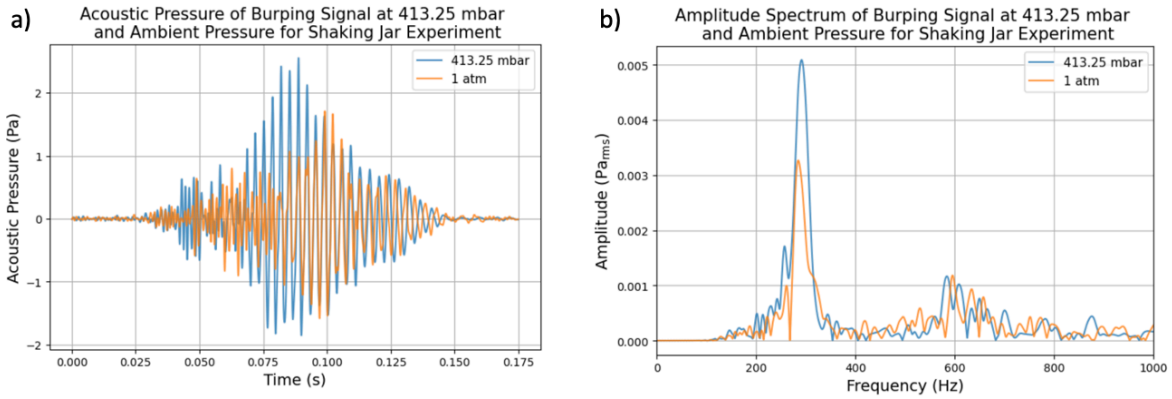

Figure 3.14: Comparison between burping emissions in the shaking jar experiment, at 413.25 mbar and ambient terrestrial pressure, in (a) acoustic pressure in the time domain and (b) amplitude spectrum in the frequency domain.

of the sound at 413.25 mbar is noticeably greater than that at ambient pressure without any noise in the signal, explaining the SPL_{pp} behavior. Also, the dominant frequency component represented by a sine wave-like signal, seems to begin earlier in the sound at 413.25 mbar, and is sustained at an acoustic pressure greater than that of the sound at ambient pressure for multiple signal periods. This translates to the frequency domain, where the amplitude spectrum at 413.25 mbar shows a greater peak amplitude of the dominant frequency than at ambient pressure, explaining the increase in the signal energy in the burping frequency range. From looking at multiple measurements at the different pressure levels, it is apparent that the width of this peak does not seem related to the pressure level, but rather varies from one burping emission to another. These observations would indicate that the increase in acoustic metrics from ambient pressure to 413.25 mbar is not a product of measurement error or noise, but perhaps rather of a change in the physical phenomenon of sand acoustic emissions.

The signals in the time domain show that the burping emission seems to be initiated earlier in the sand flow (in both experiments). The hypothesis is that in that early phase, slightly more sonic sand synchronizes, which increases the amplitude of the pressure wave formed by the vibrating sheared layer. This proposition would require further research including visual tools like cameras in the experimental setups, to be confirmed. The reason behind this behavior, and the consequent role of the air pressure within the sand bed remains to be elucidated. What is clear however is that sand acoustic emissions exhibit greater acoustic pressure levels and signal energy in the burping frequency range, at 413.25 mbar than at ambient pressure, whilst the sound of the grains impacting one another (referred to as the silent sand sound) is reduced. This could perhaps make these acoustic emissions easier to identify in planetary environments where such conditions are met (without considering the sound propagation involved).

Discrepancy at Low Chamber Pressure

One of the main observations from the results is the lack of consensus in SPL_{pp} and signal energy behavior of the burping emission from 413.25 to 13.25 mbar, across the shaking jar and laboratory avalanche experiments. In the former, the metrics remain higher than the expected results all the way down to the Mars-like pressure level. On the other hand, under 413.25 mbar, the acoustic metrics in the avalanche setup decrease back to around model values in the SPL_{pp} case, even going below at 13.25 mbar, and trend closely to the silent sand values in signal energy. The methods used to induce the sand acoustic emissions in the two experiments exhibit some differences, with the shaking jar method depending more on the vacuum chamber motion and creating much shorter burping sounds. Though this could perhaps lead to slight differences in the role of the air pressure on the emission produced, the observed discrepancy might also originate from setup characteristics.

The two experimental setups indeed differ in their geometry and the methods used to fixate the inner container (hosting the sand) to the vacuum chamber and reduce sound propagating through the chamber walls. While these methods proved to significantly reduce the sound propagation through the chamber walls, how much so could not be determined. This could perhaps have played a role in the differences across experiment results.

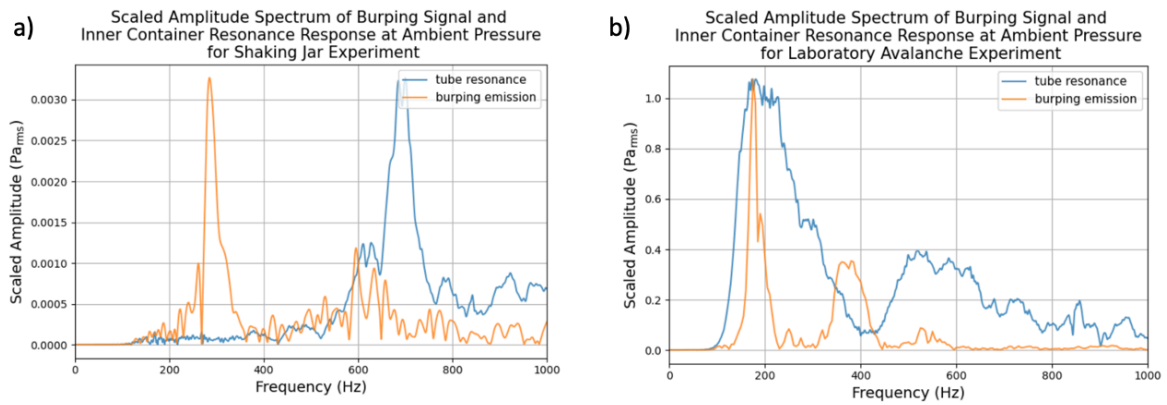

Figure 3.15: Comparison between the frequency spectrum of a burping emission and the resonance response of the inner container for (a) the shaking jar experiment and (b) the laboratory avalanche experiment. The amplitude is adjusted such that the scale of the curves match.

Then, the resonance response of the two empty inner containers was obtained, using a rubber hammer. In Figure 3.15, the inner container resonance response in both experiments is plotted with the frequency spectrum of a burping emission in the corresponding setup. In the shaking jar setup, the resonance response of the inner container features a maximum peak between 650 and 750 Hz. While the second harmonic of the burping emission produced in this setup might be slightly affected, its dominant frequency peak around 285 Hz is completely out of resonance range. The results in this experiment are hence not affected by resonance. When looking at the graph for the laboratory avalanche experiment however, it is clear that the dominant frequency peak of the sand acoustic emission coincides quite closely with the resonant frequency range of the corresponding inner container. Most of the frequencies that constitute the burping emissions are thus amplified. How much resonance plays a role in the recorded sound, and its impact at different pressure levels, remain unanswered questions. However, it is likely to have played a role in the discrepancies in SPL_{pp} and signal energy results between experiments; at lower pressure levels, the excitation amplitude becomes increasingly weaker, which might affect the resonance amplitude and overall signal in the laboratory avalanche setup.

From these observations, it is concluded that the results in SPL_{pp} and signal energy from 413.25 to 13.25 mbar from the shaking jar experiment are more reliable than those from the laboratory avalanche experiment, where resonance likely affected the resultant signal of the burping emissions. The following

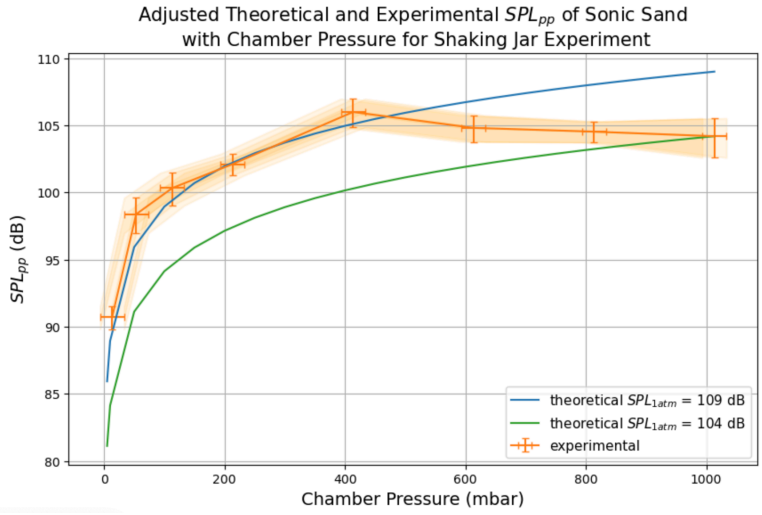

Figure 3.16: Adjusted SPL_{pp} plot of sonic sand emission in the shaking jar experiment, to show results below 413.25 mbar fit well the SPL model of a louder sound at ambient pressure.

interpretation is thus put forth to take these observations into account. From ambient pressure down to around 400 mbar, the SPL_{pp} and signal energy metrics of desert sand acoustic emissions increase (as shown in the results of both experiments) as the emission seemingly initiates earlier in the sand motion and reaches greater acoustic pressure levels despite the decrease in air pressure. As the air pressure decreases further, the emission mechanism seems to stabilize such that the trend of the SPL_{pp} follows that of the *SPL* model, as shown in Figure 3.16. This would suggest that sand acoustic emissions are able to fully develop below a certain air pressure threshold. The reason for this behavior, and the role of the interstitial air pressure in this physical change, remain unknown for the moment. This preliminary hypothesis requires further research to corroborate it, and to remove or better control certain variables that may have affected the results of this project.

3.3.2. Interpreting Changes in Frequency Spectra

Analysing the acoustic signal of burping emissions in the frequency domain gives further insights into the evolution of sonic sand behavior at low atmospheric pressure.

In the shaking jar experiment, the dominant frequency peak and second harmonic peak remain very similar in relative amplitude and shape across pressure levels (see Figure 3.7 (b)). This shows that for this particular burping emission type, no significant changes in the synchronized layer thickness or emission threshold seem to come with a change in air pressure. However, it is important to note that this setup only uses a very small amount of sonic sand and produces very short burping emissions (around 50 ms) due to the nature of the motion induced; in turn, changes in sand flow or sheared layer thickness due to interstitial air pressure might not have appeared due to the quantity of sediment available and brief sand grain motion. What does appear in the graph is the decrease in relative amplitude of the noisy frequency components (most likely corresponding to the grain to grain impacting sound) around the first and second harmonic peaks, at pressure levels of 413.25 mbar and below. This indicates that the amplitude of the burping emission sound decreases slower than that of the regular silent sand sound, which agrees with the SPL_{pp} and signal energy metrics in suggesting that the decreasing air pressure may play a role in allowing more grains to synchronize and create a louder sound than expected.

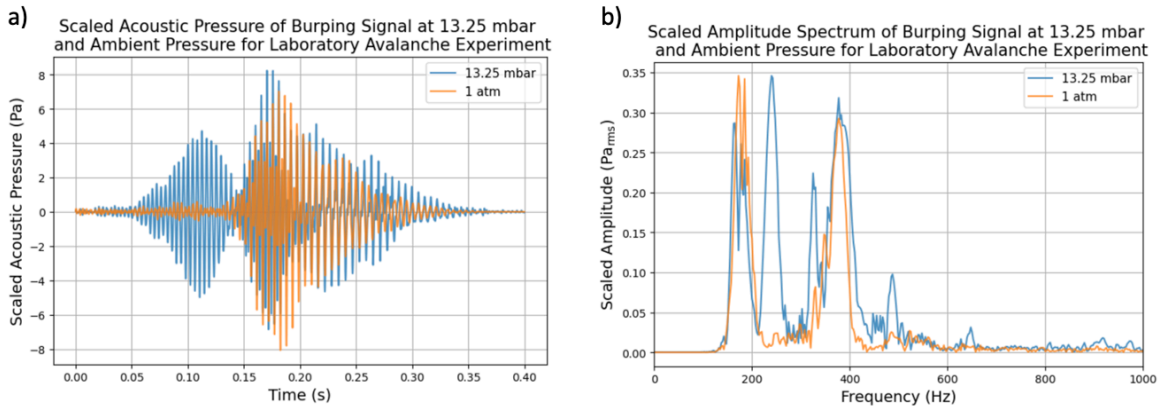

Figure 3.17: Comparison between burping emissions in the laboratory avalanche experiment, at 13.25 mbar and ambient terrestrial pressure, in (a) scaled acoustic pressure in the time domain and (b) scaled amplitude spectrum in the frequency domain. In both cases, the scaling is done by multiplying the signal of interest by a constant such that the peak value of both measurements match.

The dominant frequency of burping emissions in the laboratory avalanche experiment remains very consistent across pressure levels, similarly to the motion metric used. This seems to suggest that, like in the shaking jar experiment, the interstitial air pressure in the sand bed does not appear to affect the maximum thickness of the sheared layer. Due to the resonance effect in the laboratory avalanche experiment discussed with Figure 3.15, it is difficult to draw reliable conclusions from the changes in the different frequency components of burping emissions across pressure levels in this setup (shown in Figure 3.13 (b)). It is however interesting to note the increasingly stronger presence of a peak at around 250 Hz in the burping emission as the chamber pressure decreases (see section 3.2.4). Figure 3.17 compares the signal of a burping emission at ambient terrestrial pressure, and at 13.25 mbar, in both the time and frequency domains. The plots are scaled by multiplying the 13.25 mbar signal by a

constant such that the peak value of both measurements match. In the frequency domain, the first and second harmonics of both emissions are closely comparable in frequency, width and relative amplitude to one another. However, as mentioned in section 3.2.4, another frequency component appears at 250 Hz, as the pressure decreases. This component corresponds to the sound emission starting earlier at 13.25 mbar compared to ambient pressure, evidenced by the signal in the time domain from 0.05 s to 0.15 s, which is clearly absent at ambient pressure. This seems to indicate that burping emissions at 13.25 mbar initiate earlier in the sand flow, where a thinner sheared layer would perhaps produce the 250 Hz frequency component, after which the maximum sheared layer thickness would be reached and the dominant frequency produced. This could hence indicate that, as the interstitial air pressure decreases, the sound emission threshold also decreases, such that a thinner sheared layer of sonic sand would be required to emit a sand acoustic emission. This hypothesis would however require further research and analysis to be confirmed. Furthermore, it remains to be seen how the resonance effect may have affected this behavior.

4

Recommendations

This chapter serves to identify the limitations in the setups and nature of the project. These shortcomings are then used to provide recommendations for future research on the topic.

4.1. Experiment Limitations

Firstly, the vacuum chamber motion was controlled manually. Although it was kept as consistent as possible, and an accelerometer was used to characterise it, an inherent component of variability was added to the results. Furthermore, the motion metrics for these experiments only approximate the true displacement experienced by the sediment samples during testing.

There is also a trade-off between accuracy and sonic sand deterioration: more measurements avoids biases of small sample sizes, but in theory leads to the erosion of the grain surface desert varnish. To avoid sand deterioration, the number of measurements was kept relatively low, which led to apparent variability in the motion metric in the shaking jar experiment for example. This illustrates the important limitation of sonic sand experiments, especially considering how difficult it can be to acquire.

The *SPL* model was calculated using the free-field assumption which can be used for larger rooms (ideally equipped with sound absorption material) where sound wave reflection doesn't affect the measured signal as much. Though the model proved to agree well with the results of the silent sand measurements, the assumption would be more valid in a larger setup. Furthermore, although the inner containers within the vacuum chambers helped reduce the propagation of the sound directly through the chamber walls, it is likely that the measured signal was still slightly affected by this effect. Finally, some frequencies of the burping sound in the laboratory avalanche setup were likely amplified by the resonance of the inner container. All these factors likely played a role in the results discrepancy between experiments at lower chamber pressure, and made it difficult to give a conclusion regarding the sonic sand emission mechanism at the lowest pressure levels tested.

The measurement errors in the setups also reduced the accuracy of results at the lower pressure levels. Indeed, the vacuum gauge included in the setup for both chambers has a specified indication error of ±1.6% of the full 1 bar scale (or ±16 mbar). While this doesn't have a significant impact at 800 mbar, the measurements close to 10 mbar could have been at very high vacuum, smaller that 1 mbar or at 26 mbar. The low sonic sand sound SPL_{pp} results at 13.25 mbar in the laboratory avalanche experiment may have come from the vacuum gauge perhaps indicating a higher pressure level than the actual one. To this indication error is added the human reading error that comes with the uncertainty of analog gauge readings.

Lastly, the small size of the setups only allowed for burping emissions to be produced. These sounds require more variables to be controlled, especially the motion of the vacuum chamber which introduces uncertainty to the produced sound, compared to the naturally occurring booming emissions found in desert dunes, and reproduced in the laboratory by Dagois-Bohy et al. (2012) and Dagois-Bohy et al. (2010). A larger static avalanche setup would not only remove such variables, but also give more time for the sand flow to fully develop and overall more accurately reproduce natural booming emissions from avalanche flows in planetary environments.

4.2. Recommended Improvements

The following recommendations outline the continuation to this project and address the limitations described in section 4.1.

In order to accurately study the impact of one parameter, here the air pressure, on the emission mechanism of sonic sand, it would be beneficial to avoid manually controlling the motion of the vacuum chambers. A setup similar to the laboratory avalanche chute developed by Dagois-Bohy et al. (2012) and Dagois-Bohy et al. (2010) could thus be adapted. The chute is static, kept at the angle of repose of sonic sand, which is held back at the top of the slope by a controllable gate. Once opened, the sediment flows freely down the reproduced slipface, and sand acoustic emissions occur. The only moving part in the setup, the gate, could be remote-controlled.

The larger setup in Dagois-Bohy et al. (2012) and Dagois-Bohy et al. (2010) also reproduces booming emissions which are more sustained than burping emissions. It hence better replicates the conditions required for natural booming emissions from avalanche flows present in planetary environments like Mars. However, to achieve these sounds, a much larger quantity of sonic sand is used, making the setup larger than a portable vacuum chamber could fit. Ideally, the setup could be housed in a larger scale vacuum system, which would also more accurately measure the lower pressure levels and remove the vacuum gauge measurement errors encountered. Furthermore, by applying sound absorbing foam panels to the chamber walls, this larger experimental setup would also allow for more valid free-field assumptions, eliminating most reflections of sound waves.

The hypothesis proposed in section 3.3 regarding the impact of the chamber pressure on the sonic sand motion and consequent acoustic emission, could be corroborated not only by reproducing the results in this new setup, but also by adding a new, visual element of analysis in the form of cameras. Studying the correspondence between camera footage and audio recording could provide further insights into the changes in grain flow dynamics and acoustic emission timing occurring at lower pressure levels.

As seen in this project, the decrease in sound production of sonic sand, which may have come from surface varnish erosion, is an important factor to account for. To prevent it from affecting the experiments schedule or the results, one would ideally collect a much larger amount of sonic sand than in this project, like Dagois-Bohy et al. (2012), to have more sediment available and not rely on a single batch.

5

Conclusion

To answer the first research question posed in section 1.4, the sound of silent sand grains impacting one another at various pressure levels, from Mars-like to Earth, coincides well with the *SPL* model used, and thus follows expected trends with decreasing chamber pressure. The *SPL* model and silent sand measurements were thus further used to compare the trends of sonic sand sounds to that produced by regular sound emission mechanisms.

Regarding the second and third research questions, the results obtained with the sonic sediment show that the interstitial air pressure does seem to play a role in the sand grain synchronisation and emission mechanism of sonic sand. Indeed, the burping emission signals exhibit noticeable differences in both the time and frequency domains, as the air pressure decreases. In both experiments, the burping emissions see an increase in the SPL_{pp} and signal energy metrics from ambient pressure to 413.25 mbar, which is not predicted by the *SPL* model nor the trend of silent sand measurements with decreasing pressure. This behavior is associated to the observation in the time-domain signals that the sand acoustic emissions seem to initiate earlier at 413.25 mbar and below, resulting in greater acoustic pressure levels being produced, compared to those at ambient pressure. Below 413.25 mbar, the results suggest a stabilized behavior, with the acoustic metrics of the burping emissions following the model. A hypothesis could be that more sheared sonic sand grains synchronize at 413.25 mbar and below (compared to terrestrial air pressure), and thus increase the amplitude of the sound wave produced. It is also found that the dominant frequency very closely follows the trend of the motion metrics used, remaining very consistent across pressure levels. This suggests that the maximum sheared sonic sand layer thickness is independent of the interstitial air pressure. Furthermore, the emergence of a new frequency component slightly higher than the dominant frequency, in the laboratory avalanche burping emissions at the lower pressure levels, is shown to correspond to the sonic sand seemingly synchronizing earlier in the grain flow than at ambient pressure. It is thought that for such avalanche-like flows, the minimum sheared layer thickness threshold required to produce an emission is lowered at lower pressure, which leads to a higher frequency produced initially until the full layer forms, ultimately decreasing the frequency. However, the results at Mars-like pressure levels do somewhat suffer from different parameters, namely vacuum gauge (in)accuracy and resonance effects in the laboratory avalanche setup, making it difficult to strongly conclude about how the Martian sand acoustic emissions would sound in the field. Furthermore, the physical reason behind the air pressure affecting the sonic sand grain flow and synchronization timing remains unclear. These limitations and open questions would benefit from further research on the topic, following the proposed recommendations. An improved experimental setup could also remove the human factor, further reduce the testing variability, and introduce new tools such as cameras to visually analyze the sonic sand grain flow, which could test the hypotheses emitted in this project.

Is is important to note that other potential research areas in the overarching field of sand acoustic emissions being applied to planetary exploration exist and could help better estimate the possibilities of this phenomenon taking place on other planets. Mainly, the formation of desert varnish in Martian (and other extraterrestrial) conditions would further the understanding of its requirements, and how likely it is to form outside of Earth.

Bibliography

Ahlbrandt, T. S. (1979). Textural parameters of eolian deposits. *A study of global sand seas* (pp. 21–52). United States Geological Survey Professional Paper.

Alshibli, K. A., Batiste, S. N., & Sture, S. (2003). Strain localization in sand: Plane strain versus triaxial compression. *Journal of geotechnical and geoenvironmental engineering*, *129*(6), 483–494.

Altuhafi, F., O'Sullivan, C., & Cavarretta, I. (2013). Analysis of an image-based method to quantify the size and shape of sand particles. *Journal of Geotechnical and Geoenvironmental Engineering*, *139*(8), 1290–1307.

Andreotti, B. (2004). The song of dunes as a wave-particle mode locking. *Physical Review Letters*, *93*(23), 238001.

Andreotti, B. (2012). Sonic sands. *Reports on Progress in Physics*, *75*(2), 026602. https://doi.org/10.1088/0034-4885/75/2/026602

Andreotti, B., Claudin, P., & Pouliquen, O. (2010). Measurements of the aeolian sand transport saturation length. *Geomorphology*, *123*(3-4), 343–348.

Attenborough, K. (2014). Sound propagation in the atmosphere. *Springer handbook of acoustics*, 117–155.

Atwood-Stone, C., & McEwen, A. S. (2013). Avalanche slope angles in low-gravity environments from active martian sand dunes. *Geophysical Research Letters*, *40*(12), 2929–2934.

Aydda, A., & Algouti, A. (2014). Assessment of sand dunes movements rate in atlantic sahara desert using multi-temporal landsat imagery and gis technique.

Bagnold, R. (1941). The physics of blown sand and desert dunes. Methuen.

Baird, T., Bristow, C. S., & Vermeesch, P. (2019). Measuring sand dune migration rates with cosi-corr and landsat: Opportunities and challenges. *Remote Sensing*, *11*(20), 2423.

Bass, H. E., & Chambers, J. P. (2001). Absorption of sound in the martian atmosphere. *The Journal of the Acoustical Society of America*, *109*(6), 3069–3071.

Bass, H. E., Sutherland, L. C., Piercy, J., & Evans, L. (1984). Absorption of sound by the atmosphere. *Physical acoustics*, *17*, 145–232.

Bolton, H. C. (1890). Squeaking sand versus musical sand. *Nature*, *43*(1098), 30–30.

Bourke, M. C., Ewing, R. C., Finnegan, D., & McGowan, H. A. (2009). Sand dune movement in the victoria valley, antarctica. *Geomorphology*, *109*(3-4), 148–160.

Bracewell, R. N. (1986). *The fourier transform and its applications* (Vol. 31999). McGraw-Hill New York.

Brantley, K. S., Hunt, M. L., Brennen, C. E., & Gao, S. S. (2002). Characterization of booming sands. *MRS Online Proceedings Library (OPL)*, *759*, MM3–5.

Breed, C. S., Grolier, M. J., & McCauley, J. F. (1979). Morphology and distribution of common 'sand' dunes on mars: Comparison with the earth. *Journal of Geophysical Research: Solid Earth*, *84*(B14), 8183–8204.

Bridges, N. T., Ayoub, F., Avouac, J. P., Leprince, S., Lucas, A., & Mattson, S. (2012). Earth-like sand fluxes on mars. *Nature*, *485*(7398), 339–342.

Brown, A. E. (1964). *Musical sand: The singing sands of the seashore, part ii*. University of Newcastle upon Tyne Philosophical Society.

Burkard, R. (1984). Sound pressure level measurement and spectral analysis of brief acoustic transients. *Electroencephalography and clinical Neurophysiology*, *57*(1), 83–91.

Cabrol, N. A., Herkenhoff, K. E., Greeley, R., Grin, E. A., Schröder, C., d'Uston, C., Weitz, C., Yingst, R. A., Cohen, B. A., Moore, J. et al. (2008). Soil sedimentology at gusev crater from columbia memorial station to winter haven. *Journal of Geophysical Research: Planets*, *113*(E6).

Cardinale, M., Silvestro, S., Vaz, D. A., Michaels, T., Bourke, M. C., Komatsu, G., & Marinangeli, L. (2016). Present-day aeolian activity in herschel crater, mars. *Icarus*, *265*, 139–148.

Carus-Wilson, C. (1891). The production of musical notes from non-musical sands. *Science*, (446), 99–99.

Cate, R. B., & Nelson, L. A. (1971). A simple statistical procedure for partitioning soil test correlation data into two classes. *Soil Science Society of America Journal*, *35*(4), 658–660.

Cerna, M., & Harvey, A. F. (2000). *The fundamentals of fft-based signal analysis and measurement* (tech. rep.). Application Note 041, National Instruments.

Chen, H., Liu, Y. L., Zhao, X. Q., Xiao, Y. G., & Liu, Y. (2015). Numerical investigation on angle of repose and force network from granular pile in variable gravitational environments. *Powder technology*, *283*, 607–617.

Chojnacki, M., Burr, D. M., Moersch, J. E., & Michaels, T. I. (2011). Orbital observations of contemporary dune activity in endeavor crater, meridiani planum, mars. *Journal of Geophysical Research: Planets*, *116*(E7).

Chojnacki, M., & Fenton, L. K. (2017). The geologic exploration of the bagnold dune field at gale crater by the curiosity rover. *Journal of Geophysical Research: Planets*, *122*(11), 2216–2222.

Cooke, R. U., & Warren, A. (1973). *Geomorphology in deserts*. University of California Press.

Cooley, J. W., & Tukey, J. W. (1965). An algorithm for the machine calculation of complex fourier series. *Mathematics of computation*, *19*(90), 297–301.

Cornwall, C., Bourke, M. C., Jackson, D. W. T., & Cooper, J. A. G. (2018). Aeolian slipface dynamics and grainflow morphologies on earth and mars. *Icarus*, *314*, 311–326.

Cousin, A., Dehouck, E., Meslin, P. Y., Forni, O., Williams, A. J., Stein, N., Gasnault, O., Bridges, N. T., Ehlmann, B. L., Schröder, S. et al. (2017). Geochemistry of the bagnold dune field as observed by chemcam and comparison with other aeolian deposits at gale crater. *Journal of Geophysical Research: Planets*, *122*(10), 2144–2162.

Criswell, D. R., Lindsay, J. F., & Reasoner, D. L. (1975). Seismic and acoustic emissions of a booming dune. *Journal of geophysical research*, *80*(35), 4963–4974.

Curzon, G. N. (1923). Tales of travel. Century.

Dagois-Bohy, S., Courrech du Pont, S., & Douady, S. (2012). Singing-sand avalanches without dunes. *Geophysical research letters*, *39*(20).

Dagois-Bohy, S., Ngo, S., Courrech du Pont, S., & Douady, S. (2010). Laboratory singing sand avalanches. *Ultrasonics*, *50*(2), 127–132.

Dain, Y., & Lueptow, R. M. (2001). Acoustic attenuation in three-component gas mixtures—theory. *The Journal of the Acoustical Society of America*, *109*(5), 1955–1964.

Davidson, G. A. (1977). Propagation of audible sound through air-water fogs. *The Journal of the Acoustical Society of America*, *62*(3), 497–502.

Davis, J. M., Grindrod, P. M., Boazman, S. J., Vermeesch, P., & Baird, T. (2020). Quantified aeolian dune changes on mars derived from repeat context camera images. *Earth and Space Science*, *7*(2), e2019EA000874.

De Vet, S. J. (2016). Transport and modification of glaciovolcanic glass from source to sink on mars. *Netherlands Journal of Geosciences*, *95*(2), 171–182.

Dickens, P. G., & Ripamonti, A. (1961). Calculation of vibrational relaxation times in gases. *Transactions of the Faraday Society*, *57*, 735–745.

Douady, S. (2016, February 18). *Les dunes qui chantent, un nouveau mode d'émission sonore* [Conference session], Paris, France. https://vimeo.com/157550696

Douady, S., Manning, A., Hersen, P., Elbelrhiti, H., Protiere, S., Daerr, A., & Kabbachi, B. (2006). Song of the dunes as a self-synchronized instrument. *Physical Review Letters*, *97*(1), 018002.

Edwards, A. C. (2001). Grain size and sorting in modern beach sands. *Journal of Coastal Research*, 38–52.

Ehlmann, B. L., Edgett, K. S., Sutter, B., Achilles, C. N., Litvak, M. L., Lapotre, M. G. A., Sullivan, R., Fraeman, A. A., Arvidson, R. E., Blake, D. F. et al. (2017). Chemistry, mineralogy, and grain properties at namib and high dunes, bagnold dune field, gale crater, mars: A synthesis of curiosity rover observations. *Journal of Geophysical Research: Planets*, *122*(12), 2510–2543.

Ejakov, S. G., Phillips, S., Dain, Y., Lueptow, R. M., & Visser, J. H. (2003). Acoustic attenuation in gas mixtures with nitrogen: Experimental data and calculations. *The Journal of the Acoustical Society of America*, *113*(4), 1871–1879.

Engel, C. G., & Sharp, R. P. (1958). Chemical data on desert varnish. *Geological Society of America Bulletin*, *69*(5), 487–518.

Fenton, L. K. (2006). Dune migration and slip face advancement in the rabe crater dune field, mars. *Geophysical Research Letters*, *33*(20).

Fischer, E., Martínez, G. M., Rennó, N. O., Tamppari, L. K., & Zent, A. P. (2019). Relative humidity on mars: New results from the phoenix tecp sensor. *Journal of Geophysical Research: Planets*, *124*(11), 2780–2792.

Fisher, R. V., & Schmincke, H. U. (2012). *Pyroclastic rocks*. Springer Science & Business Media.

Folk, R. L., & Ward, W. C. (1957). Brazos river bar [texas]; a study in the significance of grain size parameters. *Journal of sedimentary research*, *27*(1), 3–26.

Fourier, J. B. J. (1822). *Théorie analytique de la chaleur*. Firmin Didot.

Fryberger, S. G., & Ahlbrandt, T. S. (1979). Mechanisms for the formation of eolian sand seas.

Goetz, W., Pike, W. T., Hviid, S. F., Madsen, M. B., Morris, R. V., Hecht, M. H., Staufer, U., Leer, K., Sykulska, H., Hemmig, E. et al. (2010). Microscopy analysis of soils at the phoenix landing site, mars: Classification of soil particles and description of their optical and magnetic properties. *Journal of Geophysical Research: Planets*, *115*(E8).

Greeley, R., Arvidson, R. E., Barlett, P. W., Blaney, D., Cabrol, N. A., Christensen, P. R., Fergason, R. L., Golombek, M. P., Landis, G. A., Lemmon, M. T. et al. (2006). Gusev crater: Wind-related features and processes observed by the mars exploration rover spirit. *Journal of Geophysical Research: Planets*, *111*(E2).

Greeley, R., & Iversen, J. D. (1985). Wind as a geological process on earth, mars, venus and titan. *Cambridge Planetary Science Series*.

Haff, P. K. (1979). Booming sands of the mojave desert and the basin and range province, california.

Haff, P. K. (1986). Booming dunes. *American scientist*, *74*(4), 376–381.

Han, F., Tian, M., Wu, F., Zhang, J., Liu, S., & Wang, L. (2017). Physical and chemical properties of sound-producing and soundless sand particles from booming sand dunes, northern china. *Arabian Journal of Geosciences*, *10*, 1–10.

Hansen, C. J., Bourke, M. C., Bridges, N. T., Byrne, S., Colon, C., Diniega, S., Dundas, C., Herkenhoff, K., McEwen, A., Mellon, M. et al. (2011). Seasonal erosion and restoration of mars' northern polar dunes. *Science*, *331*(6017), 575–578.

Hashimoto, M. (1951). Some physical properties of the singing sand. *Proc. 1st Japan Nat. Congr. App. Mech.*, 261–266.

Haughton, P. M., Lightfoot, G. R., & Stevens, J. C. (2003). Peak-to-peak equivalent sound pressure level. *International journal of audiology*, *42*(8), 494–496.

Hecht, M. H., Kounaves, S. P., Quinn, R. C., West, S. J., Young, S. M. M., Ming, D. W., Catling, D. C., Clark, B. C., Boynton, W. V., Hoffman, J. et al. (2009). Detection of perchlorate and the soluble chemistry of martian soil at the phoenix lander site. *Science*, *325*(5936), 64–67.

Henley, D. C., & Hoidale, G. B. (1973). Attenuation and dispersion of acoustic energy by atmospheric dust. *The Journal of the Acoustical Society of America*, *54*(2), 437–445.

Hidaka, J., Miwa, S., & Makina, K. (1988). Mechanism of generation of sound in shear flow of granular materials. *Int. Chem. Eng*, *28*, 99–107.

Hiremath, N., Kumar, V., Motahari, N., & Shukla, D. (2021). An overview of acoustic impedance measurement techniques and future prospects. *Metrology*, *1*(1), 17–38. https://doi.org/10.3390/metrology1010002

Holstein-Rathlou, C., Gunnlaugsson, H. P., Merrison, J. P., Bean, K. M., Cantor, B. A., Davis, J. M., Davy, R., Drake, N. B., Ellehoj, M. D., Goetz, W. et al. (2010). Winds at the phoenix landing site. *Journal of Geophysical Research: Planets*, *115*(E5).

Horgan, B. H. N., & Bell III, J. F. (2012). Seasonally active slipface avalanches in the north polar sand sea of mars: Evidence for a wind-related origin. *Geophysical Research Letters*, *39*(9).

Humphries, D. W. (1966). The booming sand of korizo, sahara, and the squeaking sand of gower, s. wales: A comparison of the fundamental characteristics of two musical sands. *Sedimentology*, *6*(2), 135–152.

Hunt, M. L., & Vriend, N. M. (2010). Booming sand dunes. *Annual Review of Earth and Planetary Sciences*, *38*, 281–301.

Jakosky, B. M. (2021). Atmospheric loss to space and the history of water on mars. *Annual Review of Earth and Planetary Sciences*, *49*, 71–93.

Karapiperis, K., Marshall, J. P., & Andrade, J. E. (2020). Reduced gravity effects on the strength of granular matter: Dem simulations versus experiments. *Journal of Geotechnical and Geoenvironmental Engineering*, *146*(5), 06020005.

Kilkenny, C., Leach, M. F., & Goldsack, D. E. (1997). Acoustic emission of silica gel. *Canadian Acoustics*, *25*(4), 28–28.

Kok, J. F. (2010a). Difference in the wind speeds required for initiation versus continuation of sand transport on mars: Implications for dunes and dust storms. *Physical Review Letters*, *104*(7), 074502.

Kok, J. F. (2010b). An improved parameterization of wind-blown sand flux on mars that includes the effect of hysteresis. *Geophysical Research Letters*, *37*(12).

Kok, J. F., Parteli, E. J. R., Michaels, T. I., & Karam, D. B. (2012). The physics of wind-blown sand and dust. *Reports on progress in Physics*, *75*(10), 106901.

Kokelaar, P. (1986). Magma-water interactions in subaqueous and emergent basaltic. *Bulletin of Volcanology*, *48*, 275–289.

Lämmel, M., Meiwald, A., Yizhaq, H., Tsoar, H., Katra, I., & Kroy, K. (2018). Aeolian sand sorting and megaripple formation. *Nature Physics*, *14*(7), 759–765.

Laukli, E., & Burkard, R. (2015). Calibration/standardization of short-duration stimuli. *Seminars in hearing*, *36*(01), 03–10.

Leach, M. F., Goldsack, D. E., & Kilkenny, C. (1999). Booming sand as a possible source of single frequency sound. *Proc. 6th Int. Congress on Sound and Vibration (Copenhagen, Denmark)*, 1983–8.

Leach, M. F., & Rubin, G. A. (1993). Acoustic emission of booming sand analyzed in the laboratory. *Journal of acoustic emission*, *11*(1), 19–20.

Ledoux, A. R. (1920). Singing sands. *Science*, *51*(1323), 462–464. https://doi.org/10.1126/science.51.1323.462.b

Leer, K., Drube, L., Goetz, W., Gunnlaugsson, H. P., Lemmon, M., Madsen, M. B., Morris, R. V., Smith, P. et al. (2009). Optical study of particles on mars phoenix magnets. *40th Annual Lunar and Planetary Science Conference*, 1923.

Leshin, L. A., Mahaffy, P. R., Webster, C. R., Cabane, M., Coll, P., Conrad, P. G., Archer Jr, P. D., Atreya, S. K., Brunner, A. E., Buch, A. et al. (2013). Volatile, isotope, and organic analysis of martian fines with the mars curiosity rover. *science*, *341*(6153), 1238937.

Lindsay, J. F., Criswell, D. R., Criswell, T. L., & Criswell, B. S. (1976). Sound-producing dune and beach sands. *Geological Society of America Bulletin*, *87*(3), 463–473.

Liu, T., Wang, S., & Zhu, M. (2017). Predicting acoustic relaxation absorption in gas mixtures for extraction of composition relaxation contributions. *Proceedings of the Royal Society A: Mathematical, Physical and Engineering Sciences*, *473*(2208), 20170496.

Malin, M. C., & Edgett, K. S. (2001). Mars global surveyor mars orbiter camera: Interplanetary cruise through primary mission. *Journal of Geophysical Research: Planets*, *106*(E10), 23429–23570.

Marshall, J. P., Hurley, R. C., Arthur, D., Vlahinic, I., Senatore, C., Iagnemma, K., Trease, B., & Andrade, J. E. (2018). Failures in sand in reduced gravity environments. *Journal of the Mechanics and Physics of Solids*, *113*, 1–12.

Martín-Torres, F. J., Zorzano, M. P., Valentín-Serrano, P., Harri, A. M., Genzer, M., Kemppinen, O., Rivera-Valentin, E. G., Jun, I., Wray, J., Bo Madsen, M. et al. (2015). Transient liquid water and water activity at gale crater on mars. *Nature Geoscience*, *8*(5), 357–361.

Maurice, S., Chide, B., Murdoch, N., Lorenz, R. D., Mimoun, D., Wiens, R. C., Stott, A., Jacob, X., Bertrand, T., Montmessin, F. et al. (2022). In situ recording of mars soundscape. *Nature*, *605*(7911), 653–658.

Mazzullo, J., Sims, D., & Cunningham, D. (1986). The effects of eolian sorting and abrasion upon the shapes of fine quartz sand grains. *Journal of Sedimentary Research*, *56*(1), 45–56.

McGlynn, I. O., Fedo, C. M., & McSween Jr, H. Y. (2011). Origin of basaltic soils at gusev crater, mars, by aeolian modification of impact-generated sediment. *Journal of Geophysical Research: Planets*, *116*(E7).

McLaughlin, D. B. (1954). Volcanism and aeolian deposition on mars. *Geological Society of America Bulletin*, *65*(7), 715–718.

Miwa, S., Hidaka, J., & Shimosaka, A. (1983). Musical sand. *KONA Powder and Particle Journal*, *1*, 64–72.

Möbius, M. E., Lauderdale, B. E., Nagel, S. R., & Jaeger, H. M. (2001). Size separation of granular particles. *Nature*, *414*(6861), 270–270.

Möhlmann, D., & Thomsen, K. (2011). Properties of cryobrines on mars. *Icarus*, *212*(1), 123–130.

Moore, H. J., & Jakosky, B. M. (1989). Viking landing sites, remote-sensing observations, and physical properties of martian surface materials. *Icarus*, *81*(1), 164–184.

Morse, P. M., & Ingard, K. U. (1986). *Theoretical acoustics*. Princeton university press.

Musiolik, G., Kruss, M., Demirci, T., Schrinski, B., Teiser, J., Daerden, F., Smith, M. D., Neary, L., & Wurm, G. (2018). Saltation under martian gravity and its influence on the global dust distribution. *Icarus*, *306*, 25–31.

Nakashima, H., Shioji, Y., Kobayashi, T., Aoki, S., Shimizu, H., Miyasaka, J., & Ohdoi, K. (2011). Determining the angle of repose of sand under low-gravity conditions using discrete element method. *Journal of terramechanics*, *48*(1), 17–26.

National Oceanic and Atmospheric Administration. (2021). *How does sand form?* https://oceanservice.noaa.gov/facts/sand.html

Ng, T. T. (2013). Numerical study of a granular material in various gravity environments. *Journal of Engineering Mechanics*, *139*(4), 489–495.

Nickling, W. G., & Neuman, C. M. (2009). Aeolian sediment transport. *Geomorphology of desert environments*, 517–555.

Nori, F., Sholtz, P., & Bretz, M. (1997). Booming sand. *Scientific American*, *277*(3), 84–89.

Nyquist, H. (1928). Certain topics in telegraph transmission theory. *Transactions of the American Institute of Electrical Engineers*, *47*(2), 617–644.

O'Connell-Cooper, C. D., Spray, J. G., Thompson, L. M., Gellert, R., Berger, J. A., Boyd, N. I., Desouza, E. D., Perrett, G. M., Schmidt, M., & VanBommel, S. J. (2017). Apxs-derived chemistry of the bagnold dune sands: Comparisons with gale crater soils and the global martian average. *Journal of Geophysical Research: Planets*, *122*(12), 2623–2643.

Papoulis, A. (1962). The fourier integral and its applications. *Polytechnic Institute of Brooklyn*.

Patitsas, A. J. (2012). Singing sands, booming dune sands, and the stick-slip effect. *Canadian Journal of Physics*, *90*(7), 611–631.

Perry, R. S., Kolb, V. M., Lynne, B. Y., Sephton, M. A., Mcloughlin, N., Engel, M. H., Olendzenski, L., Brasier, M., & Staley Jr, J. T. (2005). How desert varnish forms? *Astrobiology and Planetary Missions*, *5906*, 276–287.

Petculescu, A., & Lueptow, R. M. (2007). Atmospheric acoustics of titan, mars, venus, and earth. *Icarus*, *186*(2), 413–419.

Petculescu, A. G., & Lueptow, R. M. (2005). Fine-tuning molecular acoustic models: Sensitivity of the predicted attenuation to the lennard-jones parameters. *The Journal of the Acoustical Society of America*, *117*(1), 175–184.

Poynting, J. H., & Thompson, J. J. (1909). A text-book of physics. Charles Griffin & Co.

Pye, K. (1987). *Aeolian dust and dust deposits*. Academic Press.

Reynolds, O. (1885). Lvii. on the dilatancy of media composed of rigid particles in contact. with experimental illustrations. *The London, Edinburgh, and Dublin Philosophical Magazine and Journal of Science*, *20*(127), 469–481.

Richardson, W. D. (1919). The singing sands of lake michigan. *Science*, *50*(1300), 493–495.

Ridgway, K., & Scotton, J. B. (1973). Whistling sand beaches in the british isles. *Sedimentology*, *20*(2), 263–279.

Savage, S. B., & Lun, C. K. K. (1988). Particle size segregation in inclined chute flow of dry cohesionless granular solids. *Journal of fluid mechanics*, *189*, 311–335.

Schatz, V., Tsoar, H., Edgett, K. S., Parteli, E. J. R., & Herrmann, H. J. (2006). Evidence for indurated sand dunes in the martian north polar region. *Journal of Geophysical Research: Planets*, *111*(E4).

Sharp, R. P. (1963). Wind ripples. *The Journal of Geology*, *71*(5), 617–636.

Sharp, R. P. (1966). Kelso dunes, mojave desert, california. *Geological Society of America Bulletin*, *77*(10), 1045–1074.

Shaw, A., Arvidson, R. E., Bonitz, R., Carsten, J., Keller, H. U., Lemmon, M. T., Mellon, M. T., Robinson, M., & Trebi-Ollennu, A. (2009). Phoenix soil physical properties investigation. *Journal of Geophysical Research: Planets*, *114*(E1).

Sholtz, P., Bretz, M., & Nori, F. (1997). Sound-producing sand avalanches. *Contemporary physics*, *38*(5), 329–342.

Silvestro, S., Fenton, L. K., Vaz, D. A., Bridges, N. T., & Ori, G. G. (2010). Ripple migration and dune activity on mars: Evidence for dynamic wind processes. *Geophysical Research Letters*, *37*(20).

Simons, D. G., & Snellen, M. (2021). *Chapter 3: Propagation of sound in the atmosphere* [Powerpoint slides]. Delft University of Technology. https://brightspace.tudelft.nl/d2l/le/%20content/398020/viewContent/2502381/View

Smith, J. O. (2003). *Mathematics of the discrete fourier transform (dft)*.

Soares, C. (2015). Gas turbines (second edition).

Sochan, A., Zieliński, P., & Bieganowski, A. (2015). Selection of shape parameters that differentiate sand grains, based on the automatic analysis of two-dimensional images. *Sedimentary Geology*, *327*, 14–20.

Soderblom, L. A., Anderson, R. C., Arvidson, R. E., Bell III, J. F., Cabrol, N. A., Calvin, W., Christensen, P. R., Clark, B. C., Economou, T., Ehlmann, B. L. et al. (2004). Soils of eagle crater and meridiani planum at the opportunity rover landing site. *Science*, *306*(5702), 1723–1726.

Sullivan, R., Anderson, R., Biesiadecki, J., Bond, T., & Stewart, H. (2011). Cohesions, friction angles, and other physical properties of martian regolith from mars exploration rover wheel trenches and wheel scuffs. *Journal of Geophysical Research: Planets*, *116*(E2).

Tanczos, F. I. (1956). Calculation of vibrational relaxation times of the chloromethanes. *The Journal of Chemical Physics*, *25*(3), 439–447.

Tschiffely, A. F. (1933). Southern cross to pole star. Heinemann.

Tyler, W. (2023). *The ultimate guide to the ro-tap sieve shaker*. https://hub.wstyler.com/rotap-guide

Ulusoy, U. (2019). Quantifying of particle shape differences of differently milled barite using a novel technique: Dynamic image analysis. *Materialia*, *8*, 100434.

Van Rooyen, T. H., & Verster, E. (1983). Granulometric properties of the roaring sands in the south-eastern kalahari. *Journal of arid environments*, *6*(3), 215–222.

Vriend, N. M., Hunt, M. L., & Clayton, R. W. (2015). Linear and nonlinear wave propagation in booming sand dunes. *Physics of Fluids*, *27*(10), 103305.

Vriend, N. M., Hunt, M. L., Clayton, R. W., Brennen, C. E., Brantley, K. S., & Ruiz-Angulo, A. (2007). Solving the mystery of booming sand dunes. *Geophysical Research Letters*, *34*(16).

Vriend, N. M., Hunt, M. L., Clayton, R. W., Brennen, C. E., Brantley, K. S., & Ruiz-Angulo, A. (2008). Reply to comment by b. andreotti et al. on ”solving the mystery of booming sand dunes”. *Geophysical Research Letters*, *35*(L08).

Weitz, C. M., Anderson, R. C., Bell III, J. F., Farrand, W. H., Herkenhoff, K. E., Johnson, J. R., Jolliff, B. L., Morris, R. V., Squyres, S. W., & Sullivan, R. J. (2006). Soil grain analyses at meridiani planum, mars. *Journal of Geophysical Research: Planets*, *111*(E12).

Williams, J. P. (2001). Acoustic environment of the martian surface. *Journal of Geophysical Research: Planets*, *106*(E3), 5033–5041.

Yang, J., Dong, Z., Liu, Z., Shi, W., Chen, G., Shao, T., & Zeng, H. (2019). Migration of barchan dunes in the western quruq desert, northwestern china. *Earth Surface Processes and Landforms*, *44*(10), 2016–2029.

Zamanian, M., Mollaei-Alamouti, V., & Payan, M. (2020). Directional strength and stiffness characteristics of inherently anisotropic sand: The influence of deposition inclination. *Soil Dynamics and Earthquake Engineering*, *137*, 106304.

Zhang, K. S., Ou, W., Jiang, X., Long, F., & Hu, M. (2014). Calculation of vibrational relaxation times in multi-component excitable gases. *Journal of the Korean Physical Society*, *65*, 1028–1035.

Zimbelman, J. R. (2000). Non-active dunes in the acheron fossae region of mars between the viking and mars global surveyor eras. *Geophysical Research Letters*, *27*(7), 1069–1072.

Zorzano, M. P., Mateo-Martí, E., Prieto-Ballesteros, O., Osuna, S., & Renno, N. (2009). Stability of liquid saline water on present day mars. *Geophysical Research Letters*, *36*(20).

Zou, M., Fan, S., Shi, R., Yang, Y., & Li, J. (2015). Effect of gravity on the mechanical properties of lunar regolith tested using a low gravity simulation device. *Journal of Terramechanics*, *60*, 11–22.